UILU-ENG.-71-2015

CIVIL ENGINEERING STUDIES

STRUCTURAL RESEARCH SERIES NO. 378

QUASI-STATIC LATERAL DESIGN LOADS FOR EARTHQUAKE RESISTANT STRUCTURES

By

G. Estrada-Uribe (Ph D)

A Technical Report
of a Research Program
Sponsored by
THE OFFICE OF NAVAL RESEARCH
DEPARTMENT OF THE NAVY
Contract No. N 000-14-67-A-0305-0010

UNIVERSITY OF ILLINOIS
Urbana, Illinois
June, 1971

QUASI-STATIC LATERAL DESIGN LOADS

FOR EARTHQUAKE RESISTANT STRUCTURES

By

G. Estrada-Uribe

A Technical Report
of a Research Program
Sponsored by
THE OFFICE OF NAVAL RESEARCH
DEPARTMENT OF THE NAVY
Contract No. N 000-14-67-A-0305-0010

UNIVERSITY OF ILLINOIS
Urbana, Illinois
June, 1971

ACKNOWLEDGEMENTS

This report was prepared as a doctoral dissertation by Mr. G. Estrada-Uribe and was submitted to the Graduate College of the University of Illinois in partial fulfillment of the requirements for the degree of Doctor of Philosophy in Civil Engineering. The work was done under the supervision of Dr. John W. Melin and Dr. Steven J. Fenves, Professors of Civil Engineering.

Development of the programs was done on the Burroughs B5500 at the Civil Engineering Systems Laboratory, and on the IBM 360 at the Digital Computing Laboratory, both at the University of Illinois, Urbana, Illinois.

The study was sponsored by the Office of Naval Research under their grant N000-14-67-A-0305-0010.

TABLE OF CONTENTS

LIST OF TABLES

LIST OF FIGURES

Figure Page

CHAPTER I

INTRODUCTION

A simple procedure for computing a set of static design loads for earthquake resistant structures has been developed. The procedure is valid for a large class of multi-story shear and frame type structures.

1.1 Motivation

The process of designing a structure to resist earthquake forces consists of a preliminary design followed by a more rigorous analysis. Then modifications are introduced as necessary, and the process is repeated until satisfactory results are obtained. The selection of a better preliminary set of static loads has two advantages: a) since the final design would be closer to the preliminary design, a reduced number of analyses would be necessary; b) if the preliminary design loads are known to yield responses within a desired bound of the modal analysis for a particular range of structures, expensive modal analysis is unnecessary.

However, there are essentially two methods of analysis available: modal analysis, and numerical integration. Modal analysis is time-consuming and it gives only an approximation to inelastic behavior. Using numerical integration the inelastic behavior can be reasonably evaluated for a particular loading function but its reliability is questionable since the magnitude of the seismic motion is difficult to predict.

1.2 Scope

The primary purpose was to develop a systematic procedure for predicting a quasi-static loading such that the actual dynamic forces resulting from an earthquake would cause equivalent or smaller responses.

This procedure should be valid for a large class of multi-story structures composed of either moment resisting frames or shear wall cores, as well as box type systems. Chimneys, towers, masts, elevated water tanks and other similar structures may also be included. The foregoing also applies to building structures of various rigidities as well as to those having different stiffness and mass distributions throughout their height. The ground motions resulting from several seismic records and different earthquake magnitudes are considered.

Although this investigation was conducted on as general a basis as possible, some particular cases were excluded and certain limitations were imposed on the number and range of the parameters considered in order to keep the resulting design method practical and easy to apply.

Damping is accounted for by reducing the earthquake magnitude. Neglecting damping in the analysis reduces the number of calculations involved, makes the solution of the equations of motion easier and more suitable for computer processing, and results in a conservative design.

It was assumed that structural components are linear in their behavior. In real structures this is not generally the case. Nonlinearities arise from at least two causes: geometric nonlinearities may be induced as the structure displaces; material nonlinearities may occur when the stresses developed in the structure exceed the linear stress-strain range. Those nonlinearities and the associated hysteretic energy absorption, as well

as the ductility and yield level of the elements were not considered. However, if the building is able to stand the lateral forces within the elastic range, its inelastic properties constitute an additional beneficial factor.

The justification for not including damping or inelastic behavior is based on previous studies in which the response of various systems has been investigated over wide ranges of yield levels, damping values and natural frequencies, and for motions ranging from simple, pulse-like inputs to complex records of actual or simulated earthquakes. Such studies [18,19,20]* have shown that the maximum deformation of an inelastic system may be related in a simple manner to that of an elastic system having the same stiffness as the inelastic system. These studies have also concluded that over a wide range of natural frequencies, yield levels and damping factors, the maximum deformations of inelastic systems are generally equal to or smaller than those of the associated elastic systems.

Twisting moments or torques on the horizontal section of a building may arise from local irregularities and differences in stiffness and strength even though the building might be regular and uniform. If the building is eccentric because of non-uniform mass or stiffness distributions, large torques may be developed. Another source of twisting excitation are the irregularities of the ground motion. However, no such twisting action was considered in this study, and the models selected were assumed to be uniform plane frames or walls.

Earthquake motions are transmitted through the ground to the

---

* The numbers in parentheses refer to the References at the end of this study.

foundation of the structure and then to the structure itself. Interaction between the foundation of the structure and the earth beneath it is of particular importance in defining the nature of the forces and the motions transmitted. Equally important is the nature of the foundation upon which the structure rests, as it may behave as an amplifier of the seismic motion. Since the investigation of soil-structure interaction is a vast area that can provide material for several other research projects, no attempt was made to include it here. The building was assumed to be subjected to a single input motion equal to the resulting seismic motion considering the amplification due to soil and foundation characteristics.

Throughout the history of earthquake design of structures it has been proved that interaction between structural and so-called non-structural components is very likely to change the behavior of a structure subjected to a seismic motion. Non-structural fillers such as masonry block or brick located in all or part of the spacing between beams and columns may alter the behavior in such a way that the structure acts in a completely different fashion than intended, with points of high stress concentration away from the joints and with the chance of failure at loads lower than those which the structure alone could sustain. Again, this is matter for a separate investigation and thus was excluded from this study.

Finally, since the nature of an earthquake is such that its magnitude cannot be predicted accurately, even the most refined nonlinear dynamic analysis would be questionable.

1.3 Organization

The discussion of the results obtained, and the presentation of

the recommended method is divided into ten chapters. The mathematical theory that served as the background for this investigation is developed in Chapter 2. The models studied, the parameters considered, and the standard earthquake spectrum used are discussed in Chapter 3. Chapter 4 contains a general description of the computer programs developed and used to obtain the basic data. Chapters 5, 6, and 7 provide a detailed discussion of the effects of parameter variations upon the responses of the structure, and the interpretation of the data. This is the basis for the proposed method of computing lateral loads presented in Chapter 8 and illustrated by means of the examples given in Chapter 9. Finally, general conclusions and recommendations for further study are given in Chapter 10.

1.4 Nomenclature

Chapter 2

F_I, F_D, F_S = inertia force, damping force, and elastic force vectors, respectively.

$P(t)$ = dynamic applied load vector.

K = stiffness matrix.

U = displacement vector.

M = mass matrix.

C = damping matrix.

$Q_i^{(x)}$, $q_i^{(x)}$ = load and displacement vectors in local coordinates at point x of member i.

$k_i^{(x)}$ = stiffness properties at point x of member i.

Φ_i = interpolation function for member i.

SE = strain energy.

$\bar{Q}$, $\bar{q}$ = load and displacement vectors in global coordinates for the entire structure.

$\bar{k}_i$ = stiffness matrix for element i in local coordinates.

$\sigma_i^{(x)}$, $\epsilon_i^{(x)}$ = stress and strain at point x of member i.

B = transformation matrix from local to global coordinates.

Q, q = force and displacement vectors in local coordinates.

$\bar{K}$ = diagonal matrix componsed of member stiffness matrices.

KE = kinetic energy.

μ = mass per unit area.

$\bar{M}_i$ = mass matrix for member i in local coordinates.

α, α' = proportionality constants for damping.

Q_{ext} = externally applied load vector.

W_{ext} = virtual work done by Q_{ext}.

y(t) = displacement input at the base.

$P_{eff}(t)$ = effective load vector.

γ = participation factors.

ψ = eigenvectors.

ω = circular frequency.

η = amplification factors.

τ = period of the forcing function.

X = maximum response.

ABS = sum of the absolute values.

SRSS = square root of the sum of the squares.

BM = base magnitude - total applied lateral force

VD = vertical distribution - the portion of base magnitude concentrated at each story.

Chapter 3

$\bar{k}_{b_i}$, $\bar{k}_{c_i}$ = total beam and column stiffnesses at story i, respectively.

m_i = lumped mass at story i.

ρ = specific weight of the material.

r_t = shear-flexural ratio.

k_b = stiffness of a beam.

k_c = stiffness of a column.

r_k = stiffness distribution ratio.

f_1 = fundamental frequency of the prototype in cps.

T = fundamental period of the system in sec.

N, n = number of stories.

M_R = magnitude of the earthquake in Richter scale.

D = dimension of the building in feet in a direction parallel to the applied forces.

h_i = height of story i above the base of the building.

h_n = total height of the building above its base.

Int = intensity of the earthquake.

A = ground acceleration in in./sec.^{2}.

E = modulus of elasticity of the material.

I = moment of inertia of the cross sectional area of a member.

r_m = mass distribution ratio.

L = length of a particular member.

Chapter 4

P_i = quasi-static load at story i.

w_i = weight of story i.

A_0, A_1, A_2 = equation coefficients for best fitting parabola.

X, Y = dependent and independent variables, respectively, for least square fitting.

$\bar{X}$, $\bar{Y}$ = mean values for the dependent and independent variables X, and Y, respectively.

X_{reg} = dependent variable in regression parabola.

cr = correlation coefficient.

Chapter 5

BM^* = scaled base magnitude.

$\overline{BM}$ = reference base magnitude.

C_B = scaling coefficients for base magnitudes. Subscripts: (R) for earthquake magnitude; (T) for type of building; (N) for number of stories; (K) for stiffness distribution. Superscripts: (D) for displacement; (A) for acceleration; (S) for shear; (M) for moment.

P_B = scaling powers for base magnitudes. (Same subscripts and superscripts as C_B).

P_k = power factor for rigidity of the building.

f_1^* = scaled fundamental frequency for earthquake magnitude (model).

C_{FR} = scaling coefficient for frequency, due to earthquake magnitude.

R = total horizontal reaction at the base of the structure.

W = total weight of the building.

S_c = frequency scaling coefficient.

K' = scaled stiffness matrix.

$\bar{K}_1'$, $\bar{K}_1$ = total column stiffness divided by the column height, for the first story of the prototype, and the model, respectively.

Chapter 6

C_{FD} = frequency scaling coefficient for participation of second mode.

A^*, $\bar{A}$ = parabolic coefficients for the prototype and the model respectively. (Subscripts 0, 1, or 2. Superscripts D, A, S, or M for displacement acceleration, shear, or moment response.)

C_D, Δ_A = Scaling multiplier and increment for vertical distributions respectively. (Subscripts: (T) type of building; (N) number of stories; (K) stiffness distribution. Superscripts: D, S, A, or M for displacement, shear, acceleration, or moment. Δ_A takes also subscripts 0, 1 or 2.)

b_t', d_t', e_t' = equation coefficients for $\Delta_T A$.

a_k', b_k', d_k' = equation coefficients for $\Delta_K A$.

Chapter 7

EL_n, EL_1 = end loads at top and first stories, respectively.

b_e, d_e, b_e', d_e' = equation coefficients for end loads.

F_n, F_1 = concentrated forces at top and first stories, respectively.

CHAPTER 2

THEORETICAL BACKGROUND

A brief summary of the basic theory used throughout this project is given here. The formulation of the equation of motion and the construction of the various matrices involved in it are discussed first. Then, a method of solution for eigenvalues and eigenvectors as well as a matrix compression technique are presented. Finally, the modal analysis method and the calculation of quasi-static loads is explained.

2.1 Equations of Motion

The formulation of equations of motion for a discrete system is based on the equilibrium of the dynamic forces corresponding to the generalized coordinates of the system[1]. If F_I, F_D, and F_S are the inertia force, damping force, and elastic force vectors respectively, the dynamic equilibrium equation may be written as

$$F_I + F_D = F_S = P(t) \qquad (1)$$

in which $P(t)$ is the dynamic applied load vector.

The relationship between the elastic force vector, F_S, and the displacement vector, U, is given by

$$F_S = K\,U \qquad (2)$$

where K is the structural stiffness matrix composed of individual coefficients K_{ij} defined as the elastic force corresponding to coordinate "i" due to a unit displacement of coordinate "j." Similarly, the inertia force vector is related to the nodal accelerations, $\ddot{U}$, by means of the mass matrix, M:

$$F_I = M \ddot{U} \tag{3}$$

in which M is composed of coefficients M_{ij} representing the inertia force at coordinate "i" resulting from a unit acceleration of coordinate "j." Assuming a viscous damping mechanism, the damping forces may be expressed in terms of the nodal velocities, $\dot{U}$, by

$$F_D = C \dot{U} \tag{4}$$

where the coefficients C_{ij} of the damping matrix C, represent the damping force at coordinate "i" due to a unit velocity of coordinate "j."

Substituting Eqs. (2), (3), and (4) into Eq. (1), the equation of motion of the system becomes

$$M \ddot{U} + C \dot{U} + K U = P(t) \tag{5}$$

where P(t) is equal to zero for the case of free vibration.

2.2 Structural Properties

The first step towards the solution of a dynamic problem as indicated by Eq. (5) is to express the physical properties of the system in terms of its mass, stiffness and damping matrices.

1. Stiffness Matrix[2]. The two main phases in obtaining the stiffness matrix for a given discrete system are:

   (a) to evaluate the stiffness matrices for the individual elements, and

   (b) to assemble them into the global matrix for the system.

The member stiffness properties in local coordinates may be readily obtained from the expression for strain energy. By definition, the relation between load and displacement for an elastic medium is

$$Q_i^{(x)} = k_i^{(x)} q_i^{(x)} \tag{6}$$

where $Q_i^{(x)}$ and $q_i^{(x)}$ are the load and displacement vectors in local coordinates at point x along member i, and $k_i^{(x)}$ represents the stiffness properties at that point.

Since the stiffness properties of a structural member are generally considered distributed throughout its length, the displacement vector at any location along the member may be obtained by interpolation between the nodal displacement vectors at the ends of the member. In other words, if Φ_i is the interpolation function for member i, the displacement vector $q_i^{(x)}$ at any position x along the member is given by

$$q_i^{(x)} = \Phi_i \, q_i \tag{7}$$

The strain energy, SE, stored in the element may be expressed as

$$SE = \frac{1}{2} \int_A (\text{Force} \times \text{Displacement}) \, dA$$

or,

$$SE_i = \frac{1}{2} \int_A Q_i^{(x)^T} \, q_i^{(x)} dA \tag{8}$$

Substituting Eqs. (6) and (7) into Eq. (8)

$$SE_i = \frac{1}{2} \int_A q_i^T \, \Phi_i^T \, k_i^{(x)} \, \Phi_i \, q_i \, dA \tag{9}$$

Eq. (9) is a quadratic equation whose first derivative with respect to q_i gives the values of the elements of the member stiffness matrices in local coordinate system, $\bar{k}_i$ [4]:

$$\bar{k}_i = \int_A \Phi_i^T \, k_i^{(x)} \, \Phi_i \, dA \tag{10}$$

The stiffness properties at location x of member i may be obtained from the fundamental stress-strain relation

$$\sigma_i^{(x)} = k_i^{(x)} \, \epsilon_i^{(x)}$$

where $\sigma_i^{(x)}$ and $\epsilon_i^{(x)}$ are the stresses and strains, respectively.

Finally, the stiffness matrix for the entire structure may be

assembled by means of the so-called triple product transformation. This method requires that a transformation matrix B be defined by statics using either free body diagrams or the deformed shapes of the structure, such that the following relationship between displacements in local coordinates, q, and those in global coordinates, $\bar{q}$, is met.

$$q = B\bar{q}$$

All member stiffness matrices, whose elements are given by Eq. (10) are assembled into a diagonal matrix $\bar{K}$ to which a triple product transformation is applied in order to obtain the total stiffness matrix for the entire structure K. That is,

$$K = B^T \bar{K} B$$

2. Mass matrix[1]. The kinetic energy of the system is related to the nodal velocities by the mass matrix in the same way that the strain energy is related to the nodal displacements by the stiffness matrix. Thus, the kinetic energy may be written as

$$KE_i = \frac{1}{2} \int_A \mu_i \dot{q}_i^{(x)^2} dA \qquad (11)$$

where μ_i is the mass per unit area of the element, and $\dot{q}_i^{(x)}$ is the local velocity vector at point x of member i.

The velocity distribution along the member may be related to its nodal velocities through an interpolation function:

$$\dot{q}_i^{(x)} = \Phi_i \dot{q}_i \qquad (12)$$

Substituting Eq. (12) into Eq. (11)

$$KE_i = \frac{1}{2} \int_A \dot{q}_i^T \Phi_i^T \mu_i \Phi_i \dot{q}_i \, dA \qquad (13)$$

Eq. (13) is a quadratic equation whose first derivative with respect to $\dot{q}_i$ gives the values of the member mass matrices in local coordinates, $\bar{M}_i$:

$$\bar{M}_i = \int_A \Phi_i^T \mu_i \Phi_i \, dA \qquad (14)$$

The total mass matrix is assembled in a similar way as the stiffness matrix.

The interpolation functions Φ_i to be used in Eq. (14) may be chosen arbitrarily. However, in the case of distributed mass systems it is generally assumed that the interpolation functions for the mass matrix are the same as those used in evaluating the stiffness matrix, so that the kinetic energy of the elements will be consistent with the strain energy. If the displacement functions are compatible, the consistent mass matrix will lead to an upper bound on the natural frequency[3].

To obtain a lumped mass matrix the interpolation function Φ_i is set equal to unity over a specified portion of the element, and zero elsewhere. In general, it is desirable to use the lumped mass matrix rather than the consistent mass matrix because the first is diagonal and thus simplifies greatly the subsequent dynamic analysis, whereas the latter requires substantial additional computational effort. A careful selection of coordinates is necessary since the mass matrix may turn out to be singular if the coordinates are defined in such a way that some of them do not contribute to the kinetic energy.

3. Damping Matrix[1,6]. The same procedure used before to obtain stiffness and mass matrices may be used for damping matrices in the following two cases.

(a) When the damping forces are proportional to the velocity of the masses, the damping matrix may be evaluated as the mass matrix. Thus, if the element inertia forces are:

$$F_i^I = \mu \ddot{q}_i$$

then the damping forces may be given by

$$F_i^D = \alpha \mu \ddot{q}_i$$

where α is a proportionality constant. After making an analysis similar to that used for the mass matrix, the following expression for the elements of the damping matrix results

$$C_i = \int_A \Phi_i^T \alpha \mu_i \Phi_i \, dA = \alpha M_i \qquad (15)$$

(b) If the damping stresses are assumed to be proportional to the elastic stresses, a procedure similar to that of the stiffness matrix may be used. Therefore, if the elastic stresses are given by

$$\sigma_i^E = k_i^{(x)} \epsilon_i$$

then the damping stresses may be expressed as

$$\sigma_i^D = \alpha' \, k_i^{(x)} \epsilon_i$$

where α' is a proportionality constant. A procedure similar to that used for the stiffness matrix gives

$$C_i = \int_A \Phi_i^T \alpha' \, k_i^{(x)} \Phi_i \, dA = \alpha' \bar{k}_i \qquad (16)$$

The total damping matrix is assembled in the same way as the stiffness matrix.

The damping matrix is necessary only when a direct inegration of the equation of motion is performed. For all other methods modal damping ratios obtained experimentally are a satisfactory approximation[13].

4. Load Vector[1]. The virtual work done by the applied loads through a virtual displacement may be used to obtain the load vector. Using Eq. (7), the virtual displacements of the element may be expressed in terms of the nodal values, q_i, by means of an interpolation function Φ_i:

$$\delta q_i^{(x)} = \Phi_i \, \delta q_i \qquad (17)$$

The virtual work done by the applied force vector Q_{ext_i} is

$$\delta W_{ext_i} = \int_A (\delta q_i^{(x)})^T Q_{ext_i} \, dA \tag{18}$$

Substituting Eq. (17) into Eq. (18)

$$\delta W_{ext} = \int_A \Phi_i^T \delta q_i^T Q_{ext_i} \, dA \tag{19}$$

Differentiating Eq. (19) with respect to δq_i^T the following expression for the element load vector is obtained

$$P_i(t) = \int_A \Phi_i^T Q_{ext_i} \, dA \tag{20}$$

The total load vector may be assembled from the element load vectors in the same way as the stiffness matrix.

In the case of earthquakes the vibration is induced by a motion of the base of the structure. This problem may be handled by using relative, rather than absolute coordinates. Calling the input motion y(t), and the relative displacement vector U, it follows that the relative velocity and absolute acceleration of the masses are $\dot{U}$ and $(\ddot{U} + \ddot{y})$ respectively. Therefore, the damping and inertia forces may be expressed as

$$F_D = C \dot{U} \tag{21}$$

and

$$F_I = M(\ddot{U} + \ddot{y}) \tag{22}$$

The elastic forces are still given by

$$F_S = K U \tag{23}$$

since any displacement at the base constitutes a rigid body motion and therefore has no influence in the state of stresses of the structure.

Substituting Eqs. (21), (22), and (23) into Eq. (1) and making P(t) equal to zero for no external load applied on the structure,

$$M(\ddot{U} + \ddot{y}) + C \dot{U} + K U = 0$$

Therefore,

$$M \ddot{U} + C \dot{U} + K U = -M \ddot{y} = P_{eff}(t) \tag{24}$$

The right-hand side of Eq. (24) is generally called the effective load vector, $P_{eff}(t)$.

2.3 Eigenvalues and Eigenvectors

Once the equation of motion has been formulated and the structural properties of the system determined, the next step in solving a dynamic problem is to find the frequencies and mode shapes for the undampened free-vibration case[1].

In this instance, the equation of motion may be stated as

$$M \ddot{U} + K U = 0 \tag{25}$$

which is a homogeneous second order differential equation whose solution is a harmonic function of the form:

$$U = x \sin \omega t \tag{26}$$

Substituting Eq. (26) into Eq. (25), the general form of the eigenvalue equation becomes

$$K x = \omega^2 M x \tag{27}$$

For the solution of Eq. (27) to be feasible, it is required that the mass and stiffness matrices meet certain conditions[5].

The first condition imposed on both mass and stiffness matrices is that they be non-singular. The stiffness matrix becomes singular when rigid body motions are included in its derivation. If the coordinates are defined in a way that some of them do not contribute to the kinetic energy, then the mass matrix becomes singular.

An additional requirement for the stiffness matrix is that it should be positive definite. Such condition will follow from the fact that the quadratic equation (Eq. (9)) that originated the stiffness matrix

be positive definite. A quadratic form

$$Q(x,x) = \sum_{i=1}^{n} \sum_{j=1}^{n} k_{ij} x_i x_j = X^T K X$$

is positive definite if all choices of x_i except $x = 0$, make $Q(x,x)$ greater than zero, and $Q(x,x)$ equal to zero when $x = 0$. If $Q(x,x)$ is positive definite, then K is also positive definite. Since the strain energy is always positive, the stiffness matrix in generalized coordinates will be positive definite if:

a) no proportional rows and columns exist, or

b) in case there are proportional rows or columns, the determinant of the matrix without the rows and columns that are proportional, is zero.

Many methods of solving the eigenvalue problem (Eq. (27)) have been formulated. The only one that will be discussed here is Jacobi's method since it was the one used to obtain most of the data for this investigation. It was chosen because of its capability of handling systems up to 200 degrees of freedom with reasonable execution time on current computers, and for its ability of working with both lumped and consistent mass matrices.

The basis for Jacobi's method is a process of diagonalization of the matrices by successive rotations. First, a matrix, m, is defined such that (since M is positive definite)

$$M = m\, m^T \tag{28}$$

in which the mass matrix M can be either lumped or consistent. Next, a change of variable is performed as indicated by

$$\psi_r = m^T X_r \tag{29}$$

Substituting Eq. (29) into Eq. (27)

$$H_s \psi_r = \omega_r^2 \psi_r \tag{30}$$

where,

$$H_s = m^{-1} K (m^{-1})^T = H_s^T \tag{31}$$

Eq. (30) may be written as

$$H_s \psi_r = \psi_r \lambda \tag{32}$$

where the spectral matrix of H_s, λ, is a diagonal matrix whose elements are the eigenvalues of H_s (i.e., ω^2). Because of orthogonality of the modal matrix of H_s, ψ_r,

$$\psi_r^{-1} = \psi_r^T$$

therefore,

$$\psi_r^T H_s \psi_r = \lambda \tag{33}$$

Thus, starting with matrix H_o and multiplying it by a sequence of rotation matrices R_i for $i = 1, 2, 3, \ldots, n$ as follows

$$H_1 = R_1^T H R_1$$

$$H_2 = R_2^T H_1 R_1 = R_2^T R_1^T H R_1 R_2$$

etc., and for proper choices of R, H_n becomes essentially a diagonal matrix for numerical purposes. When this diagonal form for H_n is reached, then the diagonal elements in λ are identified as the eigenvalues of H, and

$$\psi_r = R_1 R_2 \cdots R_n = \prod_{i=1}^{n} R_i$$

Each column of ψ_r is a mode shape whose correspondent one in X coordinates is

$$X_r = (m^{-1})^T \psi_r \tag{34}$$

2.4 Matrix Compression

When the number of degrees of freedom becomes too large, a complete solution is impractical even by very efficient computers. In these instances it is necessary to reduce the number of degrees of freedom considered before the dynamic part of the analysis may be performed[7]. There is a number of so-called matrix compression techniques for this purpose. The one used in this study is discussed below.

The relationship between forces and displacements of an elastic medium may be stated as

$$\left\{\begin{array}{c} P_1 \\ \hline P_2 \end{array}\right\} = \left[\begin{array}{c|c} K_{11} & K_{12} \\ \hline K_{21} & K_{22} \end{array}\right] \left\{\begin{array}{c} X_1 \\ \hline X_2 \end{array}\right\} \tag{35}$$

where the stiffness matrix K has been partitioned in such a way that the load and displacement vectors P_2 and X_2 correspond to the degrees of freedom that are to be eliminated. Then, P_2 may be set equal to zero. Therefore,

$$K_{21}\ X_1 + K_{22}\ X_2 = 0$$

from which

$$X_2 = -K_{22}^{-1}\ K_{21}\ X_1 \tag{36}$$

On the other hand

$$P_1 = K_{11}\ X_1 - K_{12}\ X_2 \tag{37}$$

Substituting Eq. (36) into Eq. (37)

$$P_1 = K_{11}\ X_1 - K_{12}K_{22}^{-1}K_{21}X_1 = (K_{11} - K_{12}K_{22}^{-1}K_{21})\ X_{11}$$

Therefore, the reduced stiffness matrix K^* is

$$K^* = K_{11} - K_{12}\ K_{22}^{-1}\ K_{21} \tag{38}$$

The mass matrix has to be compressed consistently with the stiffness matrix. Partitioning the mass matrix in the same way as the stiffness matrix, the virtual work of inertial forces may be stated as

$$\delta X_1^T \left(-M_1^* \ddot{X}_1\right) = \delta X^T \left(-M \ddot{X}\right) \tag{39}$$

which means that the virtual work of inertial forces corresponding to the reduced mass matrix M_1^* should be equal to that of the original mass matrix M. If the total virtual displacement vector is particioned as

$$\delta X = \begin{Bmatrix} \delta X_1 \\ \hline \delta X_2 \end{Bmatrix}$$

then, from Eq. (36)

$$\delta X_2 = -K_{22}^{-1} K_{21} \delta X_1$$

therefore,

$$\delta X = \begin{Bmatrix} I \\ \hline -K_{22}^{-1} K_{21} \end{Bmatrix} \delta X_1 \tag{40}$$

where I is the identity matrix. From Eq. (36),

$$\ddot{X}_2 = -K_{22}^{-1} K_{21} \ddot{X}_1 \tag{41}$$

Substituting Eqs. (40) and (41) into Eq. (39)

$$-\delta X_1^T M_1^* \ddot{X} = -\delta X_1^T \left[I \,\vdots\, -(K_{22}^{-1} K_{21})^T\right] \left[\begin{array}{c|c} M_{11} & M_{12} \\ \hline M_{21} & M_{22} \end{array}\right] \left[\begin{array}{c} I \\ \hline -K_{22}^{-1} K_{21} \end{array}\right] \ddot{X}_1$$

Therefore, the reduced mass matrix M^* is

$$M^* = \left[I \,\vdots\, -(K_{22}^{-1} K_{21})^T\right] \left[\begin{array}{c|c} M_{11} & M_{12} \\ \hline M_{21} & M_{22} \end{array}\right] \left[\begin{array}{c} I \\ \hline -K_{22}^{-1} K_{21} \end{array}\right] \tag{42}$$

2.5 Modal Analysis

In the case of forced vibration there are two techniques to solve the equation of motion (Eq. (5)), namely direct integration, and modal analysis. The first one is used when the load input is very complicated and for non-linear systems; there are a number of direct integration schemes available[12] such as the well known Newmark's β method[11]. Since modal analysis was used in this study, it is discussed in some detail[1].

The modal analysis method is based upon the principle of super-

position, that is, the total deflection caused by a set of forces is found by adding deflections produced by the individual forces of the set acting separately. However, the principle of superposition is valid for linear systems in which the displacement coordinates and their derivatives appear in the equations of motion only to the first power with constant coefficients.

There exists a set of coordinates that are related to the geometric displacement coordinates by a linear transformation. When the differential equations are expressed in terms of normal coordinates they are found to be completely uncoupled so that they can be solved independently, thereby simplifying the solution process. This is called the principle of linear independence of vectors, and is based on the fact that coupling is not an inherent property of the system but depends on the coordinates chosen. Making use of Rayleigh's quotient, the following expression for the modal response in normal coordinates may be written

$$Y_i = \gamma_i \psi_i \tag{43}$$

where ψ_i is the eigenvector for mode i, and the participation factors γ_i are given by

$$\gamma_i = \frac{\psi_i^T \bar{P}}{\psi_i^T M \psi_i} \tag{44}$$

$\bar{P}$ is obtained from the forcing function

$$P(t) = \bar{P} f(t) \tag{45}$$

A convenient way of handling a time dependent forcing function is to establish a pattern of similarity between the multi-degree-of-freedom system and a single-degree-of-freedom system. This is done by means of amplification factors η, obtained on the basis of a single-degree-of-freedom system; the solution for the multi-degree-of-freedom system is obtained by multiplying the uncoupled eigenvectors Y_i, by η. That is

$$X_i = \eta_i Y_i \tag{46}$$

If the forcing function P(t) is a well defined mathematical expression, the amplification factors η may be obtained from Duhamel's integral

$$\eta_i = \frac{1}{\omega_i} \int_o^t f(\tau) \sin \omega_i (t - \tau) \, d\tau \qquad (47)$$

where ω_i is the circular frequency for mode i and τ is the period of the forcing function.

When the force input is a random excitation such as an earthquake, the amplification factors may be obtained from a response spectrum of the seismic motion.

Combining Eq. (43) and (46) and the principle of superposition, the maximum spectral response of the system is obtained as

$$X = \sum_{i=1}^{n} \gamma_i \psi_i \eta_i \qquad (48)$$

Eq. (48) defines only the maximum response of each mode but not the time at which it occurs. Each mode of vibration has a frequency different from that of the other modes and therefore, its maximum response generally occurs at a time different from the times of the maximum response of the other modes. To get closer to the maximum response a statistical approach is used. The summation of the absolute values of the maximum responses for the individual modes is an extreme upper bound to the response of the total system. That is,

$$X_{ABS} = \sum_{i=1}^{n} \left| \gamma_i \psi_i \eta_i \right| \qquad (49)$$

This sum of the absolute values (ABS) is also known as the possible maximum[14].

A more reasonable estimate of the maximum response is given by

the square root of the sum of the squares (SRSS) of the individual modal maxima

$$X_{SRSS} = \sqrt{\sum_{i=1}^{n} (\gamma_i \psi_i \eta_i)^2} \qquad (50)$$

The SRSS response is also called the probable maximum[14].

Eqs. (49) and (50) may be used to obtain spectral responses other than displacements, namely accelerations, shears, and moments, by using the corresponding modal vector in place of ψ_i.

2.6 Quasi-Static Loads

Although accurate analytical methods may lead directly to stresses and deformations at critical points in the structure, only an estimate of forces is needed for the purpose of preliminary design[8]. It has been traditional to use quick (but hopefully reliable) methods that give static loads which are greater than the dynamic loads, thus resulting in a conservative design. Given the unpredictable nature of the earthquake input a sophisticated analysis is out of the question for economic and practical reasons. Approximate forces may be obtained from the dynamic analysis and used as static lateral loads in order to select the proportions of the members. Quasi-static loads for the responses of interest, namely displacements, accelerations, shears, and moments may be obtained as indicated below.

In the case of displacements, a set of quasi-static forces P_i^D, may be computed by multiplying the spectral displacement vector by the stiffness matrix. Quasi-static forces for acceleration P_i^A, are calculated by multiplying the spectral acceleration vector by the mass matrix. For shears, a single differentiation step applied on the spectral shear vector gives the

quasi-static loads P_i^S. A double differentiation process has to be applied on the spectral moment vector in order to obtain the quasi-static loads for moment P_i^M. These differentiations may be carried out by any numerical scheme such as Newmark's method[9,10].

It is important to note that quasi-static forces for the various responses considered have to be obtained independently since the maximum transient values at any elevation do not necessarily appear simultaneously, and hence, arise from different loading distributions. To meet this condition the quasi-static loads should be obtained directly from the corresponding spectral responses and not exclusively from spectral displacements.

A convenient way of expressing a set of quasi-static loads is by giving the total reaction induced at the base of the structure or base magnitude (BM), and a vertical distribution vector (VD) containing the percentages of the base magnitude that ought to be applied at each floor.

CHAPTER 3

MODELS AND PARAMETERS

This chapter deals with the various types of building structures and the way they have been modeled. The parameters influencing the dynamic behavior of such structures are outlined. Finally, some generalities on the nature of earthquake motions are given and the selected standard earthquake spectrum is presented.

3.1 Types of Structures

Structures and their corresponding models generally resist lateral forces induced by ground motions through shear or flexural actions. Therefore, building structures may be subdivided into shear and flexural according to the way they behave under lateral loads. Fig. 1 illustrates these two types of structures as are usually encountered in actual practice. The frame and shear-wall elements composing the combined building shown in Fig. 1(a) have been separated and their independent behavior is presented in Figs. 1(b) and (c).

When the rotations at the joints (beam-column connections) are highly restricted as in the case of a frame with very stiff girders, and the axial deformations of the columns are small, the lateral deflections of a story relative to the next one below it decrease with increasing height above the base, as indicated by Fig. 1(b). Such effect is called shear behavior. If the axial deformation of the columns is large and the rotational restraint in the joints is small, the building behaves essentially as

a cantilever beam as shown in Fig. 1(c). Shear and flexural structures differ also in the definition of their stiffness matrix as will be discussed later.

Pure-shear and pure-flexural buildings are sometimes encountered in practice. However, the most common case is a combination of both kinds. Buildings having a complete moment resisting frame combined with shear wall elements, usually alongside elevators or stairwells as illustrated in Fig. 1(a), are frequently found.

As far as the type of members composing a structure and their disposition are concerned, building structures may be classified as frames, box systems, or shear-wall systems. A frame may be defined as a "structural system composed of interconnected members, other than bearing walls, laterally supported so as to function as a complete self-contained unit with or without the aid of horizontal diaphragms or floor bracing systems."[15] Depending on the stiffness of the girders relative to that of the columns, a frame may fall into the categories of pure-shear or pure-flexural buildings, or be somewhere in between.

A box system is a "structural system without a complete vertical load carrying space frame, in which the required lateral loads are resisted by shear walls."[15] A shear wall is a "wall designed to resist lateral forces parallel to the wall."[15] Cross-braced frames may be considered as shear walls. Box systems, shear walls and braced frames, as well as chimneys, towers, and masts, not braced laterally by cable guys, behave essentially as flexural structures.

3.2 Mathematical Model

The first step towards the investigation of the behavior of a structure subjected to earthquake motions is the establishing of an appropriate model. A mathematical model provides a general means of representing the structural systems discussed in the preceding section.

From the many possible mathematical models, the discrete one was considered the most suitable for this investigation. The discrete model is based on the concept that the structure consists of an assemblage of individual components, the properties of which are defined directly as indicated in Chapter 2, and may be synthesized into a single system.

The model is illustrated in Fig. 2. A large variety of buildings from the pure-shear to the pure-flexural, can be represented by changing the shear-flexural ratio r_t, i.e., the ratio of the total stiffness of the beams $\bar{k}_{b_i}$, to the total stiffness of the columns $\bar{k}_{c_i}$ and $\bar{k}_{c_{i+1}}$, connected to beams of a particular story i

$$r_t = \frac{\bar{k}_{b_i}}{\bar{k}_{c_i} + \bar{k}_{c_{i+1}}} \tag{51}$$

Thus, if r_t is zero the model shown in Fig. 2 represents a pure-flexural building, whereas if r_t is equal to infinity it becomes a pure-shear model.

For the intermediate cases the stiffness of the beams introduce an additional restraint on the rotation of the joints as compared to the pure-flexural case in which free rotation of the joints is attained. Thus, the rotational stiffness of the model is a function of the beam stiffness.

In general, a building has six degrees of freedom per joint. Rubenstein and Hurty[1] have shown that for buildings with a height to

width ratio (aspect ratio) of five or less, the axial deformation in all frame members can be disregarded with a small sacrifice in accuracy of the computed natural modes and frequencies of the building. In most cases, it is also permissible to simplify the response behavior by assuming that the floor slabs act as ideal diaphragms, that is, rigid in the horizontal plane, but flexible vertically.

The model may be simplified further by assuming equal rotations of the frame joints. The accuracy of the computed results when such assumptions are made was studied by Rubenstein and Hurty[16]. After investigating several cases they concluded that this assumption is satisfactory and computer time was greatly reduced (maybe up to 900%).

Thus, the model proposed in Fig. 2 may be considered in general to have two degrees of freedom per joint: a horizontal translation, and a rotation. Following the procedure outlined in Chapter 2, a general stiffness matrix for the model may be written as follows:

$$
K = \begin{bmatrix}
2(k_1+k_2) & 0 & -2k_2 & Lk_2 & & & & \\
0 & \frac{L^2}{1.5}(r_t+1)(k_1+k_2) & -Lk_2 & \frac{L^2}{3}k_2 & & & & \\
-2k_2 & -Lk_2 & 2(k_2+k_3) & 0 & & & & \\
Lk_2 & \frac{L^2}{3}k_2 & 0 & \frac{L^2}{1.5}(r_t+1)(k_2+k_3) & & & & \\
0 & 0 & -2k_3 & -Lk_3 & & & & \\
0 & 0 & Lk_3 & \frac{L^2}{3}k_3 & & & & \\
 & & & & \ddots & & & \\
 & & & & -2k_{n-1} & Lk_{n-1} & 0 & 0 \\
 & & & & -Lk_{n-1} & \frac{L^2}{3}k_{n-1} & 0 & 0 \\
 & & & & 2(k_{n-1}+k_n) & 0 & -2k_n & Lk_n \\
 & & & & 0 & \frac{L^2}{1.5}(r_t+1)(k_{n-1}+k_n) & -Lk_n & \frac{L^2}{3}k_n \\
 & & & & -2k_n & -Lk_n & 2k_n & -Lk_n \\
 & & & & Lk_n & \frac{L^2}{3}k_n & -Lk_n & \frac{L^2}{1.5}(r_t+1)k_n
\end{bmatrix} \qquad (52)
$$

In the above matrix, k_i is given by

$$k_i = \frac{6 E_i I_i}{L_i^3} \qquad (53)$$

where E_i is the modulus of elasticity of the material, I_i is the moment of inertia of the cross sectional area, and L_i is the length of member i in the model.

The preceding stiffness matrix, developed for a discrete model, may be used for the pure-shear and pure-flexural buildings as well as the intermediate cases. By making r_t equal to zero, the stiffness matrix becomes that corresponding to a flexural building. In the case of a shear building, the rows and columns corresponding to those diagonal terms containing the shear-flexural ratio r_t ought to be eliminated.

The mass is assumed to be lumped at the joints; thus the mass matrix for both discrete and analytical models is:

$$M = \begin{bmatrix} m_1 & & & & & \\ & m_2 & & & & \\ & & m_3 & & & \\ & & & \ddots & & \\ & & & & m_i & \\ & & & & & \ddots \\ & & & & & & m_n \end{bmatrix} \qquad (54)$$

By varying the parameters of the model illustrated in Fig. 2, and the corresponding stiffness and mass properties given by Eqs. (52) and (54), a total of eighteen different cases were investigated as indicated in Table 1. The various models are classified by number of stories, mass distribution,

stiffness distribution, and type of building. The properties of the models are given in terms of the stiffness distribution ratio r_k, the mass distribution ratio r_m, and the shear-flexural ratio r_t. The stiffness distribution ratio is given by

$$r_k = \frac{\bar{k}_{c_n}}{\bar{k}_{c_1}} \tag{55}$$

where $\bar{k}_{c_n}$ and $\bar{k}_{c_1}$ are the total column stiffnesses for the top and first stories respectively; and the mass distribution ratio is

$$r_m = \frac{m_n}{m_1} \tag{56}$$

where m_n and m_1 are the lumped masses at the top and first stories respectively. The shear-flexural ratio is defined by Eq. (51).

Four cases of mass and stiffness distribution were studied as shown in Fig. 3. They are:

Case A: constant mass and stiffness

Case B: constant mass and linearly varying stiffness

Case C: constant stiffness and linearly varying mass

Case D: linearly varying mass and stiffness.

Most structures fall somewhere between Case A and Case B for vertical stiffness distribution, and between pure-shear and pure-flexural buildings.

3.3 Parameters Considered

A deterministic parameter variation study was conducted. The basic parameters considered were the following:

1. Stiffness distribution ratio, r_k.

2. Mass distribution ratio, r_m.
3. Type of building (shear-flexural ratio, r_t).
4. Fundamental frequency, f_1.
5. Rigidity of the building (power factor, P_k).
6. Number of stories, N.
7. Magnitude of the earthquake motion, M_R.

The first three parameters, i.e., r_k, r_m, and r_t, are defined by Eqs. (55), (56), and (51), respectively. The fundamental frequency of the building may be obtained by means of a standard eigenvalue routine (for small structures) or by using any of the several approximate formulas encountered in the literature on this subject, an example of which is the one given below[17].

$$f_1 = \frac{1}{T} = \frac{\sqrt{D}}{0.05\ h_n} \qquad (57)$$

where T is the fundamental period of the building, D is the dimension of the building in feet in a direction parallel to the applied forces, h_n is the total height of the building above its base, and f_1 is the fundamental frequency in cycles per second (cps.). Finally, the rigidity power factor P_k, and the earthquake magnitude M_R, are defined in Chapter 5.

The effect of these parameters was measured by base magnitudes and vertical distributions of concentrated lateral static loads corresponding to dynamic displacements, accelerations, shears, and overturning moments.

3.4 Standard Earthquake Spectrum

Given the number of seismic records available, their random nature and the many factors influencing the motion of the ground, it is necessary to define a standard earthquake spectrum which serves as the forcing function in the analysis of the various models. In order to define

such a standard tremor it is convenient to consider first certain characteristics of earthquake motions.

During an earthquake the ground oscillates in an irregular pattern both horizontally and vertically for a certain period of time. Such a motion of the surface may be recorded by a seismograph in the form of an acceleration trace or acceleragram. As an example, Fig. 4 shows the recorded ground acceleration for the North-South component of El Centro earthquake of May 18, 1940. The velocity and displacement traces shown in Fig. 4 were computed by integration of the acceleration records.

The displacement record shown in Fig. 4 may be input at the base of an elastic single-degree-of-freedom system having various damping factors and natural frequencies. If the responses of the system are plotted in a four-way logarithmic chart, the so-called pseudo-velocity response spectrum is obtained as illustrated by Fig. 5. Finally, the pseudo-velocity spectrum may be transformed into a tripartite response spectrum by drawing constant displacement, constant velocity, and constant acceleration lines through its maximum peaks.

For the purpose of this study, a tripartite spectrum was considered to be an acceptable approximation of the ground motion as well as an easy method of handling the earthquake input. A standard earthquake spectrum was defined from the ground motion pseudo-velocity spectrum for El Centro earthquake shown in Fig. 5 by means of the amplification factors given in Ref. 21. The resulting spectrum as shown in Fig. 6 is the standard earthquake spectrum used throughout this investigation. The reasons for having selected the North-South component of El Centro earthquake of May, 1940 as the basis for the standard earthquake spectrum are discussed below.

Earthquakes may be of tectonic or volcanic nature depending on the kind of energy released. Volcanic earthquakes are of meager importance; thus, when talking about earthquakes one usually refers to tectonic earthquakes. These seismic motions are produced by the sudden release of strain energy accumulated on the adjacent surfaces of a geological fault. The amount of energy released, or, in other words, the importance of an earthquake, may be measured by either its intensity or its magnitude. Intensity is a relative measuring quantity that indicates the extent to which the effect of a seismic motion appears at a given site; intensity decreases as the distance from the point considered to the epicenter of the earthquake increases. The following experimental formulas to calculate the intensity of an earthquake at a given site knowing the ground acceleration at that point were presented by Richter[22]:

$$Int_1 = 1.5 + 3.0 \log A \tag{58}$$

$$Int_2 = 2.1 + 2.3 \log A \tag{59}$$

where Int_1 and Int_2 are two different measures for the intensity of the earthquake and A is the ground acceleration at that point in $in./sec^2$. If the ground acceleration at the epicenter is used, these equations give the maximum intensity of the earthquake. Magnitude, on the other hand, is an absolute measurement that indicates the amount of energy released by the source, thus defining a given earthquake motion independently of the location of the site. Two well known magnitude scales have been formulated: Richter's magnitude scale (1942)[22], and Mercalli's modified intensity scale (1931)[23]. The first one grades earthquakes from 1 to 8 according to the amount of energy released by the source as discussed above, and is the one used here since a direct relationship may be established between

the magnitude of the motion and the acceleration of the ground by the following experimental formula[22]:

$$M_R = 2.2 + 1.8 \log A \tag{60}$$

where M_R is the magnitude of the earthquake in Richter scale, and A is the acceleration of the ground at the epicenter, in in./sec.^{2}.

The modified Mercalli scale is a subjective estimate of the intensity of the seismic motion that classifies them in categories ranging from 1 to 12 according to the damaging effect of the earthquake.

Intensities and magnitudes of the most important earthquakes that have occurred in the past 50 years and whose records are available, were computed by means of Eqs. (58), (59), and (60), and are tabulated in Table 2. It can be readily seen that the maximum quantities for intensity and magnitude correspond to the North-South component of El Centro earthquake of May, 1940. This was the main reason for selecting such a tremor as the basis for constructing the tripartite standard earthquake spectrum to be used in this study and shown in Fig. 6.

The selected standard earthquake spectrum illustrated in Fig. 6 has a constant displacement branch of 20.7 in., a constant velocity branch of 54.72 in./sec., and a constant acceleration branch of 2.05 g. Its Richter magnitude may be calculated by means of Eq. (60) as follows:

$$M_R = 2.2 + 1.8 \log (2.05 \times 386) = 7.4 \tag{61}$$

which is very close to the maximum value of 8 in the scale, and far more severe than that of the North-South component of El Centro, 1940 earthquake.

For structures that require a high security standard such as nuclear reactors, design spectrum curves resulting from a combination of several different earthquakes are being used[24,25]. Newmark has shown[21]

that such spectra are bound by a tripartite spectrum similar to the one selected here and shown in Fig. 6.

When studying the effect of earthquake magnitude upon the response of the various models, other spectra of smaller magnitudes were used as will be discussed in Chapter 5.

CHAPTER 4

RESPONSE DATA

In this chapter, a general description of the computer programs used in obtaining the data for the subsequent analysis, is given. The format in which the data obtained is presented is also discussed.

4.1 General Description of Computer Programs

Two major programs were developed. The first one was used to generate the equivalent stiffness matrix for the model shown in Fig. 2 corresponding to multi-story multi-bay frames. The second one computed the dynamic response of the structure. These two programs are discussed below in more detail.

1. Matrix Generator. This program, called GEUGEN, is a stiffness and mass matrix generator. It was written in POST (Problem Oriented Subroutine Translator)[26], so that it would be able to handle large matrices by using the secondary memory (disks) dynamic allocation characteristics of the POST compiler. The structure is treated as a finite element grid and its mass and stiffness matrices are generated as discussed in Chapter 2. The generated mass matrix may be either lumped or consistent, or a combination of both in the case, for instance, of a heavy piece of machinery installed in a floor of a structure that has distributed mass.

Once the mass and stiffness matrices for the entire system are generated, they might undergo a reduction process if desired. Two types of matrix reduction are built into the program: reduction by compression, and

reduction by summation. The first one was discussed in detail in Chapter 2. The second one consists in adding up certain rows and columns of the matrix so as to account for such reductions in the number of degrees of freedom resulting from neglecting the axial deformation of the beams and/or columns. Either of these reduction processes or both simultaneously can be applied to the generated matrices.

Finally, the matrices are printed out or stored in a data file to be used as input stream for the dynamic analyzer. A block diagram of the program is shown in Fig. 7.

In summary, GEUGEN has the following present capabilities:

- Mass and stiffness matrices can be generated for any plane structure (frame, truss, finite element grid, etc.), size limitations being those of the computer secondary storage.
- The mass and stiffness matrices can be generated either from the simple memeber properties (E, A, I, L, G, ρ) or from given elementary matrices in local coordinates.
- Three types of mass matrix can be generated: lumped, consistent, or a combination of both.
- Two types of reduction processes can be applied on both mass and stiffness matrix: reduction by compression or reduction by summation. Either one of them can be performed, or both simultaneously.
- Shear deformation can be also included in generating the stiffness matrix.
- Any type of support conditions can be handled.

2. Dynamic Analyzer. This program, called GEUDYN, is a dynamic modal analyzer that takes the matrices generated by GEUGEN as input and through a process of modal analysis, as discussed in Chapter 2, calculates the responses of the system. Assuming that the matrices at the input stream have been already compressed to a manageable size, the main consideration when writing this program was the speed of the numerous calculations involved, rather than the size of the memory used. Therefore, it was written in FORTRAN.

In general terms, the various steps involved in this program are the following. First, an additional reduction process similar to that used in GEUGEN may be executed here in case the matrices are input directly into this program. Then, an eigenvalue routine is called to calculate natural frequencies and mode shapes which are processed through a modal analysis routine to obtain spectral responses for a given earthquake. Next, the quasi-static loads as well as their corresponding base magnitudes and vertical distributions are computed. Finally, a least-square fitting procedure is applied to the vertical distributions, and equation coefficients as well as correlation coefficients are determined. This process may be repeated in a cyclic manner so as to sweep part or all of the frequency range of the earthquake spectrum as discussed below. A block diagram of the program is shown in Fig. 8.

The process of computing modal responses, spectral responses, quasi-static loads, and base magnitudes and vertical distributions can be made regenerative in such a way that in each cycle the model is scaled to be in a different place in the spectrum, thus sweeping it out. The scaling is carried out by multiplying the mass and stiffness matrices by a constant quantity or scaling factor. In such a case, the eigenvalues do not have to

be recalculated, but they are simply multiplied or divided (depending on whether the stiffness or the mass matrices were multiplied by that coefficient, respectively) by the square of the scaling factor. This operation shifts the frequency bound of the model through the spectrum, although the logarithmic separation of the modes and the band width remain unchanged. The purpose of sweeping the spectrum is to find the effect of the rigidity of the building on the base magnitudes as will be discussed in Chapter 5.

In summary, GEUDYN has the following present capabilities:

- Any type of structure (frame, truss, finite element grid, etc., can be treated, with the limitations imposed by the size of the computer memory (core).
- Three types of mass matrix can be treated: lumped, consistent, or a combination of both.
- An additional reduction by compression of the mass and stiffness matrices can be performed here.
- A unit or any other given load vector can be used.
- Any tripartite ground motion spectrum can be specified as well as any amount of damping.
- The spectrum can be swept partially or automatically from one end to the other.

The programs were executed on two different computers. GEUGEN was executed on the Burroughs B5500 at the Civil Engineering Systems Laboratory, whereas, GEUDYN was run on an IBM 360/75 at the Digital Computer Laboratory, both at the University of Illinois.

4.2 Format of Response Data

The responses of the system were obtained in terms of quasi-static concentrated loads as discussed in Chapter 2. These forces were transformed into dimensionless parameters, namely base magnitudes and vertical distributions so that they could be used directly in design and at the same time compared most meaningfully among themselves and with those obtained by other methods.

Base magnitudes BM, were computed from the quasi-static loads by the following expression:

$$BM = \frac{\sum_{i=1}^{n} P_i}{\sum_{i=1}^{n} w_i} \tag{62}$$

where P_i is the quasi-static load applied at story i, and w_i is the weight of story i. The corresponding vertical distributions VD, were computed by

$$VD = \frac{P_i \sum_{i=1}^{n} w_i}{w_i \sum_{i=1}^{n} P_i} \tag{63}$$

Eqs. (62) and (63) are discussed in more detail in Chapters 5 and 6. Vertical distributions given by Eq. (63) indicate the fraction of the base reaction that is applied as a concentrated force at each story.

Since vertical distributions were found to be close to a parabola within certain range of the spectrum, least-square parabolic functions were fitted[27]. The equation of the regression parabola in an X - Y coordinate system is

$$X_{reg} = A_0 + A_1 Y + A_2 Y^2 \tag{64}$$

where coefficients A_2, A_1 and A_0 are given respectively by

$$A_2 = \frac{\left\{\Sigma Y^2 X - \Sigma YX\left(\frac{\Sigma Y^2}{\Sigma Y}\right)\right\} - \left\{\left[\Sigma YX - \Sigma X\left(\frac{\Sigma Y}{N}\right)\right]\left[\frac{\Sigma Y^3 - \Sigma Y^2\left(\frac{\Sigma Y^2}{\Sigma Y}\right)}{\Sigma Y^2 - \Sigma Y\left(\frac{\Sigma Y}{N}\right)}\right]\right\}}{\left\{\Sigma Y^4 - \Sigma Y^3\left(\frac{\Sigma Y^2}{\Sigma Y}\right)\right\} - \left\{\left[\Sigma Y^3 - \Sigma Y^2\left(\frac{\Sigma Y}{N}\right)\right]\left[\frac{\Sigma Y^3 - \Sigma Y^2\left(\frac{\Sigma Y^2}{\Sigma Y}\right)}{\Sigma Y^2 - \Sigma Y\left(\frac{\Sigma Y}{N}\right)}\right]\right\}} \quad (65)$$

$$A_1 = -\left\{\frac{\left[\Sigma Y^3 - \Sigma Y^2\left(\frac{\Sigma Y}{N}\right)\right] A_2 - \left[\Sigma YX - \Sigma X\left(\frac{\Sigma Y}{N}\right)\right]}{\left[\Sigma Y^2 - \Sigma Y\left(\frac{\Sigma Y}{N}\right)\right]}\right\} \quad (66)$$

$$A_0 = \frac{\Sigma X - A_1 \Sigma Y - A_2 \Sigma Y^2}{N} \quad (67)$$

where N is the number of stories, X is the dependent variable, in this case the vertical distribution quantities, and Y is the independent variable, in this case (h_i/h_n). Correlation coefficients that would indicate how well the best fitting parabola approximates the actual vertical distribution curve, were calculated as follows:

$$cr = \sqrt{\frac{\Sigma\ (X_{reg} - \bar{X})^2}{\Sigma\ (X - \bar{X})^2}} \quad (68)$$

where $\bar{X}$ and $\bar{Y}$ are the mean values for the dependent and independent variables, respectively. A more detailed discussion on the best fitting parabola will be presented in Chapter 6.

4.3 Data Obtained

The output of the computer program (GEUDYN) contains the following quantities.

1. Modal Responses: natural frequencies, mode shapes, modal participation factors, modal story shears, modal overturning moments and modal accelerations.
2. Spectral Responses: spectral amplification factors, ABS and SRSS spectral responses for displacement, acceleration, shear, and moment.
3. Quasi-static loads: actual values, base magnitudes, vertical distributions, best fitting regression parabola, equation coefficients, and correlation coefficients all for ABS and SRSS responses for displacement, acceleration, shear and moment, and for any sweeping position in the spectrum.

Due to the large amount of data generated it is impossible to include here all of it either in numerical form or plotted. Therefore, the most significant pieces of data and those on which the discussion and conclusions of this thesis are based, are presented in the tables and figures at the end. It is worth noting that most plots were limited to SRSS responses since they represent a probable maximum estimate and are a more reasonable value than the ABS responses. The frequency range of the plots was also limited to a band width from 1 to 10 cps. where most common buildings are located. The data generated constituted the basis for the entire investigation and its conclusions, and will be the subject of discussion for the next chapter.

CHAPTER 5

BASE MAGNITUDE

In this and the following two chapters, the data obtained as indicated in Chapter 4 are discussed and interpreted, in order to obtain a more rational estimate of lateral loads that can be used as a preliminary design method for earthquake resistant structures. It is assumed that the building is designed by subjecting it to a static lateral loading.

The loading system shown in Fig. 9 may be decomposed into three parts: (1) a reaction force at the base of such magnitude and direction as to equilibrate the loads acting along the height of the building; (2) a parabolically varying set of forces concentrated at each story level; and (3) two concentrated loads located at the first and top stories to account for the effects which will be referred to as end forces. The effects of variations in the parameters upon base magnitudes, vertical distributions and end forces are discussed in this and the next two chapters, respectively.

A reference point is necessary to provide a basis of comparison in the analysis and interpretation of data. Models ranging from 4 to 30 stories and from pure-shear to pure-flexural buildings with various mass and stiffness distributions were studied. It was convenient to choose as a reference the 10SA model corresponding to a 10-story pure-shear Case A building as indicated by Table 1. This model was selected as a standard not only because of its simplicity but also because it represents a building typical of this study. Scaling coefficients are given to convert the responses from the reference model to the prototype or structure being designed.

Base magnitudes are obtained by dividing the total reaction, at the base of the structure produced by the static loading, by the weight of the building. This was defined by Eq. (62) as

$$BM = \frac{\sum_{i=1}^{n} P_i}{\sum_{i=1}^{n} w_i} \qquad (62)$$

where BM is the base magnitude, P_i is the quasi-static load at story i, and w_i is the weight of story i. The units of base magnitude are actually "force/force;" however, for purpose of design it may be considered as a non-dimensional measuring quantity.

The base magnitude obtained from the dynamic analysis is a function of the fundamental frequency of the building. The base magnitude curve has well defined displacement, velocity, and acceleration branches, similar to those in the earthquake spectra. This is illustrated by Fig. 10, which is a typical example of an SRSS base magnitude spectrum family, for this case of moment response in model 10SA. Similar SRSS base magnitude spectra were obtained for other responses and models. The frequency range is limited to 1 to 10 cps. in subsequent figures. Thus, the acceleration branch and part of the velocity branch appear in subsequent base magnitude spectra.

In Figs. 11 and 12 are shown base magnitude responses for displacement and acceleration, and for shear and moment, respectively, corresponding to the reference model (10SA). This response serves as a basis for discussing the effects of the main parameters, namely earthquake magnitude, rigidity of the structure, type of building, number of stories, and stiffness and mass distribution, on the responses of interest.

The various parameters are coupled in a very complicated manner. However, by assuming that they are coupled only with the fundamental frequency, and by using some scaling factors as discussed below, the errors resulting from ignoring the other couplings were found minimal for the most part and certainly acceptable for preliminary design purposes. The magnitude of the maximum error found was 45.5% on the conservative side.

In the following sections the effect of each parameter is considered separately. The plots for shear and moment base magnitudes were found to be very similar and consequently were combined into one plot.

5.1 Effect of Earthquake Magnitude

The response of a building to a seismic motion, and in particular the base magnitudes, depends directly on earthquake magnitude. Four different earthquakes with Richter magnitudes, M_R, of 6.1, 6.6, 7.1, and 7.4 were investigated. The resulting base magnitudes for displacement, acceleration, shear, and moment are shown in Figs. 13, 14, and 15 respectively. Shear and moment are treated together since earthquake magnitude affects both of them in a similar manner. From Figs. 13, 14 and 15 it may be concluded that the effect of earthquake magnitude is a parallel shifting of the base magnitude curves in two directions: to the left and down from the reference curves shown in Figs. 11, and 12, for a decreasing Richter magnitude. This double movement of the curves can be accounted for by using two separate multipliers, one for the frequency scale, and the other for the base magnitude scale. Such multipliers are the ratios of base magnitudes and fundamental frequencies for a curve of a given magnitude M_R to those corresponding to the reference magnitude ($M_R = 7.4$) at the kink, as indicated below

$$C_{BR} = \frac{\text{base magnitudes for any } M_R \text{ at the kink}}{\text{reference base magnitudes } (M_R = 7.4) \text{ at the kink}}$$

$$C_{FR} = \frac{\text{fundamental frequency for any } M_R \text{ at the kink}}{\text{fundamental frequency for } M_R = 7.4 \text{ at the kink}}$$

These ratios are scaling coefficients such that when multiplied by the reference values, give the base magnitude for the prototype. The base magnitude and frequency coefficients for the four cases studied are given in Table 3, and plotted in Fig. 16. The frequency coefficients are the same for displacements, accelerations, and shears, and moments.

The process of scaling the reference curve ($M_R = 7.4$) for a given M_R is as follows. First, the fundamental frequency is divided by the value of C_{FR} given in Fig. 16 for the M_R being used, in order to obtain a model frequency f_1^*

$$f_1^* = f_1/C_{FR} \tag{69}$$

where f_1 is the fundamental frequency of the prototype, and C_{FR} is the scaling coefficient for frequency due to Richter magnitude.

With this model frequency, f_1^*, a reference value of base magnitude, $\overline{BM}$, is obtained for the model from the curves in Figs. 11 or 12. Then a base magnitude is obtained using the following formula

$$BM^* = \overline{BM} \times C_{BR} \tag{70}$$

where BM^* is the scaled base magnitude for the prototype and C_{BR} is the scaling coefficient for base magnitudes due to Richter magnitude as given in Fig. 16. The superscripts D, A, S, or M refer to displacement, acceleration, shear or moment, respectively.

5.2 Effect of Rigidity of the Structure

The rigidity of the structure is a measure of its stiffness independent of how it is distributed. To investigate the effect of rigidity of the structure, the stiffness was scaled to sweep the frequency spectrum using the following scaling equation.

$$K' = K \times (S_c)^{P_k} \tag{71}$$

where K' is the new stiffness matrix, K is the original stiffness matrix, S_c is a frequency scaling coefficient equal to the ratio of the desired new fundamental frequency to the original fundamental frequency of the model, and P_k is a power factor. By changing the scaling coefficient S_c, a single base magnitude spectrum curve is generated for a given P_k. If the power factor P_k is varied, a family of curves is obtained as shown in Fig. 12. Power factors were varied from 1.0 to 2.0. The resulting family of base magnitude curves for shear and moment is shown in Fig. 12 for model 10SA. Similar plots were obtained for other models.

For the purpose of design, the power factor P_k has to be calculated first in order to locate a particular base magnitude curve. From Eq. (71),

$$P_k = \frac{\log (\bar{K}_1'/\bar{K}_1)}{\log S_c} \tag{72}$$

When a prototype is being compared to the model as is the case in obtaining a value of P_k for design purposes, the terms in Eq. (72) are described as follows. S_c is the ratio of the fundamental frequency of the prototype to that of the model (0.075 cps. for model 10SA), $\bar{K}_1'$ is the total column stiffness divided by the column height, for the first story of the prototype,

and $\bar{K}_1$ is the corresponding quantity for the model as given by

$$\bar{K}_1' = \frac{\bar{k}_{c_1}'}{h_1'} \qquad \text{(prototype)} \qquad (73)$$

and

$$\bar{K}_1 = \frac{\bar{k}_{c_1}}{h_1} \qquad \text{(model)}$$

where $\bar{k}_{c_1}$ is the total column stiffness $\left(\frac{6EI}{L^3}\right)$ at the first story, h_1 is the height of the first story. For model 10SA, $\bar{K}_1 = 10$. Therefore, if Fig. 12 is used to obtain base magnitudes for a given prototype, Eq. (72) becomes

$$P_k = \frac{\log\ (\bar{K}_1'/10)}{\log\ (f_1/0.075)} \qquad (74)$$

where $\bar{K}_1'$ is given by Eq. (73) and f_1 is the fundamental frequency for the prototype.

Variations in the rigidity of the structure change the original base magnitudes for displacement shown in Fig. 11, by the same amount as the stiffness matrix (Eq. (71)). Therefore, reference base magnitudes for displacement, $\overline{BM}^D$, are given by

$$\overline{BM}^D = BM^D \times (f_1/0.075)^{P_k} \qquad (75)$$

where BM^D is the value obtained from Fig. 11. Base magnitudes for acceleration are not affected by the rigidity of the building.

The power factor P_k, reflects the rigidity of the prototype with respect to that of the model. The more rigid the prototype is, i.e., the larger P_k is, the greater the base magnitude for a given frequency, as expected. P_k is also an important factor to be considered in determining the effects of type of building, stiffness distribution, and number of stories as discussed below.

5.3 Effect of Type of Building

Buildings may be of different kinds: frames, shear walls, box systems, etc., but they may be gathered into three main categories; pure-shear, pure-flexural, and intermediate cases. Thus, in general, the type of building may be measured by the amount of pure-shear or pure-flexural elements present in it, or in other words, by the shear-flexural ratio r_t as given by Eq. (51). The expression for r_t may be redefined as:

$$r_t = \frac{\bar{k}_{b_1}}{\bar{k}_{c_1}} \tag{76}$$

where $\bar{k}_{b_1}$ and $\bar{k}_{c_1}$ are total beam and column stiffnesses for the first story, respectively. In a pure-shear building the beams are assumed to be infinitely stiff and thus, $r_t = \infty$. In a pure-flexural structure no restrictions are placed upon the rotation of the joints which means that the stiffnesses of the beams are zero, i.e., $r_t = 0$, as is the case for shear walls. For intermediate buildings r_t takes values between zero and infinity.

Besides the pure-shear model (10SA) and the pure-flexural model (10FA) three intermediate cases were studied: models 10SFA1, 10SFA2, and 10SFA3 with values of r_t of 1.0, 0.66, and 0.33 respectively. Base magnitudes for these five models can be seen in Figs. 17, 18, and 19. From these figures it may be concluded that in general terms, the effect of changing the shear-flexural ratio r_t is again a parallel shifting of the base magnitude curves towards the left as r_t decreases. This is discussed below for each response, independently.

1. Displacement. In the case of displacement, the family of curves shown in Fig. 17 may be shifted parallel to their positions to form a

single base magnitude curve. Inverting the process, the reference base magnitude spectrum for displacement shown in Fig. 11 may be converted back into the actual curve for a given r_t by multiplying it by a scaling coefficient C_{BT}^{D}. This coefficient is defined as

$$C_{BT}^{D} = \frac{\text{base magnitude for any } r_t}{\text{reference base magnitude}}$$

Values of C_{BT}^{D} were thus calculated for the five cases considered; they are plotted in Fig. 20.

It is important to note in Fig. 20 that even if a small amount of shear resistance is added to a pure-flexural building it tends to behave as a shear structure. This means that a great number of the actual buildings behave like shear structures.

For purpose of design, a reference value of base magnitude $\overline{BM}$ may be scaled according to the type of building by the following expression

$$BM^{*} = \overline{BM} \times C_{BT}^{D} \qquad (77)$$

where BM^{*} is the scaled base magnitude and C_{BT}^{D} is the scaling coefficient obtained from Fig. 20 for a given r_t.

2. Acceleration. The base magnitude curves for acceleration shown in Fig. 18 indicate that for cases in which r_t is greater than 0.33, buildings may be assumed to be shear structures and therefore no scaling of the reference values is necessary. This statement follows from the fact that it is very difficult to differentiate between the base magnitude curves for r_t greater than 0.33. Again, this indicates that the inclusion even of a small amount of shear resistance makes the building behave as a shear structure.

In the event that the shear-flexural ratio, r_t, be smaller than 0.33 an independent scaling is needed for the velocity and the acceleration branches since the curves do not shift parallel as a unit. In the velocity branch a rotation occurs which may be corrected by a power coefficient $P^A_{BT_v}$. Thus, when the reference base magnitude $\overline{BM}$ is elevated to such a power, it rotates and gives the scaled value BM^* for a given r_t smaller than 0.33. From Fig. 18 it can be seen that for $r_t = 0$, $P^A_{BT_v}$ has the value 0.35. If the variation of $P^A_{BT_v}$ as a function of r_t is assumed to be a straight line in semi-log scale, i.e., a logarithmic function, an expression for $P^A_{BT_v}$ may be derived as indicated below. Using Eqs. (7) and (9) given in Appendix B and setting $a = 0.33$, then

$$b = \frac{0 - 0.33}{\log 0.35} = \frac{-0.33}{\bar{1}.545} = \frac{-0.33}{-0.455} = 0.725$$

Therefore,

$$P^A_{BT_v} = \log^{-1}\left[\frac{r_t - 0.33}{0.725}\right] \quad \text{for } r_t < 0.33 \qquad (78)$$

In the acceleration branch a parallel shifting of the base magnitude curve may be considered for values of r_t less than 0.33. This shifting is taken care of by means of a scaling coefficient $C^A_{BT_a}$. Fig. 18 yields a value of $C^A_{BT_a}$ equal to 1.4 for $r_t = 0$. Since $C^A_{BT_a}$ varies approximately linearly with r_t in a semi-log scale, Eqs. (7) and (9) of Appendix B give for $a = 0.33$,

$$b = \frac{0 - 0.33}{\log 1.4} = \frac{-0.33}{0.145} = -2.27$$

therefore,

$$C^A_{BT_a} = \log^{-1}\left[\frac{0.33 - r_t}{2.27}\right] \quad \text{for } r_t < 0.33 \qquad (79)$$

For values of $r_t > 0.33$ no scaling is necessary as pointed out before. Nevertheless, to make the scaling process more general it may be assumed that

$$C^A_{BT_a} = 1.0 \text{ for } r_t > 0.33 \tag{80}$$

and

$$P^A_{BT_v} = 1.0 \text{ for } r_t > 0.33 \tag{81}$$

Also,

$$C^A_{BT_v} = 1.0 \tag{82a}$$

and

$$P^A_{BT_a} = 1.0 \tag{82b}$$

Then reference base magnitudes $\overline{BM}$ are scaled by

$$BM^* = (\overline{BM})^{P^A_{BT}} \times C^A_{BT} \tag{83}$$

where $C^A_{BT_a}$ and $P^A_{BT_v}$ are given by Eqs. (78) through (82).

3. Shear and Moment. As far as shears and moments are concerned, the same parallel shifting effect is observed in Fig. 19. However, in this case the scaling coefficients by which the reference base magnitudes ought to be multiplied to obtain the actual values, depend not only upon r_t but also on the power factor P_k.

Scaling coefficients $C^{S,M}_{BT}$ for the five cases studied are tabulated in Table 4 and plotted in Fig. 21. $C^{S,M}_{BT}$ is defined as

$$C^{S,M}_{BT} = \frac{\text{base magnitude for any } r_t \text{ for a given } P_k}{\text{reference base magnitude for a given } P_k}$$

Since the $C^{S,M}_{BT}$ vs. P_k functions are straight lines in a semi-log

scale, the procedure outlined in Appendix B may be used to obtain an expression for the scaling coefficient. The slope b_t, of these lines and their pivot or intercept with the 1.0 abscissa, P_t, are plotted in Fig. 22. From Eqs. (7) and (9) of Appendix B the following expressions may be derived.

For the pivot:

$$\text{for } 1 > r_t > 0.33,\ a = 0.73.$$

therefore

$$b = \frac{1.0 - 0.73}{\log 0.86} = \frac{0.27}{\bar{1}.935} = \frac{0.27}{-0.065} = -4.15$$

then

$$P_t = \log^{-1}\left[\frac{0.73 - r_t}{4.15}\right] \quad (\text{for } r_t > 0.33) \tag{84}$$

For $r_t < 0.33$, $a = 0.54$. Therefore

$$b = \frac{0 - 0.54}{\log 1.75} = -\frac{0.54}{0.244} = -2.21$$

then

$$P_t = \log^{-1}\left[\frac{0.54 - r_t}{2.21}\right] \quad (\text{for } r_t < 0.33) \tag{85}$$

For the slope:

$$\text{for } 1 > r_t > 0.33,\ a = -0.33. \quad \text{Therefore}$$

$$b = \frac{1.0 - (-0.33)}{\log 8.78} = \frac{1.33}{1.944} = 0.68$$

Then

$$b_t = \log^{-1}\left[\frac{r_t + 0.33}{1.41}\right] \quad (\text{for } r_t > 0.33) \tag{86}$$

For $r_t < 0.33$, $a = 0.06$. Therefore,

$$b = \frac{0 - 0.06}{\log 0.79} = \frac{-0.06}{\bar{1}.896} = \frac{-0.06}{-0.104} = 0.58$$

then

$$b_t = \log^{-1}\left[\frac{r_t - 0.06}{0.58}\right] \quad (\text{for } r_t < 0.33 \qquad (87)$$

The final equations for the scaling coefficient are

$$C_{BT}^{S,M} = \log^{-1}\left[\frac{P_k - P_t}{b_t}\right] \quad (\text{for } r_t < 1) \qquad (88)$$

where P_t and b_t are given by Eqs. (84) through (87), and

$$C_{BT}^{S,M} = 1.0 \qquad (\text{for } r_t > 1) \qquad (89)$$

The scaling of the reference base magnitudes is performed in the usual manner:

$$BM^* = \overline{BM} \times C_{BT}^{S,M} \qquad (90)$$

5.4 Effect of Number of Stories

Most of this investigation was conducted on the basis of a 10-story model (10SA). However, to make the study complete and the conclusions as general as possible buildings of various heights ranging from 4 to 30 stories were analyzed. The common trend is once more a parallel shifting of the reference curves towards the left with increasing number of stories. The effect of changing the total number of stories N, is discussed for each response independently.

1. Displacement. Base magnitudes for displacement are shifted as shown in Fig. 23 when the number of stories is changed. Scaling coefficients C_{BN}^{D} defined as

$$C_{BN}^{D} = \frac{\text{base magnitudes for any N}}{\text{reference base magnitudes}}$$

were computed and plotted. They were found to vary linearly with N on a log-log scale. This represents a geometric function for which an expression may be derived using the equations presented in Appendix A. Taking two points on the straight line of coordinates

$$\left(C^{D}_{BN} = 2, \quad N = 7\right), \text{ and } \left(C^{D}_{BN} = 1, \quad N = 10\right)$$

and using Eqs. (1) and (4) of Appendix A, then

$$b = \frac{\log 7 - \log 10}{\log 2 - \log 1} = \frac{0.845 - 1}{0.3 - 0} = \frac{-0.155}{0.3} = -0.52$$

therefore

$$C^{D}_{BN} = \log^{-1}\left[\frac{1-\log N}{0.52}\right] \tag{91}$$

The scaled base magnitudes BM^{*}, are

$$BM^{*} = \overline{BM} \times C^{D}_{BN} \tag{92}$$

2. Acceleration. In Fig. 24 is shown that the effect of number of stories N on the base magnitudes for acceleration is negligible. Therefore, no scaling is necessary and the reference base magnitude spectrum for acceleration shown in Fig. 11 may be used for buildings of any number of stories. Thus,

$$C^{A}_{BN} = 1.0 \tag{93}$$

3. Shear and Moment. A parallel shifting of the reference base magnitude spectra for shear and moment occurs when the number of stories changes as illustrated in Fig. 25. Following the same procedure used before, scaling coefficients defined as

$$C^{S,M}_{BN} = \frac{\text{base magnitude for any N for a given } P_k}{\text{reference base magnitude for a given } P_k}$$

are tabulated in Table 5 and plotted in Fig. 26.

Again, the values for $C_{BN}^{S,M}$ depend not only upon N but also on the power factor P_k, the relationship being a straight line in semi-log scale as shown in Fig. 26. In this case, there is a common pivot or intercept of the $C_{BN}^{S,M}$ - P_k functions with the 1.0 abscissa. The logarithmic slopes b_N, of the lines shown in Fig. 26 were found to be also a straight line function in semi-log scale having two points of coordinates ($1/b_N = 0.271$, $N = 30$), and ($1/b_N = 0$, $N = 10$). Using Eqs. (5) and (6) of Appendix B the following expression for b_N is obtained.

$$b = \frac{0.271 - 0}{\log 30 - \log 10} = \frac{0.271}{1.476 - 1} = \frac{0.271}{0.476} = 0.57$$

therefore

$$\frac{1}{b_N} = 0.57 \quad (\log N - 1)$$

Substituting into Eq. (9) of Appendix B and noting that the pivot a is equal to 2.6, then the following equation for $C_{BN}^{S,M}$ results:

$$C_{BN}^{S,M} = \log^{-1}\left[0.57\ (P_k - 2.6)\ (\log N - 1)\right] \qquad (94)$$

The scaled base magnitudes BM^* are

$$BM^* = \overline{BM} \times C_{BN}^{S,M} \qquad (95)$$

5.5 Effect of Stiffness Distribution

The distribution of stiffness along the height of the building has a shifting effect on the reference curves for base magnitudes. This effect varies in a different way for each of the four responses being considered, namely displacements, accelerations, shears, and moments. The

conclusions made about the effect of stiffness distribution on base magnitudes were derived from the comparison of the results obtained for models 10SA, 10SB1, and 10SB2 with values of r_k of 1.0, 0.182, and 0.0825 respectively. The change in stiffness through the height of the building is measured by the stiffness distribution ratio, r_k, defined by Eq. (55) as follows:

$$r_k = \frac{\bar{k}_{c_n}}{\bar{k}_{c_1}} \tag{55}$$

where $\bar{k}_{c_n}$ and $\bar{k}_{c_1}$ are the total column stiffnesses for the top and first stories, respectively.

1. Displacement. Base magnitudes for displacement for the three cases are shown in Fig. 27. It can be seen that the effect of changing the stiffness distribution ratio, r_k, results in a parallel shifting of the reference curve ($r_k = 1$) towards the right. The amount of shift may be measured by the ratio of the base magnitudes for the various cases to those corresponding to the reference case, C^D_{BK}. Since the curves shift parallel to their original position the coefficients C^D_{BK} are constant for a particular stiffness distribution ratio, r_k, and therefore, they are independent of fundamental frequency. The values of C^D_{BK} for the three cases are plotted in Fig. 30 which shows a linear log-log relationship between stiffness distribution ratio, r_k, and the ratio of base magnitudes, C^D_{BK}. Noting that the intercept "a" is equal to 1.0 and using Eqs. (2) and (3) of Appendix A, the following expression for C^D_{BK} results:

$$b = \frac{\log 5.4 - 0}{\log 0.1} = \frac{0.733}{-1} = -0.733$$

therefore

$$C^D_{BK} = r_k^{-0.733} \tag{96}$$

C^D_{BK} defined as

$$C^D_{BK} = \frac{\text{base magnitudes for any } r_k}{\text{reference base magnitudes}}$$

is a scaling coefficient by which the reference curve of Fig. 11 should be multiplied to obtain the base magnitudes for a prototype. That is,

$$BM^* = \overline{BM} \times C^D_{BK} \tag{97}$$

2. Acceleration. Fig. 28 shows the effect of stiffness distribution on acceleration base magnitudes for the three cases considered.

Changing the stiffness distribution ratio produces not only a clockwise rotation about an imaginary pivot as indicated in the figure, but it also distorts slightly the shape of the curve or angle between the two branches. The pivot is not a fixed point, but it changes its position with variations in r_k.

Any curve for a prototype can be related to the reference curve by a process of rotation and translation applied independently to each of the two branches. Since both branches represent a linear log-log relationship, they can be rotated by a power and translated by a multiplier. Thus, the scaling process, that is, converting the reference curve into the actual curve for a prototype, may be expressed as follows:

$$BM^* = \overline{BM}^{P^A_{BK}} \times C^A_{BK} \tag{98}$$

where, BM^* is the scaled base magnitude, $\overline{BM}$ is the reference base magnitude, given in Fig. 11, P^A_{BK} and C^A_{BK} are the scaling power and multiplier for acceleration base magnitudes due to stiffness distribution, respectively.

P^A_{BK} and C^A_{BK} are subdivided into $P^A_{BK_a}$ and $P^A_{BK_v}$, and $C^A_{BK_a}$ and $C^A_{BK_v}$ respectively, according to whether the velocity or the acceleration branch is being scaled. The powers and multipliers found for the three stiffness distribution cases studied are plotted in Fig. 30. Again, a linear log-log relationship exists between the scaling powers and coefficients, and the stiffness distribution ratio r_k. Using Eqs. (2) and (3) of Appendix A, the following expressions for such powers and coefficients may be derived:

$$C^A_{BK_a} = r_k^{0.26} \tag{99}$$

$$C^A_{BK_v} = r_k^{-0.05} \tag{100}$$

$$P^A_{BK_a} = r_k^{-0.235} \tag{101}$$

$$P^A_{BK_v} = r_k^{0.145} \tag{102}$$

The subscripts a and v indicate acceleration and velocity branches respectively.

3. Shear and Moment. The results obtained show that the effect of stiffness distribution on moment base magnitude is the same as that for shear base magnitude, which is in agreement with previous findings for the reference model. Comparison of Figs. 12 and 29 show that decreasing the stiffness distribution ratio r_k, "compresses" the base magnitude curves towards the right, keeping each one of them parallel to its original position, and in such a way that the curves are moved an amount proportional to their logarithmic distances to an imaginary pivot. The shifting of the curves may be accounted for by multiplying the reference curves by a scaling coefficient $C^{S,M}_{BK}$. This coefficient varies linearly with P_k in a

semi-log scale as shown in Fig. 31. Values of $C_{BK}^{S,M}$ for the three cases studied are tabulated in Table 6.

Fig. 31 indicates that the pivot is constant for all values of r_k, and equal to 1.83. The slopes b_k, of the lines in Fig. 31 were found to be linearly related to r_k. Using two arbitrary points ($1/b_k = -0.4$, $r_k = 0.1$), and ($1/b_k = 0$, $r_k = 1$), and Eqs. (7) and (8) of Appendix B, the following expression for the slope b_k results:

$$b = \frac{-0.4 - 0}{\log 0.1} = \frac{-0.4}{-1} = 0.4$$

then,

$$1/b_k = 0.4 \log r_k$$

Substituting $1/b_k$ into Eq. (9) of Appendix B, then

$$C_{BK}^{S,M} = \log^{-1}[0.4\ (P_k - 1.83)\ \log\ r_k] \qquad (103)$$

In summary, the effect of stiffness distribution on shear and moment base magnitudes may be accounted for by the following expression:

$$BM^* = \overline{BM} \times C_{BK}^{S,M} \qquad (104)$$

where BM^* is the scaled base magnitude, $\overline{BM}$ is the reference base magnitude, and $C_{BK}^{S,M}$ is the scaling coefficient for shear and moment base magnitudes due to stiffness distribution as given by Eq. (103).

5.6 Effect of Mass Distribution

The major effect of mass upon base magnitudes is caused by the total weight of the building. Such an effect can be described by a simple rule of direct proportionality between base magnitudes and total weight of building. Therefore; from Eq. (62)

$$R = BM \times W \tag{105}$$

where, R is the total horizontal reaction at the base of the structure for displacement, acceleration, shear, or moment (superscripts D, A, S, or M, respectively), BM is the corresponding base magnitude, and W is the total weight of the building.

5.7 Scaling of Base Magnitudes

The scalings developed throughout this chapter to account for the various effects of the parameters upon base magnitudes may be considered independent as indicated previously. Therefore, Eqs. (70), (77), (83), (90), (92), (95), (97), (98), and (104) may be included into a single equation as follows:

$$BM^* = (\overline{BM})^{P_{BT} \times P_{BK}} \times C_{BR} \times C_{BT} \times C_{BK} \times C_{BN} \tag{106}$$

where $\overline{BM}$ is the reference base magnitude for the model, and BM^* is the scaled base magnitude for the prototype. The scaling powers P_{PT} and P_{BK} for displacement, shear, and moment are taken to be unity so that the same equation can be used for all responses. These powers, together with scaling coefficients C_{BT} and C_{BK} for acceleration response depend on spectrum branch.

The effects of the most significant parameters upon the reference base magnitude spectra have been discussed in this chapter, and are summarized in Table 12. How those parameters affect the vertical distribution of the loads is the subject of the next chapter.

CHAPTER 6

VERTICAL DISTRIBUTION

The total reaction at the base, discussed in Chapter 5, counteracts both the end forces and the concentrated quasi-static story forces so as to maintain the equilibrium of the system shown in Fig. 9. The variation of these concentrated forces along the height of the structure is presented and the effect of the various parameters is discussed. Scaling coefficients are given to convert the vertical distribution for the reference model to that for the prototype.

6.1 Parabolic Coefficients and Correlation

Vertical distributions for the various models were obtained by means of Eq. (63), i.e.,

$$VD_i = \frac{P_i \sum_{i=1}^{n} w_i}{w_i \sum_{i=1}^{n} P_i} \qquad (63)$$

where P_i is the quasi-static force at story i, and w_i is the weight of that story. Eq. (63) is a convenient non-dimensional measurement of the fraction of the base reaction that should be applied at each story. Vertical distributions for displacement, acceleration, shear, and moment responses were calculated by means of Eq. (63) for the various models and at different positions in the spectrum. Typical plots taken directly from the computer output for model 10SA in the displacement, velocity and acceleration branches of the spectrum are shown in Figs. 32, 33, and 34, respectively. The curves

labelled as "actual" correspond to values given by Eq. (63). Similar plots were obtained for other models and frequencies. In general, the shape of these curves agrees with those presented in previous studies[8].

Except for the very extreme displacement branch (frequencies lower than 0.1 cps), the vertical distribution curves for the four responses may be approximated by a best-fit parabola with increasing accuracy for the increasing frequency. This is illustrated in Figs. 32, 33, and 34. The parabolic fitting was performed by the method of least squares[27]. Parabolic coefficients A_0, A_1, and A_2 were calculated by means of Eqs. (65), (66), and (67). The regression parabolas shown in Figs. 32, 33, and 34 were computed by Eq. (64), i.e.,

$$X_{reg} = A_0 + A_1 Y + A_2 Y^2 \qquad (64)$$

where X is the dependent variable or value of response, and Y is the independent variable (h_i/h_n).

The extent to which these parabolas approximate the actual curves was measured by correlation coefficients as indicated by Eq. (68), i.e.,

$$cr = \sqrt{\frac{\Sigma\ (X_{reg} - \bar{X})^2}{\Sigma\ (X - \bar{X})^2}}$$

where $\bar{X}$ is the mean value for the dependent variable. Typical maximum and minimum correlation coefficients are given in Table 7 for model 10SA, for frequencies between 1.12 and 9.40 cps. A correlation value of 1.0 means an exact superposition of the parabola over the actual curve.

Such a good correlation between best-fitting parabola and actual curve may be atrributed to the high degree of participation of the fundamental mode into the total responses as shown in Figs. 35, 36, and 37.

These figures illustrate the modal contributions to the various spectral responses. The largest percentage contribution for all responses is that of the first mode, with the second mode next. The influence of the second mode on the vertical distributions shows up in the parabolic coefficient plots as discussed later.

The actual vertical distribution curves are thus replaced by the corresponding best fitting parabolas. Since these curves are defined by the same equation (Eq. (64)) they may be conveniently described by sets of parabolic coefficients A_0, A_1, and A_2. Such coefficients, obtained from the computer output, were plotted against frequency as typically illustrated in Fig. 38 for the case of acceleration response of model 10SA. Similar plots were obtained for other models and responses. Subsequent figures are limited to a frequency range from 1 to 10 cps. In all of the figures A_0 is multiplied by a factor of 10 due to its small magnitude.

It can be observed throughout the various parabolic coefficient plots, and in particular in Fig. 38, that there is a double kink and a plateau between the velocity and acceleration parts of the curve. The kink of highest frequency is due to the significant presence of the second mode in the total response as illustrated in Figs. 35, 36, and 37. This secondary kink may be eliminated by shifting part of the frequency scale thus smoothing out the parabolic coefficient curve. For this purpose, a frequency scaling coefficient C_{FD} is used as indicated by:

$$f_1^{*'} = f_1 \times C_{FD} \tag{107}$$

where f_1 and $f_1^{*'}$ are the fundamental frequencies for the prototype and the model respectively. The values for C_{FD} are

$$C_{FD} = 1 \text{ for } f_1 < 2.35 \text{ cps.} \tag{108a}$$

$$C_{FD} = 0.75 \text{ for } f_1 > 3.15 \text{ cps.} \qquad (108b)$$

$$f_1^{*'} = 2.35 \text{ cps. for } 2.35 \text{ cps.} < f_1 < 3.15 \text{ cps.} \qquad (108c)$$

Using the above procedure, smooth reference parabolic coefficient plots were obtained from those for model 10SA as shown in Figs. 39, 40, and 41. Again, shear and moment are treated together because of the similitude in their plots. Those curves serve as reference for comparison and discussion of the effects of variations in the parameters, namely, type of building, number of stories, and stiffness and mass distributions, upon the vertical distributions expressed in terms of the parabolic coefficients A_0, A_1, and A_2. Such effects are discussed independently, below.

6.2 Effect of Type of Building

The type of a building is defined by the amount of pure-shear or pure-flexural elements present, indicated in Chapter 5. This is measured by the shear-flexural ratio r_t given by Eq. (76).

Parabolic coefficients for models 10SA, 10SFA1, 10SFA2, 10SFA3, and 10FA with values of r_t of ∞, 1.0, 0.66, 0.33, and 0 respectively are shown in Figs. 42, 43, and 44. In general, the effect of changing r_t is a parallel shifting of the curves up and down with a slight change in the average slope of the velocity and acceleration branches.

The scaling process to convert parabolic coefficients from the model to the prototype is done by using both a scaling multiplier C_D, to account for changes in slope, and a scaling increment ΔA, to shift the curves, That is,

$$A^* = \bar{A} \times C_D + \Delta A \qquad (109)$$

where A^*, and $\bar{A}$ are the parabolic coefficients for the prototype and the

model, respectively. A takes subscripts 0, 1, or 2, and superscripts D, A, S, or M for displacement, acceleration, shear, and moment respectively. A_0 and ΔA_0 are always multiplied by a factor of 10, and written as $A_0 \times 10$, and $\Delta A_0 \times 10$. The scaling mulitplier and increment are defined respectively as

$$C_D = \frac{\text{"average" slope of velocity branch for prototype}}{\text{"average" slope of velocity branch for reference model}} \quad (110)$$

$$\Delta A = A^*_{kink} - \bar{A}_{kink} \times C_D \quad (111)$$

where A^*_{kink}, and $\bar{A}_{kink}$ are the values of the parabolic coefficients at the first mode kink for the prototype and the model, respectively. For the case of type of building the subscript T is added: C_{DT}, and $\Delta_T A$. Values of C_{DT} for A_2, A_1, and $A_0 \times 10$ and for all responses were calculated using Eq. (110). Their deviation was very small, and thus, an average value of 1.35 was used. Therefore

$$C_{DT} = 1.35 \quad \text{(for all responses)} \quad (112)$$

Values of ΔA were calculated using Eqs. (111), and (112), and plotted as illustrated in Fig. 45. The equations of these logarithmic functions (straight lines in semi-log scale) have the general form (see Appendix B):

$$\Delta_T A = \log^{-1}\left[d'_t + \frac{r_t - e'_t}{b'_t}\right] \quad (113)$$

The coefficients b'_t, and d'_t, and e'_t are given in Table 8 for the various responses. Eq. (113) gives values of $\Delta_T A_0 \times 10$, $-\Delta_T A_1$, and $\Delta_T A_2$.

As an example of the acceptable accuracy of this scaling method, parabolic coefficients $A^S_0 \times 10$ for $r_t = 1$ were computed from those for $r_t = \infty$ using Eqs. (109), (112), and (113). The results are given in Table 9 and compared to the values taken directly from the $A^S_0 \times 10$ curve in Fig. 44.

6.3 Effect of Number of Stories

Parabolic coefficients for buildings with 6, 10, 20, and 30 stories, and for all responses are shown in Figs. 46, 47, and 48. The effect of increasing the number of stories N is to shift the parabolic coefficient plots towards the zero line. Slight changes in slope in the velocity and acceleration branches also occur. The same scaling method described in the preceding section may be used to convert the parabolic coefficients for the 10-story model (10SA) to a prototype having any number of stories N. In this case the scaling multiplier and increment given by Eqs. (110), and (111), take the subscript N: C_{DN}, and $\Delta_N A$.

Values of C_{DN} were calculated for the various curves shown in Figs. 46, 47, and 48. They could be easily approximated by three straight lines in log-log scale. These three geometric functions for A_2, A_1 and $A_0 \times 10$ and for all responses are given by the following equation (See Appendix A):

$$C_{DN} = \log^{-1}\left[\frac{1 - \log N}{b_N}\right] \tag{114}$$

where $b_N = 0.354$ for $A_0 \times 10$, $b_N = 0.8$ for A_1, and $b_N = 0.51$ for A_2.

Scaling increments $\Delta_N A$ were calculated by Eq. (111). The results are plotted in Fig. 49. It can be observed that for buildings of more than 10 stories the scaling necessary is very small and becomes constant for more than 20 stories. Most of the scaling is required for buildings of less than 10 stories.

6.4 Effect of Stiffness Distribution

Parabolic coefficients for models 10SA, 10SB1, and 10SB2 having values

of stiffness distribution ratio r_k, of 1.0, 0.182, and 0.0525, respectively, are shown in Figs. 50, 51, and 52. Again, the effect of changing r_k is a shifting up and down of the plots with slight rotations of the velocity and acceleration branches. Thus, the same scaling procedure described in section 6.2 may be used. Scaling multipliers and increments defined by Eqs. (110), and (111), use the subscript K in this case: C_{DK}, and $\Delta_K A$.

Values of C_{KN} were calculated for the various curves shown in Figs. 50, 51, and 52. They were approximated by three straight lines in log-log scale. These three geometric functions for displacement, acceleration and shear and moment are given by the following equation (See Appendix A):

$$C_{DK} = \log^{-1}\left[\frac{\log r_k}{b_k}\right] \qquad (115)$$

where $b_k = -1.72$ for displacement, $b_k = 1.09$ for acceleration, and $b_k = 4.0$ for shear and moment.

Scaling increments $\Delta_k A$ were calculated by Eq. (111). The results are plotted in Fig. 53. The equations of these logarithmic functions have the general form (See Appendix B):

$$\Delta_K A = a'_k + b'_k\ (\log r_k - d'_k) \qquad (116)$$

The values of a'_k, b'_k, and d'_k for the various responses are tabulated in Table 10. Eq. (116) gives values of $\Delta_k A_0 \times 10$, $-\Delta_k A_1$, and $\Delta_k A_2$.

6.5 Effect of Mass Distribution

The distribution of mass along the height of the building has an important effect on the vertical distributions of quasi-static loads. This effect is shown in Fig. 54 for model 10SD having linearly distributed mass. The curves labelled "no mass correction" were calculated

by simply dividing the quasi-static load at each story by the reaction at the base, that is:

$$VD' = \frac{P_i}{\sum_{i=1}^{n} P_i}$$

The dashed curve is obtained by correcting the above equation in proportion to the individual story weights relative to the total weight as indicated by Eq. (63), i.e.,

$$VD = \frac{P_i \sum_{i=1}^{n} w_i}{w_i \sum_{i=1}^{n} P_i} \qquad (63)$$

Then a best-fitting parabola may be obtained, consistently with previous cases, as indicated in Fig. 54. Thus, the force at story i of the prototype is calculated from Eq. (63) as

$$P_i = VD_i \times BM \times w_i \qquad (117)$$

where BM was substituted from Eq. (62).

6.6 Scaling of Vertical Distributions

The scaling multipliers and increments developed throughout this chapter to account for the various effects of the parameters upon vertical distributions may be considered independent as indicated previously. Therefore, Eq. (109) may be written as

$$A^{*'} = \bar{A} + (\bar{A} \times C_{DT} + \Delta_T A - \bar{A}) + (\bar{A} \times C_{DK} + \Delta_K A - \bar{A}) \qquad (118a)$$

and

$$A^{*} = A^{*'} \pm (\bar{A} \times C_{DN} + \Delta_N A - \bar{A}) \qquad (118b)$$

where the (-) sign is used if $A^{*'} > 0$, and the (+) sign is used if $A^{*'} < 0$. If no scalings for type of building or stiffness distribution are necessary,

then $A^{*'} = \bar{A}$.

The effects of the most significant parameters upon the reference parabolic coefficients and therefore, upon the corresponding vertical distributions, have been discussed in this chapter and are summarized in Table 12.

It can be observed in the figures presented that there are differences between the actual vertical distribution curves and the best fitting parabolas at the top and first stories, besides the fact that the actual curves have peaks at those points. These are the so-called end effects which are discussed in the next chapter.

CHAPTER 7

END LOADS

The discussion of the proposed quasi-static loading shown in Fig. 9 is completed in this chapter. The nature of end loads and their relation to both vertical distributions and base magnitudes are considered.

7.1 Nature of End Loads

The vertical distribution plots presented in Chapter 6 show peaks at the top and first floors. In addition, concentrated forces should be added at those points to adjust the parabolic loading to the actual loading. This incidates that there is a different behavior of the system at its ends such that those points absorb a greater percentage of the total base reaction than the rest of the structure. This situation is known as end effects and they are directly related to the boundary conditions of the system.

The nature of these end effects is complicated. This phenomenon may be partially explained by comparing the discrete system to an analytical model such as a solid homogeneous bar with mass and stiffness properties uniformly distributed along its axis. The bar is assumed clamped at one end and free at the other to simulate an actual building. If the bar is hit at the fixed end with a forcing pulse a stress wave travelling along the bar results. The mathematical characteristics of the axial vibration of the bar, and the one-dimensional wave equation governing it, are given in Ref. 28. The bar subjected to axial vibrations behaves in a manner similar to a pure-shear building having the same mode shapes and frequency separations.

The stress wave travelling along the bar may be one of tension or compression depending on the direction of the applied forcing pulse. For purposes of this discussion a compression wave is assumed. When the wave reaches the free end the wave reflects back reversing the sign of the stress due to the inertia forces of the particles at the end. Thus the reflected wave is a tensile one. In the process of reversing the sign of the wave at the end, a tensile stress (in this particular case) of twice the magnitude of the original compressive stress is developed at that point. The same phenomena can be observed when the tensile wave travelling down hits the fixed end: a compressive stress of twice the original value develops at that point. The magnitude of the stresses at the ends when the wave is reflected back are diminished by damping present in the material.

The nature of the end effects in the discrete system is the same as that in the analytical model as discussed above. However, because of lumping of parameters and other disturbing causes the stresses at the ends, or end loads, are more difficult to predict in the discrete case than in the analytical case.

7.2 Relationship to Vertical Distributions

The parabolic distributions of quasi-static loads presented in Chapter 6 automatically concentrate part of the total base reaction, at the ends of the structure. However, the actual loading curve still shows peaks at the ends that go beyond the parabola. Such peaks are taken care of by additional concentrated end forces as shown in Fig. 9.

End force coefficients for the various models studied were calculated as the difference between the actual and parabolic vertical

distribution curves at first and top stories, and plotted for various positions in the spectrum. A typical plot of end force coefficients EL, is the one shown in Fig. 55 corresponding to the reference model 10SA. It can be observed that the curves shown are very similar to the parabolic coefficient plots presented in Chapter 6. The end force coefficient curves for this and other models were compared to the corresponding parabolic coefficient plots and a relationship between the two was established as follows:

$$EL_n = (A_2 + b_e) * 0.05\ d_e \quad \text{(top story)} \tag{119}$$

$$EL_1 = (-A_0 \times 10 + b'_e) * 0.05\ d'_e \quad \text{(first story)} \tag{120}$$

where the coefficients b_e, d_e, b'_e and d'_e are given in Table 11. Eqs. (119), and (120) apply for all responses, namely, displacements, accelerations, shears, and moments. The end force coefficients EL at the top and first stories are fractions of the total base reaction to be distributed along the height of the building.

7.3 Relationship to Base Magnitudes

The load system shown in Fig. 9 must remain in equilibrium since the forces are static. Therefore, the total base reaction R, must be divided between the end forces F and the distributed loads P_i. That is,

$$R = F_1 + F_n + \sum_{i=1}^{n} P_i \tag{121}$$

Thus, the end forces are related to the base magnitudes through the equilibrium expression, Eq. (121). In other words, once a value for the total reaction at the base R, is known, the end forces F_1 and F_n must be subtracted from it before distributing the load into story forces P_i. End forces are

given by

$$F_k = EL_k \times R \quad (k = 1 \text{ or } n) \tag{122}$$

Finally, the parameters affecting base magnitudes and vertical distributions were found to be similar to the effects on the end loads. Thus the effects of variation in the parameters on the end loads are accounted for through their direct dependency upon base magnitudes and in particular, vertical distributions.

Equations and concepts developed from the interpretation of the computer data in this and the two preceding chapters are combined in Chapter 8 in the form of a systematic method of analysis.

CHAPTER 8

PROCEDURE FOR THE DETERMINATION OF QUASI-STATIC LATERAL DESIGN LOADS FOR EARTHQUAKE RESISTANT STRUCTURES

The procedure for determination of the lateral design loads is summarized here and is presented in the form of block diagrams in Figs. 56 and 57. In the first figure are shown the steps necessary to calculate the base reaction, and in the second figure those for computing vertical distributions and end load coefficients, and the procedure for combining them together with the base reaction to finally obtain the quasi-static lateral design loads. Each step is accomplished by using the figures and equations indicated in the block diagrams.

8.1 Base Reaction

The input parameters necessary in calculating the reaction at the base are: earthquake magnitude, fundamental frequency, stiffness properties of the structure, number of stories, and total weight of the building. The fundamental frequency may be obtained either by using a standard eigenvalue routine, or from many approximate formulas available in the literature, one of which is[17]

$$f_1 = \frac{\sqrt{D}}{0.05\ h_n} \qquad (57)$$

where h_n is the height in feet above the base to level n, and D is the dimension of the building in feet in a direction parallel to the applied forces. The stiffness properties of the structure, k_i, are defined in

terms of

$$k_i = \frac{6E_i I_i}{L_i^3} \tag{53}$$

where E_i is the modulus of elasticity, I_i is the moment of inertia of the cross sectional area and L_i is the length of member i. The earthquake magnitude is always expressed on Richter scale[22].

The process is subdivided into the following steps:

1. Obtain frequency and base magnitude scaling coefficients, C_{FR}, and C_{BR}, for a given value of earthquake magnitude, M_R, from Fig. 16. Scale the fundamental frequency for the prototype, f_1, by

$$f_1^* = f_1/C_{FR} \tag{69}$$

where f_1^* is the scaled fundamental frequency.

2. Calculate the rigidity power factor P_k, from

$$P_k = \frac{\log\ (\bar{K}_1'/10)}{\log\ (f_1/0.075)} \tag{74}$$

where $\bar{K}_1'$ is the unit total column stiffness for the first story of the prototype as given by

$$\bar{K}_1' = \frac{\bar{k}_{c_1}'}{h_1'} \tag{73}$$

where $\bar{k}_{c_1}'$ is the total column stiffness at the first story (in terms of $\frac{6EI}{L^3}$), and h_1' is the height of the first story in the prototype. The rigidity power factor P_k applies to displacement, shear, and moment response.

3. Obtain reference values of base magnitude $\overline{BM}$, from Figs. 11 and 12, using the scaled fundamental frequency f_1^*, and the rigidity power factor P_k (for shear and moment responses). Reference base magnitudes for displacement, $\overline{BM}^D$, are given by:

$$\overline{BM}^D = BM^D \times (f_1/0.075)^{P_k} \qquad (75)$$

where BM^D are the values obtained directly from Fig. 11.

4. Evaluate the shear-flexural ratio r_t from

$$r_t = \frac{\bar{k}_{b_1}}{\bar{k}_{c_1}} \qquad (76)$$

where $\bar{k}_{b_1}$ and $\bar{k}_{c_1}$ are the total beam and column stiffness at the first story in the prototype.

5. Calculate scaling powers and coefficients, P_{BT} and C_{BT}, using Fig. 20 for displacement response, and the following equations for acceleration, shear, and moment responses. Acceleration response, velocity branch ($f_1^* < 2.35$ cps.):

$$P^A_{BT_v} = \log^{-1}\left[\frac{r_t - 0.33}{0.725}\right] \quad (r_t < 0.33) \qquad (78)$$

$$P^A_{BT_v} = 1.0 \quad (r_t > 0.33) \qquad (81)$$

$$C^A_{BT_v} = 1.0 \qquad (82a)$$

Accleration response, acceleration branch ($f_1^* > 2.35$ cps.):

$$C^A_{BT_a} = \log^{-1}\left[\frac{0.33 - r_t}{2.27}\right] \quad (r_t < 0.33) \qquad (79)$$

$$C^A_{BT_a} = 1.0 \quad (r_t > 0.33) \qquad (80)$$

$$P^A_{BT_v} = 1.0 \qquad (82b)$$

Shear and moment responses:

$$C^{S,M}_{BT} = \log^{-1}\left[\frac{P_k - P_t}{b_t}\right] \quad (r_t < 1) \qquad (88)$$

$$C_{BT}^{S,M} = 1.0 \quad (r_t > 1) \tag{89}$$

where P_t and b_t are given by

$$P_t = \log^{-1}\left[\frac{0.73 - r_t}{4.15}\right] \quad (r_t > 0.33) \tag{84}$$

$$P_t = \log^{-1}\left[\frac{0.54 - r_t}{2.21}\right] \quad (r_t < 0.33) \tag{85}$$

$$b_t = \log^{-1}\left[\frac{r_t + 0.33}{1.41}\right] \quad (r_t > 0.33) \tag{86}$$

$$b_t = \log^{-1}\left[\frac{r_t - 0.06}{0.58}\right] \quad (r_t < 0.33) \tag{87}$$

6. Evaluate the stiffness distribution ratio r_k from

$$r_k = \frac{\bar{k}_{c_n}}{\bar{k}_{c_1}} \tag{55}$$

where $\bar{k}_{c_n}$ and $\bar{k}_{c_1}$ are total column stiffnesses at the top and first stories respectively.

7. Calculate scaling powers and coefficients, P_{BK}, and C_{BK}, from the following equations.

Displacement:

$$C_{BK}^{D} = r_k^{-0.733} \tag{96}$$

Accleration response, velocity branch ($f_1^* < 2.35$ cps.)

$$C_{BK_v}^{A} = r_k^{-0.05} \tag{100}$$

$$P_{BK_v}^{A} = r_k^{0.145} \tag{102}$$

Acceleration response, acceleration branch ($f_1^* > 2.35$ cps.):

$$C_{BK_a}^A = r_k^{0.26} \tag{99}$$

$$P_{BK_a}^A = r_k^{-0.235} \tag{101}$$

Shear and moment responses:

$$C_{BK}^{S,M} = \log^{-1} [0.4 \ (P_k - 1.83) \ \log r_k] \tag{103}$$

8. Calculate scaling coefficients for number of stories, C_{BN}, from the following equations.

Displacement:

$$C_{BN}^D = \log^{-1} \left[\frac{1 - \log N}{0.52} \right] \tag{91}$$

Acceleration:

$$C_{BN}^A = 1.0 \tag{93}$$

Shear and Moment:

$$C_{BN}^{S,M} = \log^{-1} [0.57 \ (P_k - 2.6) \ (\log N - 1)] \tag{94}$$

where N is the number of stories.

9. Scale the reference value of base magnitude $\overline{BM}$, as indicated in the following equation.

$$BM^* = (\overline{BM})^{P_{BT} \times P_{BK}} \times C_{BR} \times C_{BT} \times C_{BK} \times C_{BN} \tag{106}$$

where BM^* is the scaled base magnitude for the prototype. The superscripts D, A, S, or M represent displacement, acceleration, shear, or moment responses, respectively for the scaling powers and coefficients. The scaling powers P_{BT} and P_{BK} are used for acceleration response only.

10. Calculate the total reaction at the base R, for each of the responses, by

$$R = BM^{*} \times W \tag{105}$$

where W is the total weight of the building.

8.2 Quasi-Static Lateral Loads

The input parameters necessary in calculating the quasi-static lateral loads are: fundamental frequency (Eq. (57)), stiffness properties (Eq. (53)), number of stories, story weights, and total reaction at the base as obtained above. The process is subdivided into the following steps (See Fig. 57).

11. Scale the fundamental frequency for the prototype f_1, by

$$f_1^{*'} = f_1 \times C_{FD} \tag{107}$$

where $f_1^{*'}$ is the scaled fundamental frequency. The scaling coefficient C_{FD} is given by

$$C_{FD} = 1.0 \qquad (f_1 < 2.35 \text{ cps.}) \tag{108a}$$

$$C_{FD} = 0.75 \qquad (f_1 > 3.15 \text{ cps.}) \tag{108b}$$

$$f_1^{*'} = 2.35 \text{ cps.} \qquad (2.35 \text{ cps.} < f_1 < 3.15 \text{ cps.}) \tag{108c}$$

12. Obtain reference values for the parabolic coefficients $\bar{A}_0$, $\bar{A}_1$, and $\bar{A}_2$ for the model, from Figs. 39, 40, and 41, using the scaled fundamental frequency $f_1^{*'}$ from step (11).

13. Using the shear-flexural ration r_t, from step 4 above, calculate scaling multipliers and increments, C_{DT}, and $\Delta_T A$, as given by the following equations.

$$C_{DT} = 1.35 \qquad \text{(for all responses)} \tag{112}$$

$$\Delta_T A = \log^{-1}\left[d_t' + \frac{r_t - e_t'}{b_t'}\right] \tag{113}$$

where d_t', e_t', and b_t' are given in Table 8.

14. Using the stiffness distribution ratio r_k, from step 6 above, calculate scaling multipliers and increments, C_{DK}, and $\Delta_K A$, as given by the following equation.

$$C_{DK} = \log^{-1}\left[\frac{\log r_k}{b_k}\right] \tag{115}$$

where b_k equals

-1.72 for displacement,

1.09 for acceleration,

4.0 for shear and moment responses.

$$\Delta_k A = a'_k + b'_k (\log r_k - d'_k) \tag{116}$$

where a'_k, b'_k, and d'_k are given in Table 10.

15. Calculate scaling multipliers and increments for number of stories, C_{DN}, and $\Delta_N A$, as indicated below.

$$C_{DN} = \log^{-1}\left[\frac{1 - \log N}{b_N}\right] \tag{114}$$

where N is the number of stories, b_N equals

0.354 for $A_0 \times 10$,

0.8 for A_1,

0.51 for A_2.

The values of $\Delta_N A$ are obtained from Fig. 49.

16. Scale the parabolic coefficients $\bar{A}_0$, $\bar{A}_1$, and $\bar{A}_2$ obtained from step 12 by

$$A^{*'} = \bar{A} + (\bar{A} \times C_{DT} + \Delta_T A - \bar{A}) + (\bar{A} \times C_{DK} + \Delta_K A - \bar{A}) \tag{118a}$$

and

$$A^{*} = A^{*'} \pm (\bar{A} \times C_{DN} + \Delta_N A - A) \tag{118b}$$

where A^* is the scaled parabolic coefficient for the prototype (subscripts 0, 1, or 2, and superscripts D, A, S, or M, corresponding to displace-

ment, acceleration, shear, or moment responses, respectively). A_0^* and $\bar{A}_0$ are always multiplied by a factor of 10. The (-) sign is used if $A^{*'} > 0$, and the (+) sign is used if $A^{*'} \leq 0$. If no scalings for type of buildings or stiffness distribution are necessary, then $A^{*'} = \bar{A}$.

17. Obtain end load coefficients for the top and first stories, EL_n, and EL_1, from the following equations

$$EL_n = (A_2 + b_e) \times 0.05\, d_e \qquad \text{(top story)} \qquad (119)$$

$$EL_1 = (-A_0 \times 10 + b'_e) \times 0.05\, d'_e \qquad \text{(first story)} \qquad (120)$$

where b_e, d_e, b'_e, and d'_e are given in Table 11.

18. Calculate end forces at the top and first stories F_n, and F_1, by

$$F_k = EL_k \times R \qquad (k = 1 \text{ or } n) \qquad (122)$$

where R is the total reaction at the base as obtained in step 10 above.

19. Calculate vertical distribution coefficients VD by:

$$VD_i = A_0^* + A_1^* \left(\frac{h_i}{h_n}\right) + A_2^* \left(\frac{h_i}{h_n}\right)^2 \qquad (123)$$

where h_i and h_n are the height of story i and the top story above the base, respectively.

20. Calculate the concentrated lateral forces P_i by

$$P_i = VD_i \times w_i \times \frac{R - F_1 - F_n}{W} \qquad (124)$$

where w_i is the weight of story i and W is the total weight of the building.

The concentrated lateral loads P_i, calculated in step 20, the end forces F_1, and F_n, calculated in step 18, and the total reaction at the base R, calculated in step 10 of the preceding section, constitute a quasi-static lateral loading as shown in Fig. 9, that can be used for design purposes.

CHAPTER 9

EXAMPLE

A typical 10-story shear-wall is shown in Fig. 58. The story weight, w_i, and stiffness, $k_i = 6EI_i/L_i^3$, are also given. The wall is made of concrete of the following properties.

$$E = 3 \times 10^3 \text{ ksi}$$

$$\rho = 150 \text{ lb./ft}^3$$

The structure is to be subjected to the proposed method. The resulting quasi-static loads are compared to those obtained from a rigorous computer analysis.

9.1 Base Reaction

The fundamental frequency of the structure calculated by means of and eigenvalue routine is

$$f_1 = 1.42 \text{ cps.}$$

The method is applied by following the same steps given in Chapter 8 and illustrated in Figs. 56 and 57. The various results obtained are shown in Table 13.

1. A standard earthquake spectrum of magnitude $M_R = 7.4$ was used. Therefore, from Fig. 16, $C_{FR} = C_{BR}^D = C_{BR}^A = C_{BR}^{S,M} = 1.0$, and from Eq. (69) $f_1^* = f_1 = 1.42$ cps.

2. Using $\bar{k}'_{c_1} = 179$ and $h'_1 = 120$ as shown in Fig. 58, the rigidity power factor given by Eq. (74) is

$$P_k = \frac{\log\left(\frac{179 \times 10^3}{120 \times 10}\right)}{\log\left(\frac{1.42}{0.075}\right)} = 1.7$$

3. Using $P_k = 1.7$ and $f_1^* = 1.42$, reference base magnitudes $\overline{BM}$, were obtained from Figs. 11, and 12, as indicated in Table 13. Base magnitudes for displacement are scaled as indicated by Eq. (75):

$$\overline{BM}^D = 3.1 \times 10^{-4} \times (1.42/0.075) = 4.65 \times 10^{-2}$$

4. The shear-flexural ratio is zero, since this may be considered as a pure-flexural structure as shown in Fig. 58.

5. Scaling powers and coefficients P_{BT}, and C_{BT} given by Eqs. (78), and (88), and Fig. 20 are:

$$C_{BT}^D = 0.005 \qquad \text{(Fig. 20)}$$

Since $f_1^* < 2.35$ cps. the building behaves in the velocity branch.

$$P_{BT_v}^A = \log^{-1}\left[\frac{0 - 0.33}{0.725}\right] = 0.35 \qquad \text{(Eq. (78))}$$

$$C_{BT_v}^A = 1.0 \qquad \text{(Eq. (82a))}$$

$$P_t = \log^{-1}\left[\frac{0.54 - 0}{2.21}\right] 1.76 \qquad \text{(Eq. (85))}$$

$$b_t = \log^{-1}\left[\frac{0 - 0.06}{0.58}\right] = 0.79 \qquad \text{(Eq. (87))}$$

$$C_{BT}^{S,M} = \log^{-1}\left[\frac{1.7 - 1.76}{0.79}\right] = 0.84 \qquad \text{(Eq. (88))}$$

6. Again using $\bar{k}$ from Fig. 58, the stiffness distribution ratio is:

$$r_k = \frac{4.85}{179.0} = 0.027 \qquad \text{(Eq. (55))}$$

7. Scaling powers and coefficients for stiffness distribution r_k are:

$$C_{BK}^{D} = 0.027^{-0.733} = 13.5 \qquad \text{(Eq. (96))}$$

$$C_{BK_V}^{A} = 0.027^{-0.05} = 1.2 \qquad \text{(Eq. (100))}$$

$$P_{BK_V}^{A} = 0.027^{0.145} = 0.59 \qquad \text{(Eq. (102))}$$

$$C_{BK}^{S,M} = \log^{-1}[0.4(1.7-1.83)\ \log 0.027] = 1.21 \qquad \text{(Eq. (103))}$$

8. Since N = 10, no correction for number of stories is necessary. Therefore, $C_{BN}^{D} = C_{BN}^{A} = C_{BN}^{S,M} = 1.0$.

9. The scaled base magnitudes are given by Eq. (106).

$$BM^{D*} = 4.65 \times 10^{-2} \times 1.0 \times 0.005 \times 13.5 \times 1.0 = 0.3 \times 10^{-2}$$

$$BM^{A*} = (1.37)^{0.35 \times 0.59} \times 1.0 \times 1.0 \times 1.2 \times 1.0 = 1.28$$

$$BM^{S,M*} = (0.32) \times 1.0 \times 0.84 \times 1.21 \times 1.0 = 0.325$$

10. Using W = 236.6 from Fig. 58, the total reactions at the base as given by Eq. (105) are

$$R^{D} = 0.3 \times 10^{-2} \times 236.6 = 0.71 \text{ kips}$$

$$R^{A} = 1.28 \times 236.6 = 302.0 \text{ kips}$$

$$R^{S,M} = 0.325 \times 236.6 = 77.0 \text{ kips}$$

9.2 Quasi-Static Lateral Loads

11. $f_1 < 2.35$ cps. Therefore, $C_{FD} = 1$ and $f_1^{*'} = f_1 = 1.42$ cps.

12. Using $f^{*'} = 1.42$, reference values for the parabolic coefficients were obtained from Figs. 39, 40, and 41, and tabulated in Table 14.

13. $C_{DT} = 1.35$ for all responses (Eq. (112)). Values of $\Delta_T A$ calculated by Eq. (113), are given in Table 14.

14. $C_{DK}^{D} = \log^{-1}\left[\frac{\log 0.027}{-1.72}\right] = 1.65$ (Eq. (115))

$C_{DK}^{A} = \log^{-1}\left[\frac{\log 0.027}{1.09}\right] = 0.46$ (Eq. (115))

$C_{DK}^{S,M} = \log^{-1}\left[\frac{\log 0.027}{4.0}\right] = 0.81$ (Eq. 115))

Values of $\Delta_K A$ calculated by Eq. (116) are given in Table 14.

15. Since N = 10, then $C_{DN} = 1$ and $\Delta_N A = 0$.

16. Scaled parabolic coefficients are obtained from Eq. (118) and tabulated in Table 14.

17. End load coefficients obtained from Eqs. (119), and (120) are given in Table 15.

18. Forces at top and first stories given by Eq. (122) are presented in Table 15.

19. Vertical distributions given by Eq. (123) are shown in Table 16.

20. Concentrated lateral loads P_i given by Eq. (124) are also shown in Table 16.

All these steps are condensed in Tables 13 to 16. Values of base magnitudes, and vertical distributions obtained from a rigorous computer analysis are given in the tables for purpose of comparison. The error between the equivalent static loads obtained from the computer analysis and those obtained by the procedure presented is less than 45%. The sum of the vertical distributions is approximately 1.0 which indicates that the equilibrium equation (Eq. (121)) is satisfied. The resulting quasi-static lateral design loads are shown in Fig. 59 for each response independently.

CHAPTER 10

CONCLUSIONS

A procedure for determining the design lateral loads for earthquake resistant structures is presented. These quasi-static lateral loads are obtained as indicated in Chapter 8 without the need for either a modal analysis or time-domain iteration procedure. A parameter variation study of the dynamic behavior of multi-story buildings subjected to seismic motions was performed. Parameters such as earthquake magnitude, rigidity of the structure, shear-flexural ratio, stiffness and mass distributions, and number of stories, were changed and the effect on the responses of interest, namely, displacement, acceleration, shear, and overturning moment, were observed.

For each structure a modal analysis was performed and the square root of the sum of the squares of the maximum modal response was determined. Plots of equivalent static loads were developed. From these plots a set of concentrated loads composed of forces distributed parabolically throughout the height of the structure plus concentrated forces at the top and first stories were developed which correlated extremely well with the plots resulting from modal analysis. The linear variations used in the present California Code[15] corresponds to the special case ($f_1 \approx 2$ cps.) in which the parabolic lateral load shape changes from concave to convex.

Although some correlation in the effects of parameters on the responses occurs, it is shown that a unique lateral loading is necessary for each response, i.e., displacement, acceleration, shear, and moment.

In an effort to simplify the procedure the effect of each parameter

was assumed to be independent. The errors resulting from this assumption were less than 22 per cent on the average and the largest discrepancy was less than 45 per cent on the conservative side. These errors are acceptable in view of the present gross inability to predict the magnitude of future earthquakes.

10.1 Further Studies

Additional simplification of the method may be achieved by elimination of some charts such as Figs. 16, 20, and 49 which may be approximated by straight lines and thereby reduced to a set of equations. Then the proposed method could be programmed for solution by computer or by hand.

Responses obtained by this method bound the SRSS (square root of the sum of the squares) modal responses of the system. A similar procedure could be developed, the response of which bounds the absolute (ABS) responses. A combination of these procedures could be developed which would represent more nearly the response of actual structures.

In addition, these procedures could be extended to include other structures and parameters. Damping may be incorporated as a coefficient affecting the magnitude of the earthquake. Amplification factors for soil structure interaction affecting the magnitude of the base motion may be included in the method.

Safety factors resulting from inelastic response need to be evaluated. Ideally, a structure should be elastic and useful after an earthquake. However, future earthquake magnitudes are unknown; thus the additional resistance to collapse, introduced by inelastic action, should be studied.

Finally, since it has been shown that a separate loading is desirable for each response, namely, displacement, acceleration, shear, and overturning moment, these loadings should be incorporated into the building codes.

APPENDIX A

A. Geometric Function

A straight line in log-log scale corresponds to a geometric function of the form $Y = a\ x^b$ as will be demonstrated here.

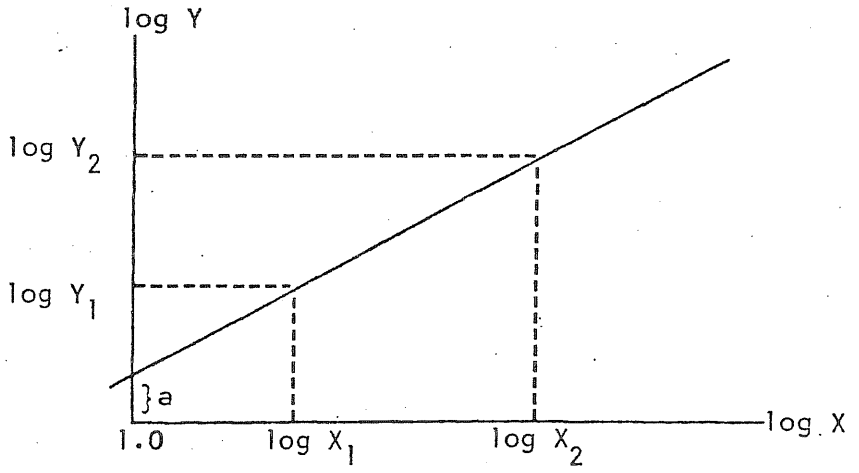

From the figure above, the logarithmic slope of the line is given by

$$b = \frac{\log Y_2 - \log Y_1}{\log X_2 - \log X_1} \qquad (1)$$

from which it follows that

$$\log Y_2 = \log Y_1 + b\ (\log X_2 - \log X_1)$$

The interception a, of the line with the 1.0 abscissa is called the pivot. If $Y_1 = a$ for $X_1 = 1$ ($\log X_1 = 0$), then,

$$b = \frac{\log Y_2 - \log a}{\log X_2} \qquad (2)$$

and

$$\log Y_2 = \log a + b \log X_2$$

or

$$Y = ax^b \qquad (3)$$

which is the equation of the geometric function.

From Eq. (1),

$$\log X_2 = \log X_1 + \frac{\log Y_2 - \log Y_1}{b}$$

If $Y_1 = a$ for $X_1 = 1$ ($\log X_1 = 0$), then,

$$\log X_2 = \frac{\log Y_2 - \log a}{b}$$

or

$$X_2 = \log^{-1}\left[\frac{\log Y_2 - \log a}{b}\right] \qquad (4)$$

Eqs. (3) and (4) are two ways of expressing the geometric function, and thus they represent a straight line in a log-log scale.

B. Logarithmic Function

A straight line in a semi-log scale corresponds to a logarithmic function of the form

$$X = \log^{-1}\left[\frac{Y - a}{b}\right]$$

as demonstrated below.

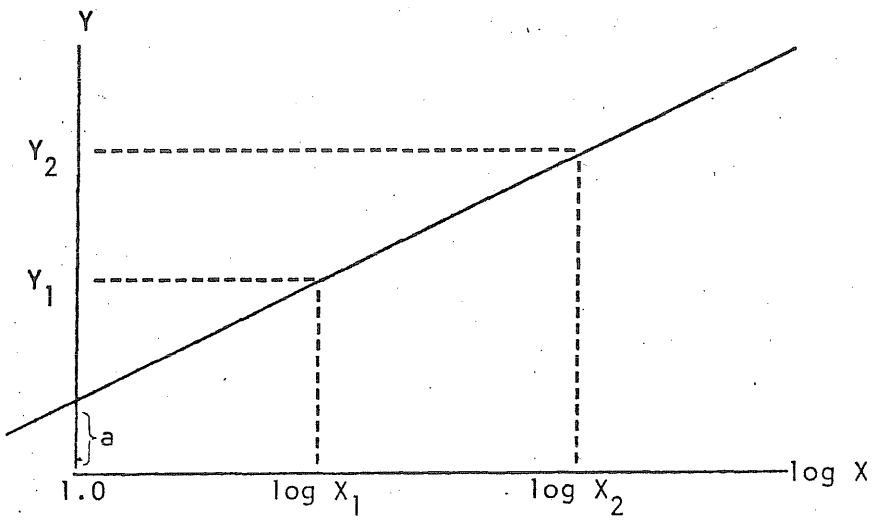

From the figure above, the semi-log slope of the line is

$$b = \frac{Y_2 - Y_1}{\log X_2 - \log X_1} \tag{5}$$

Therefore,

$$Y_2 = Y_1 + b\ (\log X_2 - \log X_1) \tag{6}$$

The interception a, of the line with the 1.0 abscissa is called the pivot. If $Y_1 = a$ for $X_1 = 1$ ($\log X_1 = 0$), then,

$$b = \frac{Y_2 - a}{\log X_2} \tag{7}$$

and

$$Y_2 = a + b \log X_2 \tag{8}$$

From Eq. (7)

$$\log X_2 = \log X_1 + \frac{Y_2 - Y_1}{b}$$

If $Y_1 = a$ and $X_1 = 1$, then,

$$\log X_2 = \frac{Y_2 - a}{b}$$

or

$$X_2 = \log^{-1}\left[\frac{Y_2 - a}{b}\right] \tag{9}$$

which is the equation of the logarithmic function. Thus, Eqs. (4) and (5) represent a straight line in a semi-log scale.

REFERENCES

1. W. C. Hurty, M. F. Rubinstein, Dynamics of Structures, Prentice-Hall, 1964.

2. J. S. Przemieniecki, Theory of Matrix Structural Analysis, McGraw-Hill, 1968.

3. J. S. Archer, "Consistent Mass Method for Distributed Mass Systems," Journal of the Structural Division, ASCE, Aug. 1963.

4. H. L. Langhaar, Energy Methods in Applied Mechanics, John Wiley & Sons, 1962.

5. R. E. Bishop, G. M. L. Gladwell, S. Michaelson, The Matrix Analysis of Vibration, Cambridge University Press, 1965.

6. J. W. Strutt, Baron Rayleigh, The Theory of Sound, Dover Publications, 1945.

7. J. N. Ramsden, J. R. Stoker, "Mass Condensation: A Semi-automatic Method for Reducing the Size of Vibration Problems," International Journal for Numerical Methods in Engineering, Vol. 1, No. 4, 1969.

8. S. J. Fenves, N. M. Newmark "Seismic Forces and Overturning Moments in Buildings, Towers, and Chimneys," Proc. 4th World Conference on Earthquake Engineering, Santiago de Chile, 1969.

9. N. M. Newmark, "Numerical Procedure for Computing Deflections, Moments and Buckling Loads, Proc. ASCE, Vol. 68, 1942.

10. W. G. Godden, Numerical Analysis of Beam and Column Structures, Prentice-Hall, 1965.

11. N. M. Newmark, "A Method of Computation for Structural Dynamics, Journal of the Engineering Mechanics Division, ASCE, Vol. 85, No. EM3, July 1959.

12. J. M. Biggs, Introduction to Structural Dynamics, McGraw Hill, 1964.

13. E. L. Wilson, R. W. Clough, "Dynamic Response by a Step-by-Step Analysis," Proc. Symposium on the Use of Computers in Civil Engineering, Lisbon, 1962.

14. J. A. Blume, N. M. Newmark, L. H. Corning, Design of Multi-story Reinforced Concrete Buildings for Earthquake Motions, Portland Cement Association, 1961.

15. Recommended Lateral Force Requirements and Commentary, Seismology Committee, Structural Engineers Association of California, 1968.

16. M. F. Rubinstein, W. C. Hurty, "Effect of Joint Rotation on Dynamics of Structure," Journal of the Engineering Mechanics Division, Proc. of the ASCE, Vol. 87, No. EM 86, December, 1961.

17. A. W. Anderson, J. A. Blume, H. J. Degenkolb, H. B. Hammill, E. M. Knapik, H. L. Powers, J. E. Rinne, G. A. Sedgwick, and H. O. Sjoberg, "Lateral Forces for Earthquake and Wind," Transactions, ASCE, Vol. 117, 1962, pp. 716-780.

18. A. S. Veletsos, N. M. Newmark, "Effect of Inelastic Behavior on the Response of Simple Systems to Earthquake Motions," Proc. Second World Conference on Earthquake Engineering, Tokyo, 1960, Vol. II, pp. 895-912.

19. G. V. Berg, S. S. Thomaides, "Energy Consumption by Structures in Strong Motion Earthquakes," University of Michigan, College of Engineering, Progress Report on UMRI Project 2881, March, 1960.

20. J. Penzien, "Elasto-Plastic Response of Idealized Multi-story Structures Subjected to a Strong Motion Earthquake," Proc. Second World Conference on Earthquake Engineering, Tokyo, 1960, Vol. II, pp. 739-760.

21. N. M. Newmark, W. J. Hall, "Seismic Design Criteria for Nuclear Reactor Facilities," Proc. 4th World Conference on Earthquake Engineering, Santiago de Chile, 1969, Vol. II.

22. B. Gutenberg, C. F. Richter, "Earthquake Magnitude, Intensity, Energy, and Acceleration," Bull. Seismic Society of America, Vol. 32, p. 163, 1942, Second paper, ibid., Vol. 46, p. 105, 1956.

23. H. O. Wood, F. Newmann, "Modified Mercalli Intensity Scale of 1931," Bull. Seismic Society of America, Vol. 23, p. 277, 1931.

24. G. W. Housner, "Design Spectrum," Earthquake Engineering, R. L. Wiegel, ed., Prentice-Hall, 1970, Chapter 5, p. 95.

25. U. S. Atomic Energy Commission, Nuclear Reactors and Earthquakes, TID-7024, Washington, D.C.: Office of Technical Services, 1963.

26. J. W. Melin, "POST - Problem Oriented Subroutine Translator," Civil Engineering Studies, Civil Engineering Systems Laboratory Research Series No. 3, Department of Civil Engineering, University of Illinois, Urbana, Illinois, March, 1969.

27. M. R. Spiegel, Statistics, Schaum's Publishing Company, New York, 1961.

28. L. S. Jacobsen, R. S. Ayre, Engineering Vibrations, McGraw-Hill Company, New York, 1968.

TABLE 1

Properties of the Models Studied

Models Reference	Number of Stories	Case	r_k	r_m	r_t
4SA	4	A	1	1	∞
5SA	5	A	1	1	∞
6SA	6	A	1	1	∞
7SA	7	A	1	1	∞
10SA	10	A	1	1	∞
10SB1	10	B	0.0525	1	∞
10SB2	10	B	0.182	1	∞
10SC	10	C	1	0.0525	∞
10SD	10	D	0.0525	0.0525	∞
10FA	10	A	1	1	0
10FB	10	B	0.0525	1	0
10FC	10	C	1	0.0525	0
10SFA1	10	A	1	1	1.0
10SFA2	10	A	1	1	0.66
10SFA3	10	A	1	1	0.33
20SA	20	A	1	1	∞
30SA	30	A	1	1	∞

TABLE 2

Magnitudes of Some Past Earthquakes

Earthquake	Int_1	Int_2	Magnitude	
			Richter	Mercalli
El Centro, 1940 (N-S)	7.8	6.9	6.0	7.5
El Centro, 1940 (E-W)	7.1	6.4	5.6	7.5
El Centro, 1934 (N-S)	7.6	6.8	5.9	6.0
El Centro, 1934 (E-W)	7.7	6.9	5.9	6.0
Taft, 1952 (N-E)	7.0	6.4	5.5	---
Taft, 1952 (S-E)	7.2	6.5	5.6	---
Olympia, 1949	7.2	6.5	5.6	8.0
Ferndale, 1954	7.2	6.5	5.6	6.0

TABLE 3

Effect of Earthquake Magnitude on Base Magnitudes

M_R	C_{FR}	C_{BR}^{D}	C_{BR}^{A}	$C_{BR}^{S,M}$
6.1	0.69	0.41	0.195	0.223
6.6	0.83	0.54	0.355	0.397
7.1	0.96	0.76	0.638	0.695
7.4	1.00	1.00	1.000	1.000

TABLE 6

Effect of Stiffness Distribution on Base Magnitudes

P_k	$C_{BK}^{S,M}$	
	$r_k = 0.182$	$r_k = 0.0525$
1.1	1.64	2.39
1.2	1.54	2.11
1.3	1.44	1.88
1.4	1.34	1.67
1.5	1.26	1.48
1.6	1.18	1.33
1.7	1.10	1.16
1.8	1.03	1.04
1.9	0.97	0.93
2.0	0.91	0.82

TABLE 7

Correlation Coefficients for Model 10SA

Response	cr maximum	cr minimum
Displacement	0.9977	0.9975
Acceleration	1.0106	0.9976
Shear	1.0000	0.9973
Moment	1.0000	0.9986

TABLE 8

Coefficients for Scaling Increment $\Delta_T A$ (Eq. 113)

$\Delta_T A$	r_t	b'_t	d'_t	e'_t
$\Delta_T A_0^D \times 10$	> 0.66	-7.73	-0.864	1.00
$\Delta_T A_0^D \times 10$	$0.33 < r_t < 0.66$	4.13	-0.820	0.66
$\Delta_T A_0^D \times 10$	< 0.33	0.53	-0.900	0.33
$-\Delta_T A_1^D$	> 0.33	-17.2	-0.655	1.00
$-\Delta_T A_1^D$	< 0.33	-1.82	-0.616	0.33
$\Delta_T A_2^D$	> 0.33	-6.30	-0.761	1.00
$\Delta_T A_2^D$	< 0.33	-1.18	-0.655	0.33
$\Delta_T A_0^A \times 10$	> 0.33	---	1.000	$= r_t$
$\Delta_T A_0^A \times 10$	< 0.33	-0.92	-2.000	0.30
$-\Delta_T A_1^A$	> 0.33	-33.5	-1.030	1.00
$-\Delta_T A_1^A$	< 0.33	-1.05	-1.010	0.33
$\Delta_T A_2^A$	> 0.33	-3.35	-1.430	1.00
$\Delta_T A_2^A$	< 0.33	-0.45	-1.230	0.33
$\Delta_T A_0^{S,M} \times 10$	all r_t	-3.0	-0.540	1.00
$-\Delta_T A_1^{S,M}$	> 0.33	-3.95	-0.560	1.00
$-\Delta_T A_1^{S,M}$	< 0.33	-1.12	-0.390	0.33
$\Delta_T A_2^{S,M}$	> 0.33	-3.25	-0.610	1.00
$\Delta_T A_2^{S,M}$	< 0.33	-1.33	-0.480	0.33

TABLE 9

Example of Scaling Parabolic Coefficients

Frequency	$\bar{A}_0^S \times 10$ ($r_t = \infty$)	$A_0^{S*} \times 10$ ($r_t = 1$)	$A_0^S \times 10$ (real)
2.2 cps.	0.1	0.418	0.42
1.775	0.2	0.555	0.57
1.475	0.3	0.695	0.73
1.275	0.4	0.830	0.87
1.150	0.5	0.960	0.98

TABLE 12

Summary of Effect of Parameters

Effect of	On BM		On VD	
	Parameter	Scaling	Parameter	Scaling
Earthquake Magnitude	M_R	C_{BR}, C_{FR}	---	---
Rigidity of Structure	$\bar{K}_1'$	P_k	---	---
Type of Building	r_t	C_{BT}, P_{BT}	r_t	$C_{DT}, \Delta_T A$
Number of Stories	N	C_{BN}	N	$C_{DN}, \Delta_N A$
Stiffness Distribution	r_k	C_{BK}, P_{BK}	r_k	$C_{DK}, \Delta_K A$
Mass Distribution	r_m	W	r_m	w_i

TABLE 13

Example, Base Reaction

	Displacement	Acceleration	Shear & Moment
BM^D (Fig. 11)	3.1×10^{-4}	---	---
$\overline{BM}$ (Eq. 75 or Figs. 11 and 12)	4.65×10^{-2}	1.37	0.32
C_{BR} (Fig. 16)	1.0	1.0	1.0
C_{BT}^D (Fig. 20	0.0054	---	---
C_{BK}^D (Eq. 96)	13.5	---	---
$P_{BT_v}^A$ (Eq. 78)	---	0.35	---
$C_{BT_v}^A$ (Eq. 82a)	---	1.0	---
$C_{BK_v}^A$ (Eq. 100)	---	1.2	---
$C_{BT}^{S,M}$ (Eq. 88)	---	---	0.84
$C_{BK}^{S,M}$ (Eq. 103)	---	---	1.21
C_{BN} (Eqs. 91-94)	1.0	1.0	1.0
BM^* (Eq. 106)	0.3×10^{-2}	1.28	0.325
BM (Computer)	0.38×10^{-2}	1.429	0.177
R (kips) (Eq. 105)	0.71	302.0	77.0

TABLE 14

Example, Parabolic Coefficients

	Displacement			Acceleration			Shear and Moment		
	$A_o \times 10$	A_1	A_2	$A_o \times 10$	A_1	A_2	$A_o \times 10$	A_1	A_2
Reference Values, $\bar{A}$	0.19	0.19	-0.055	0.68	0.05	0.012	0.32	0.09	0.05
C_{DT}	1.35	1.35	1.35	1.35	1.35	1.35	1.35	1.35	1.35
C_{DK}	1.65	1.65	1.65	0.46	0.46	0.46	0.81	0.81	0.81
Total C (1)	3.0	3.0	3.0	1.81	1.81	1.81	2.16	2.16	2.16
(1) - 1 (2)	2.0	2.0	2.0	0.81	0.81	0.81	1.16	1.16	1.16
(2) x $\bar{A}$ (3)	0.38	0.38	-0.110	0.55	0.0405	0.0098	0.37	0.104	0.058
b'_t (Table 8)	0.53	-1.82	-1.18	-0.92	-1.05	-0.45	-3.0	-1.12	-1.33
d'_t (Table 8)	-0.900	-0.616	-0.655	-2.000	-1.010	-1.230	-0.540	-0.390	-0.480
e'_t (Table 8)	0.33	0.33	0.33	0.30	0.33	0.33	1.00	0.33	0.33
$\Delta_T A$ (4)	0.0361	-0.3654	0.420	-0.2121	-0.2480	0.320	0.6221	-0.6347	0.696
a'_k (Table 10)	0.3933	-0.4236	0.3770	0.4031	-0.1537	0.2420	0.0825	-0.0980	0.1390
b'_k (Table 10)	-0.600	0.460	-0.395	-0.510	0.260	-0.269	-1.320	0.380	-0.040
d'_k (Table 10)	-1.28	-1.28	-1.28	-1.28	-1.28	-1.28	-1.28	-1.28	-1.28
$\Delta_k A$ (5)	0.566	-0.552	0.49	0.552	-0.215	0.32	0.095	-0.109	0.148
A^* (3) + (4) + (5)	0.9821	-0.5374	0.800	0.8899	-0.4225	0.6498	1.0871	-0.6397	0.902

TABLE 15

Example, End Forces

	Displacement	Acceleration	Shear	Moment
b'_e (Table 11)	0	0.02	0	0.8
d'_e (Table 11)	1.0	0.9	0.8	0.7
EL_1 (Eq. 120)	-0.049	-0.039	-0.043	-0.036
b_e (Table 11)	-0.40	0.08	-0.02	1.0
d_e (Table 11)	1.0	0.6	1.0	0.9
EL_n (Eq. 119)	0.002	0.022	0.044	0.025
F_1 (kips)(Eq. 122)	-3.53×10^{-2}	-11.8	-3.30	-2.77
F_n (kips) (Eq. 122)	1.42×10^{-2}	6.65	3.40	1.92
$F_1 + F_n$	-2.11×10^{-2}	-5.15	0.10	-0.85
$R - F_1 - F_n$	73.11×10^{-2}	296.85	76.90	76.15

TABLE 16

Example, Quasi-Static Loads

Story	Displacement			Acceleration			Shear and Moment		
	VD	P_i (10^{-2} kips)	VD (Computer)	VD	P_i (kips)	VD (Computer)	VD	P_i (kips)	VD (Computer)
10	0.358	25.0	0.204	0.319	94.0	0.160	0.369	28.1	0.228
9	0.262	18.2	0.156	0.239	71.0	0.133	0.260	19.8	0.151
8	0.176	12.2	0.107	0.159	47.0	0.122	0.173	13.2	0.094
7	0.108	7.5	0.087	0.114	33.8	0.097	0.099	7.58	0.082
6	0.061	4.22	0.052	0.070	20.7	0.083	0.049	3.75	0.048
5	0.028	1.94	0.047	0.041	12.2	0.071	0.014	1.07	0.043
4	0.010	0.69	0.030	0.025	7.4	0.049	-0.002	-0.153	0.029
3	0.008	0.55	0.022	0.022	6.5	0.036	-0.002	-0.153	0.021
2	0.022	1.54	0.011	0.029	8.6	0.019	0.017	1.30	0.012
1	0.052	3.60	0.005	0.052	15.4	0.010	0.054	4.15	0.006

Check: $1.085 \approx 1.0 \therefore$ o.k. $1.070 \approx 1.0 \therefore$ o.k. $1.031 \approx 1.0 \therefore$ o.k.

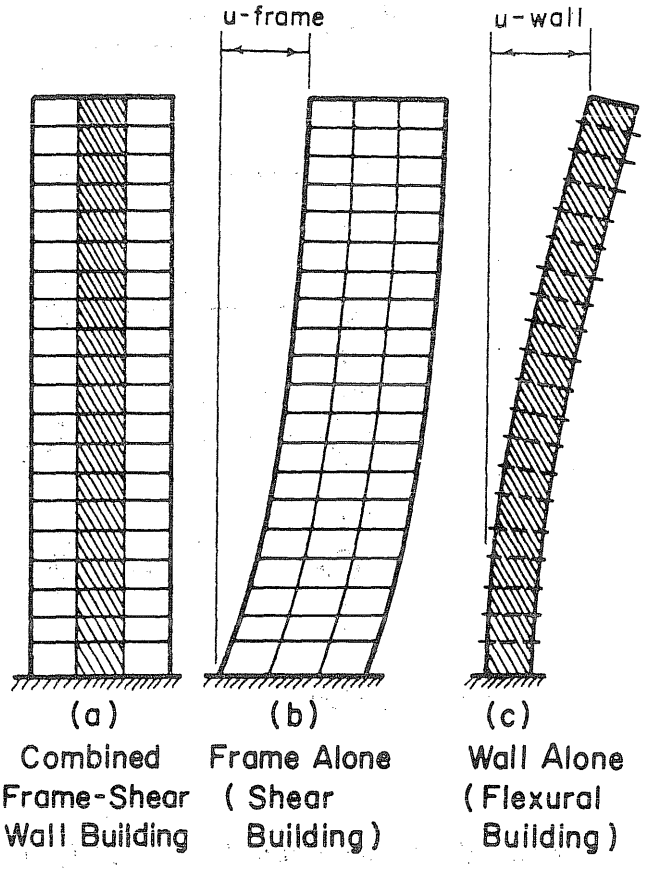

FIG. 1 SHEAR AND FLEXURAL STRUCTURES

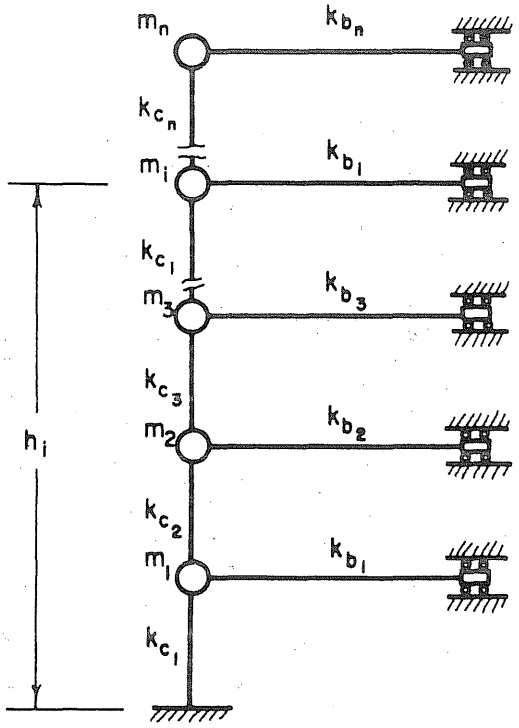

FIG. 2 MATHEMATICAL MODEL

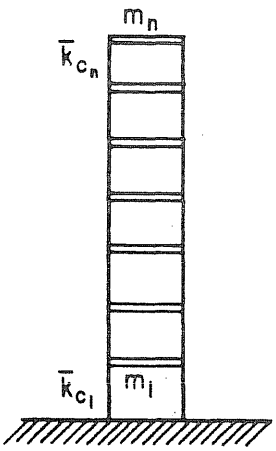

Constant Stiffness (K)
Constant Mass (M)

Case A

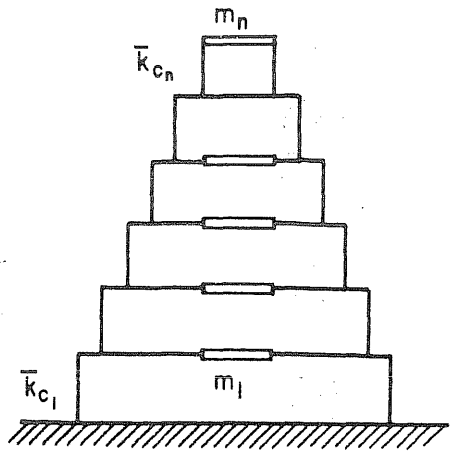

Linear Varying Stiffness (K)
Constant Mass (M)

Case B

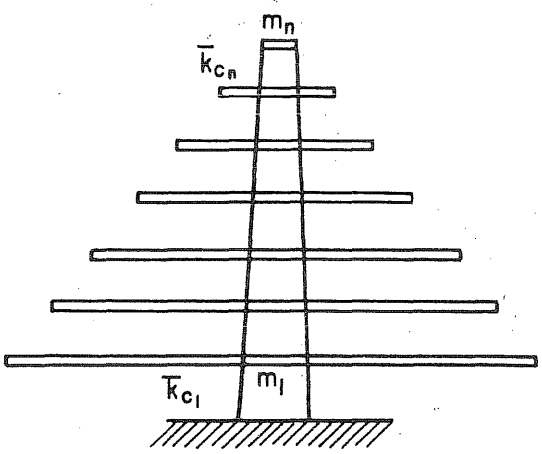

Constant Stiffness (K)
Linear Varying Mass (M)

Case C

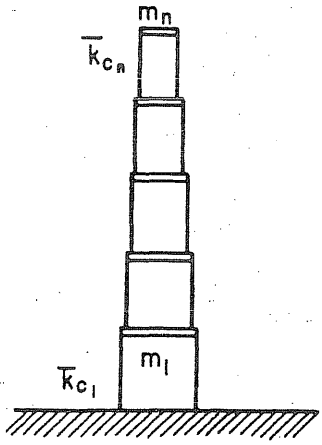

Linear Varying Stiffness (K)
Linear Varying Mass (M)

Case D

FIG. 3 BASIC CASES STUDIED

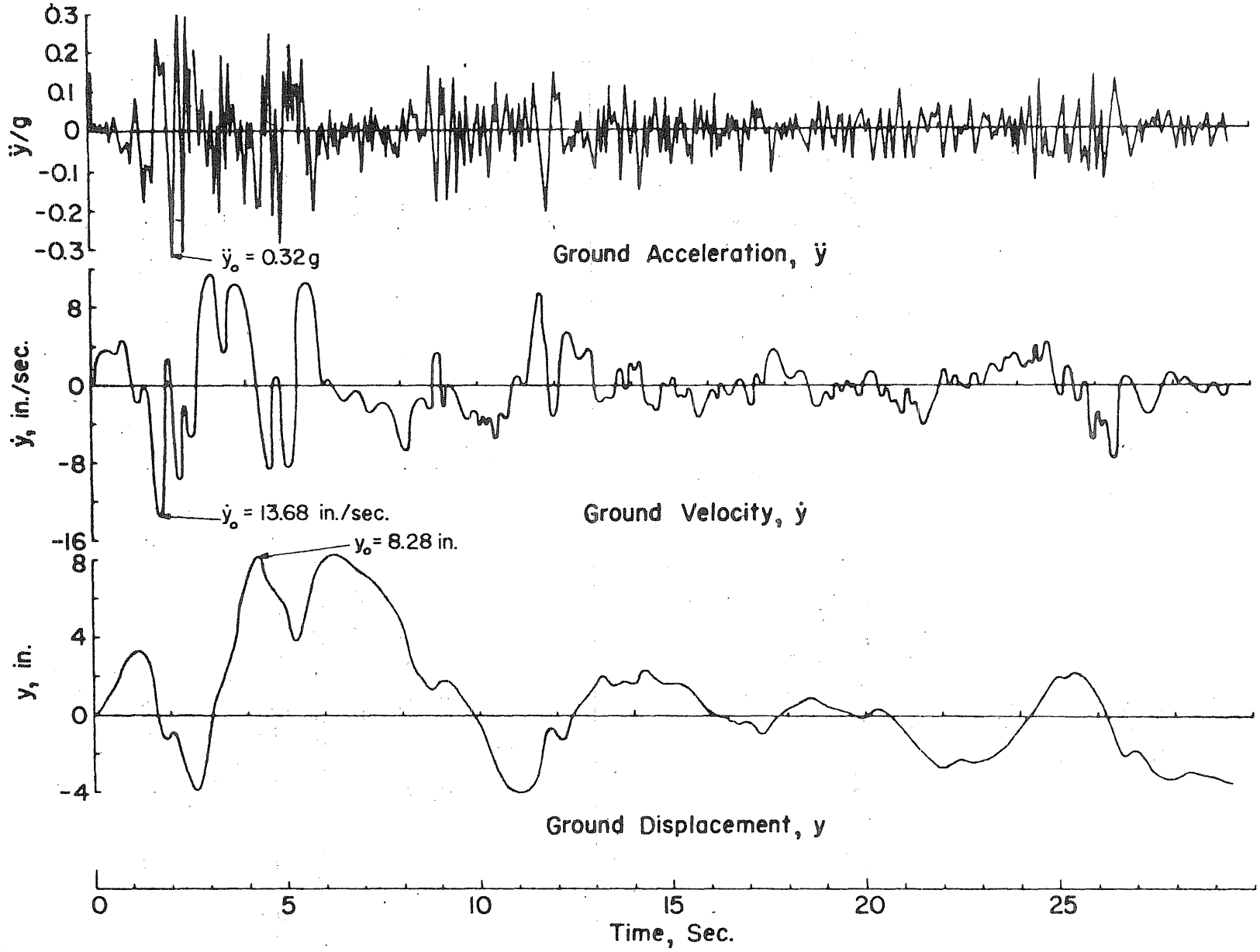

FIG. 4 EL CENTRO, CALIFORNIA EARTHQUAKE OF MAY 18, 1940, N-S COMPONENT

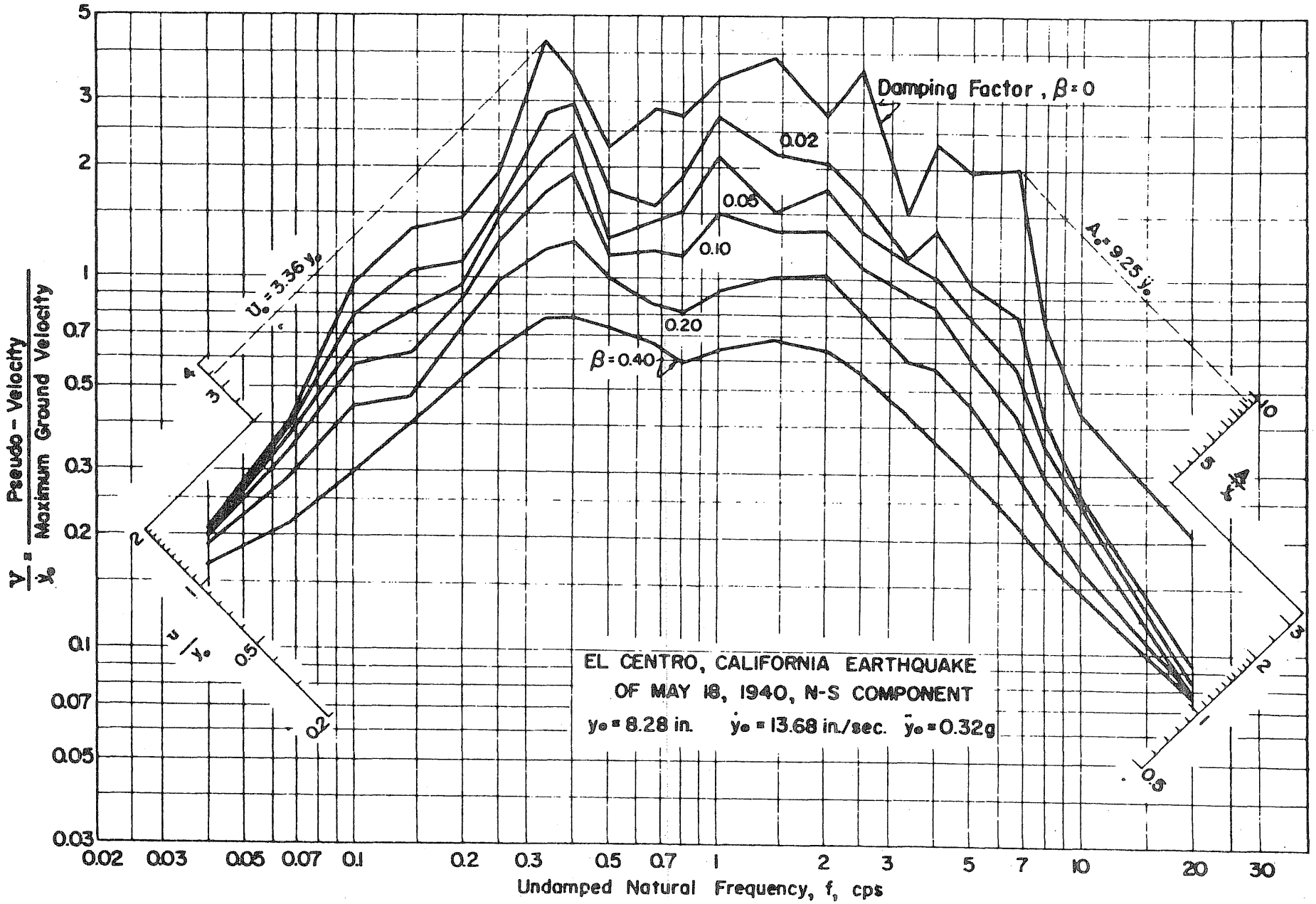

FIG. 5 DEFORMATION SPECTRA FOR ELASTIC SYSTEMS – EL CENTRO QUAKE

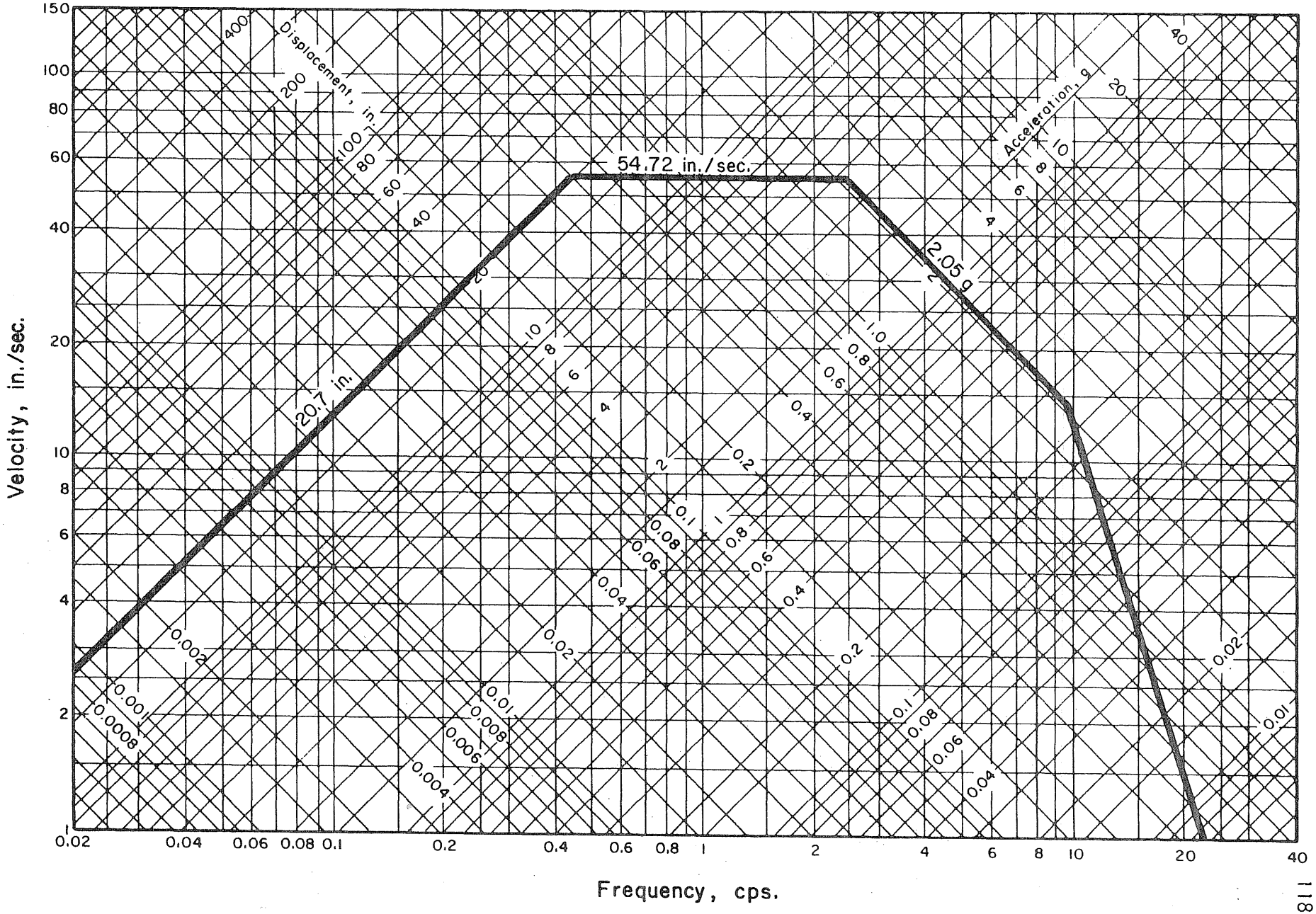

FIG. 6 STANDARD EARTHQUAKE SPECTRUM

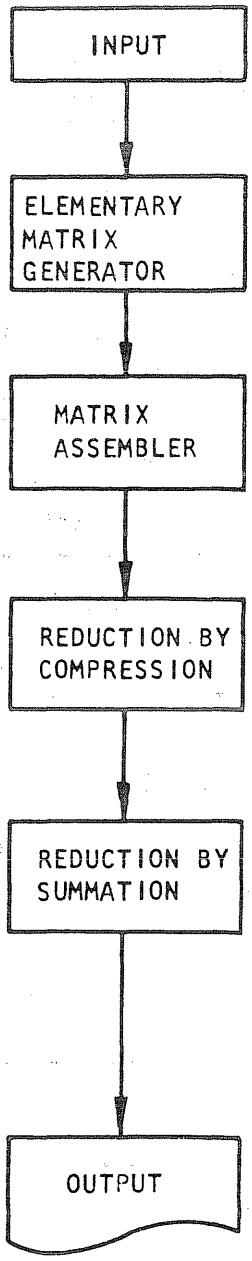

FIG 7, BLOCK DIAGRAM FOR GEUGEN

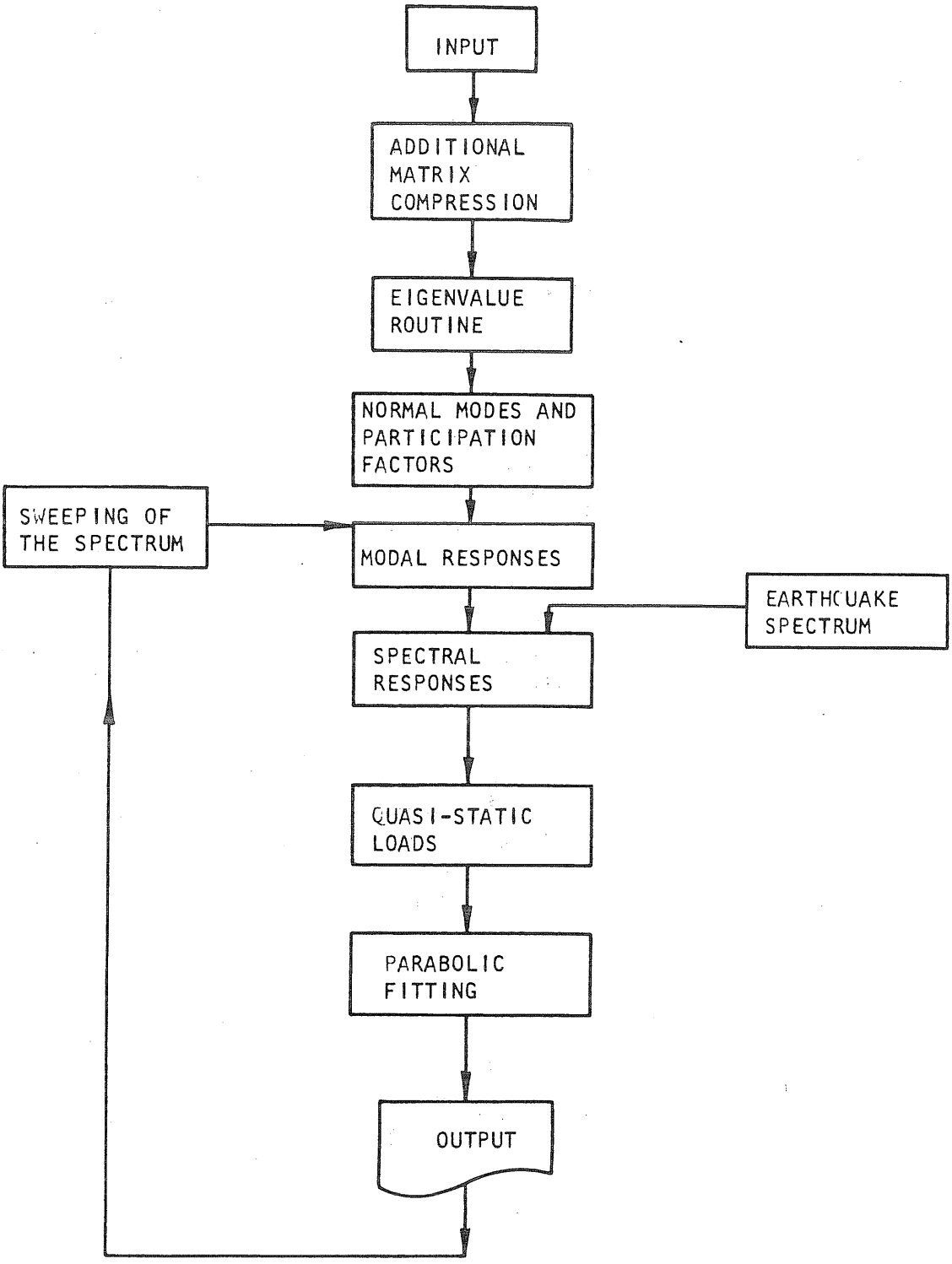

FIG. 8, BLOCK DIAGRAM FOR GEUDYN

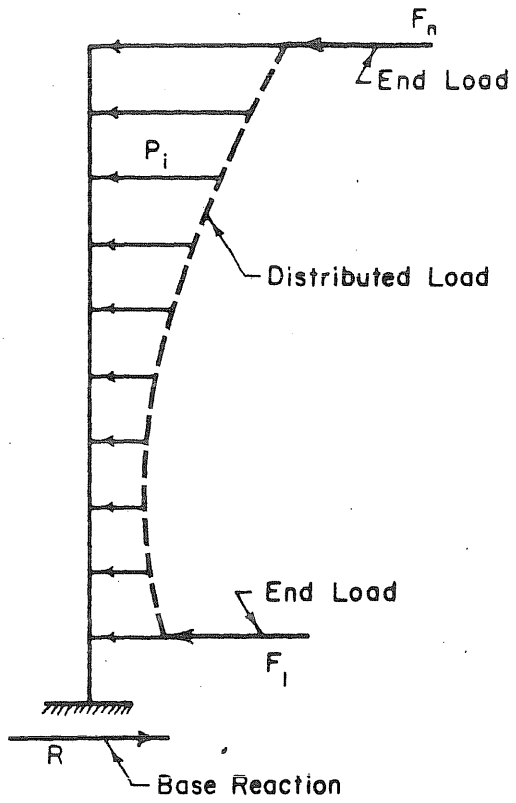

FIG. 9 STATIC LATERAL LOADING FOR EARTHQUAKE RESISTANT DESIGN

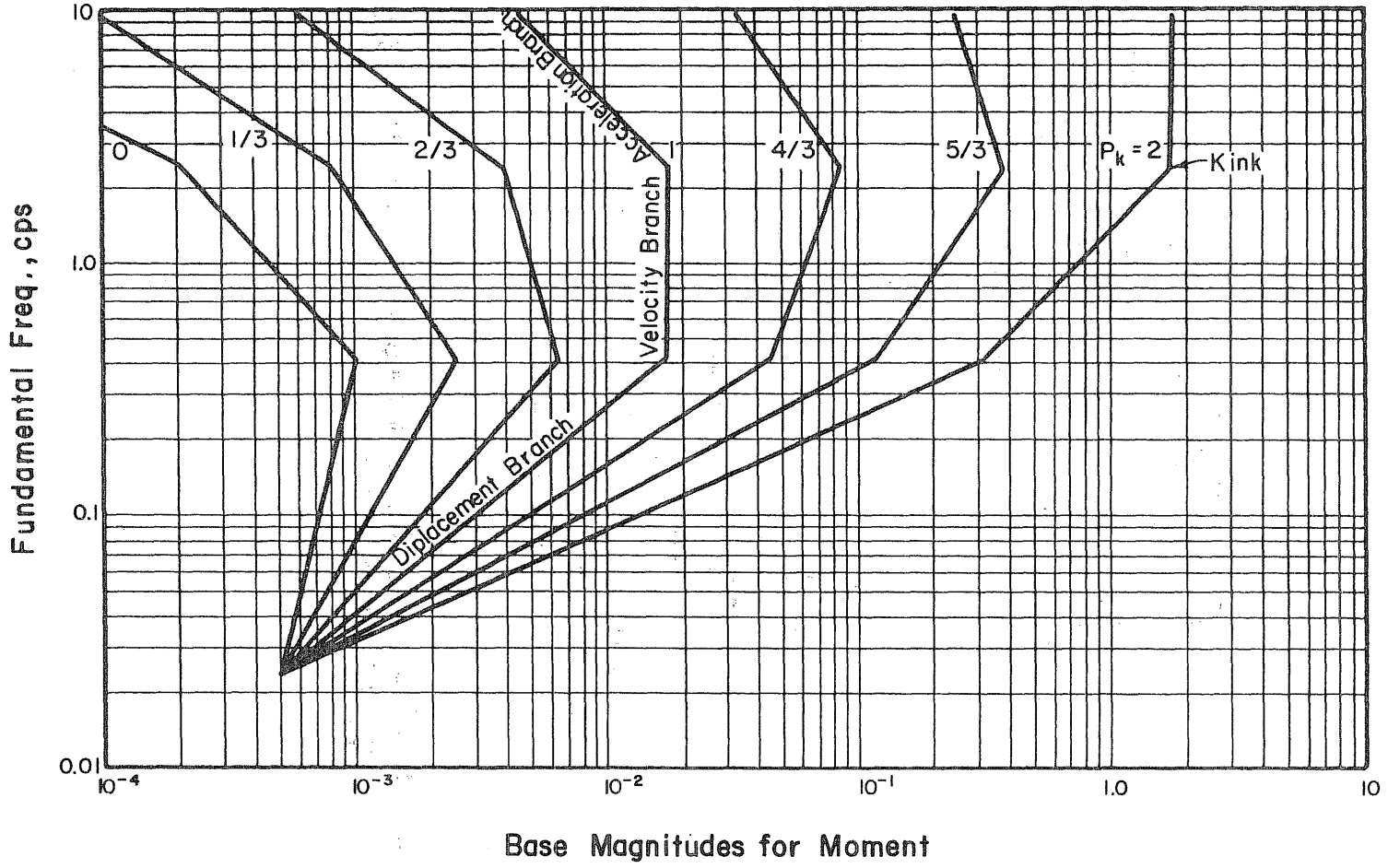

FIG. 10 BASE MAGNITUDES FOR MOMENT—MODEL 10SA

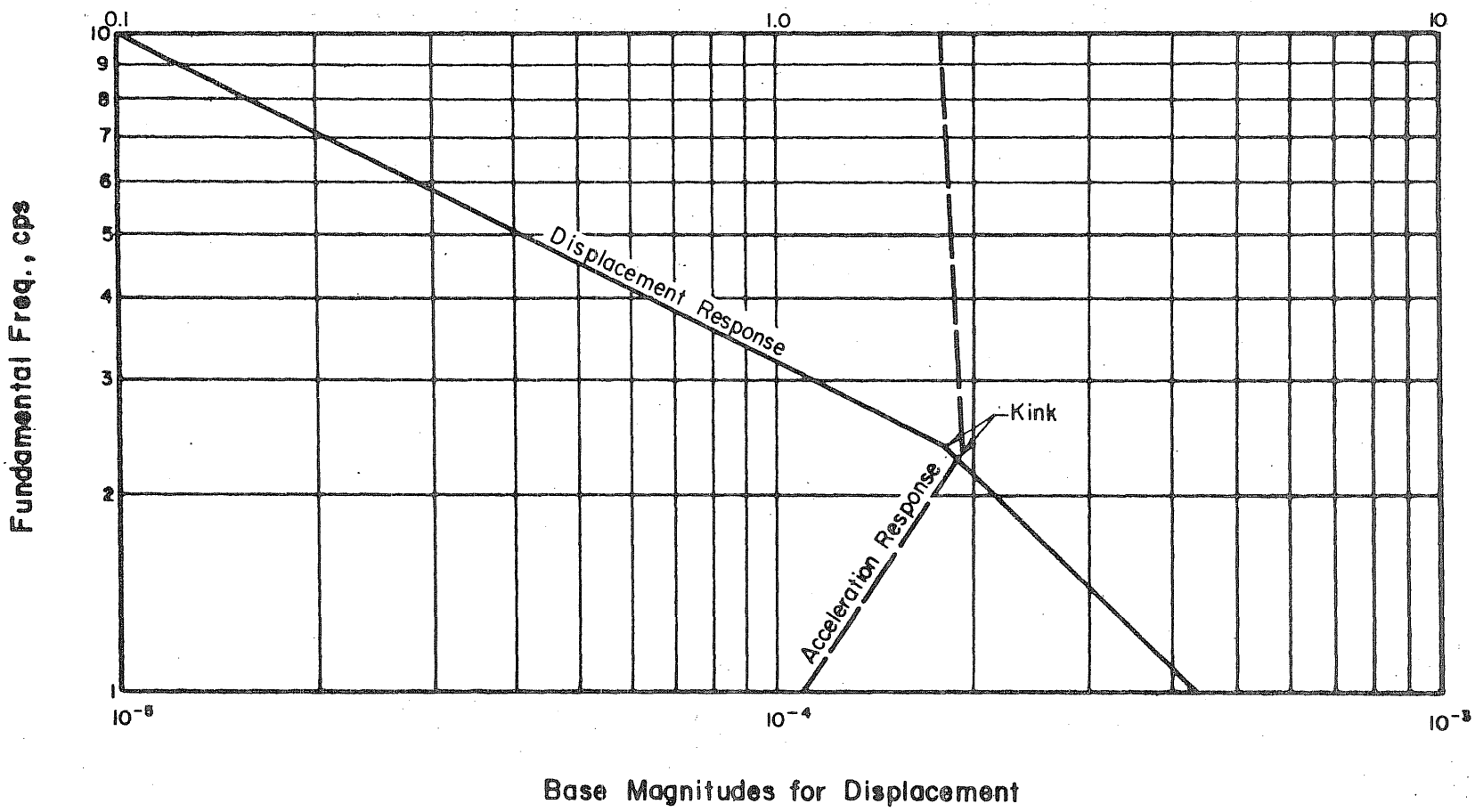

FIG. 11 REFERENCE BASE MAGNITUDE SPECTRA FOR DISPLACEMENT AND ACCELERATION

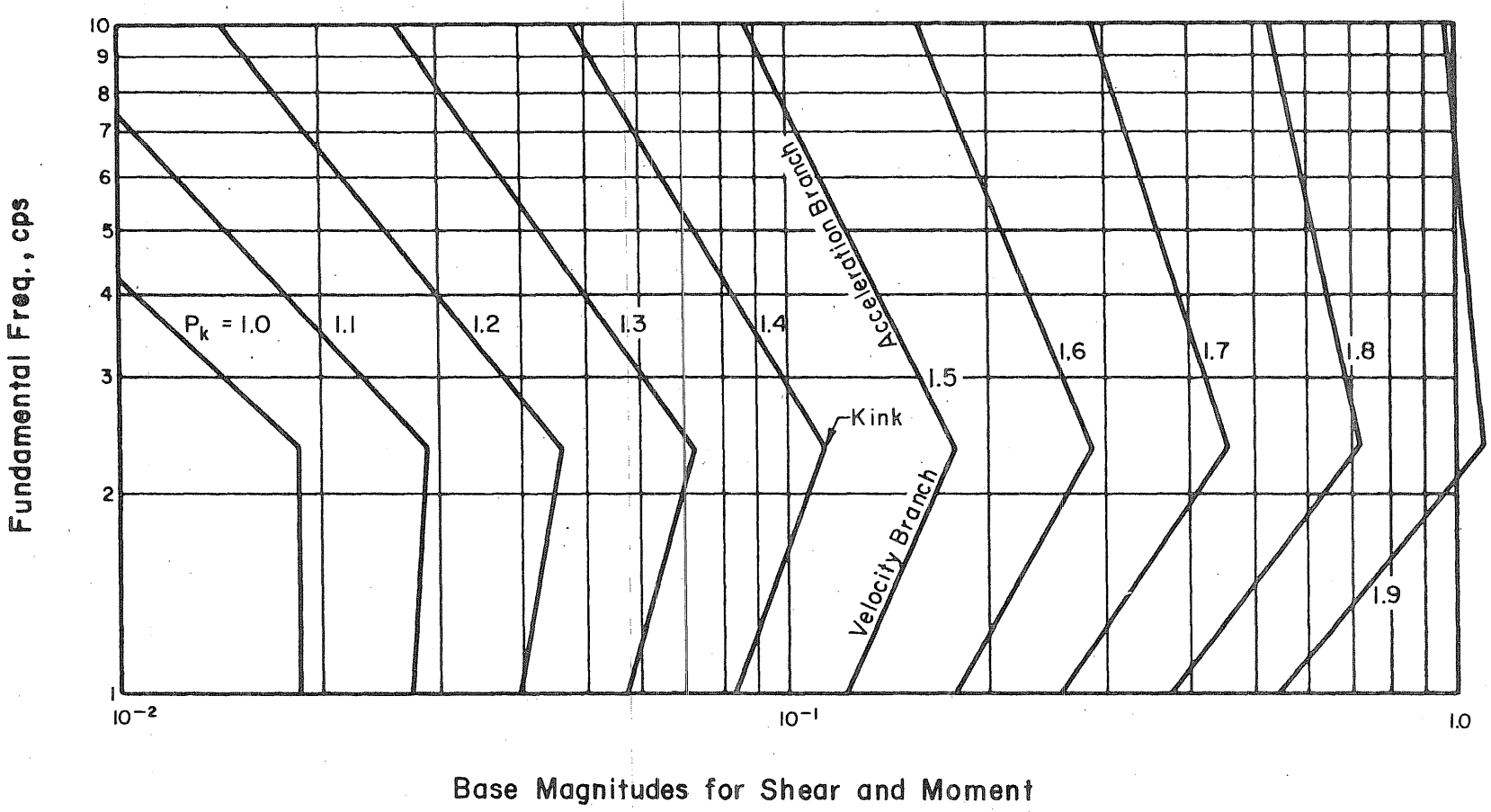

FIG. 12 REFERENCE BASE MAGNITUDE SPECTRA FOR SHEAR AND MOMENT

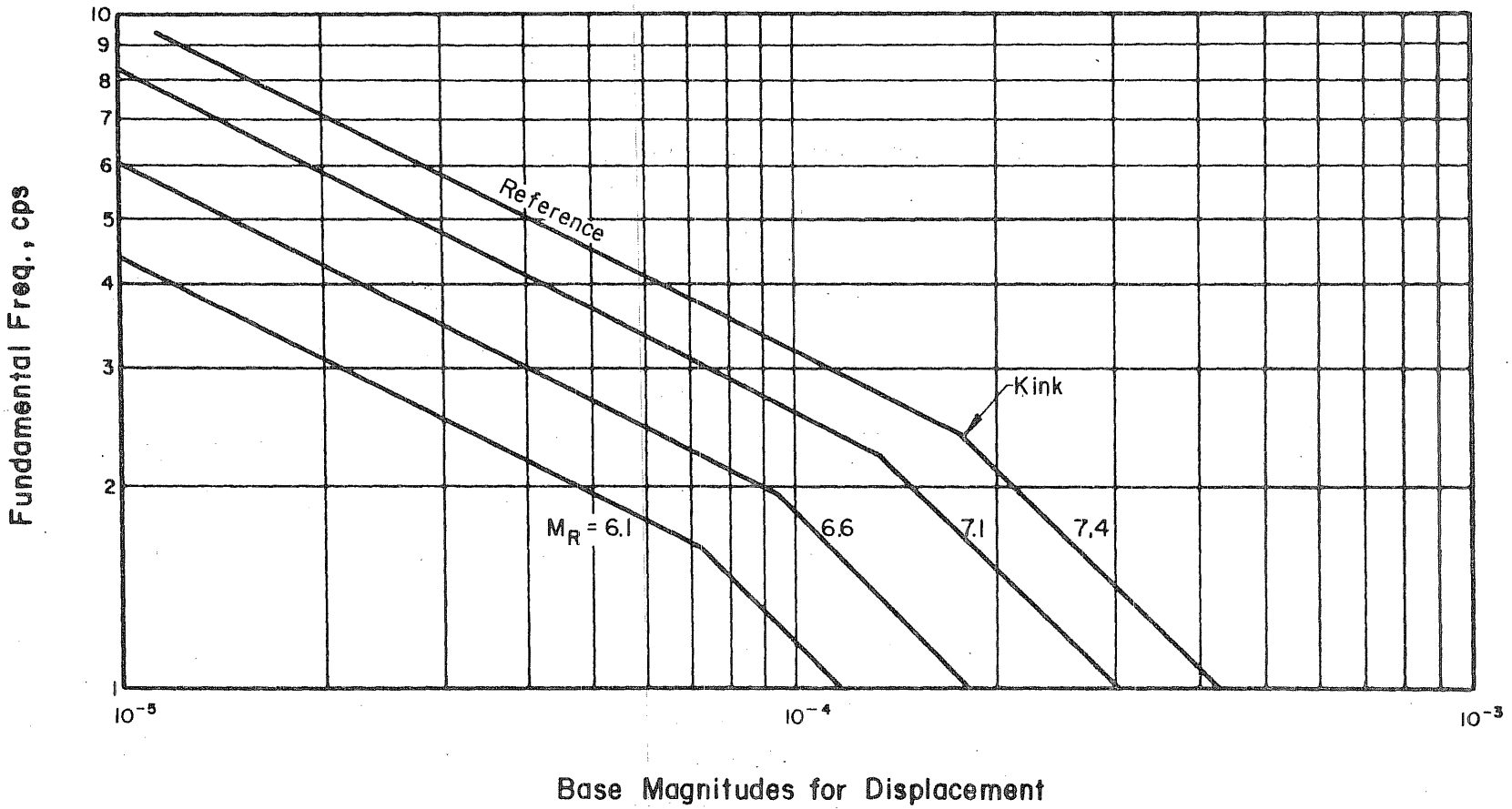

FIG. 13 BASE MAGNITUDES FOR DISPLACEMENT-EFFECT OF EARTHQUAKE MAGNITUDE (MODEL 10SA)

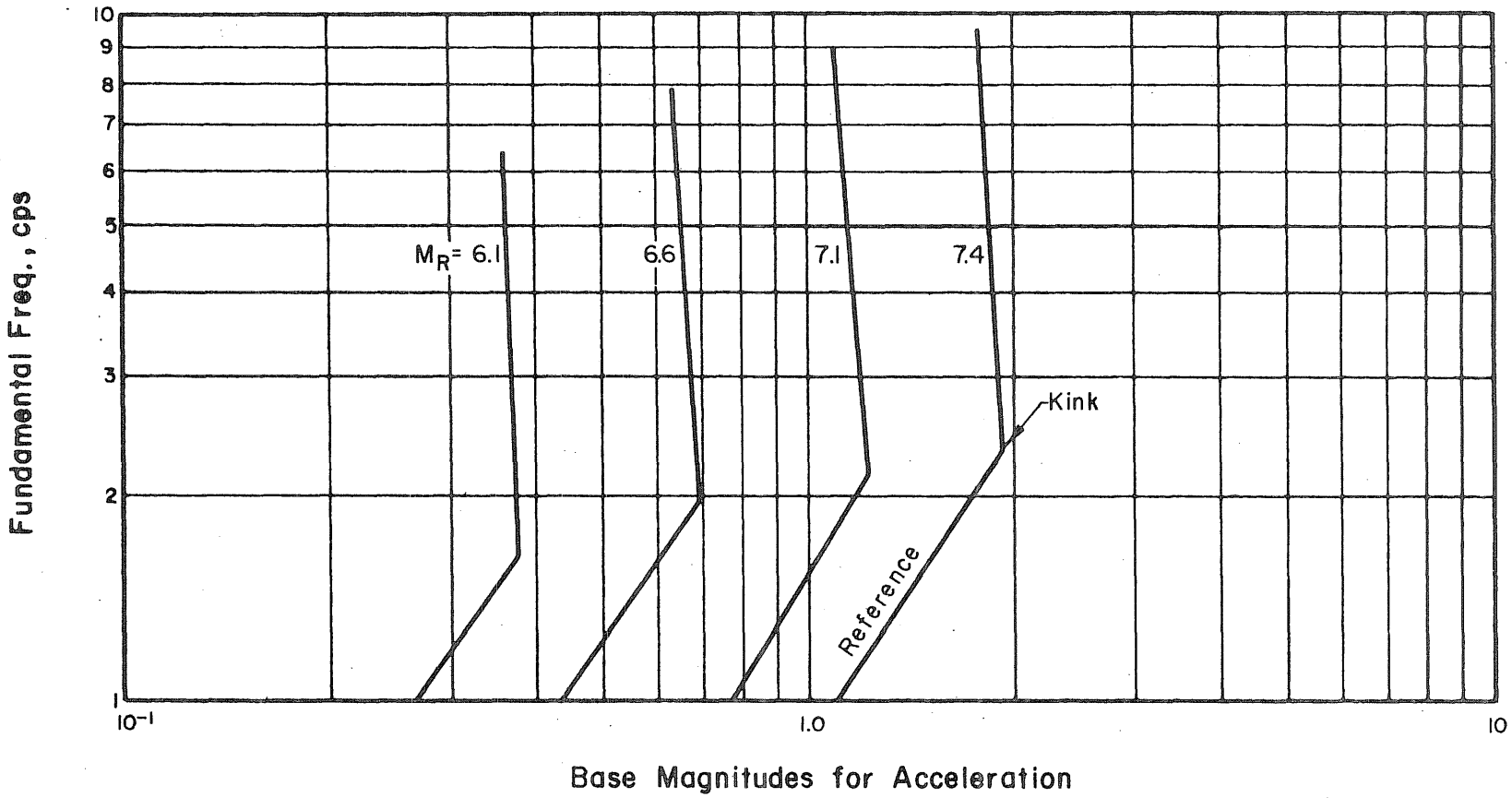

FIG. 14 BASE MAGNITUDES FOR ACCELERATION—EFFECT OF EARTHQUAKE MAGNITUDE (MODEL IOSA)

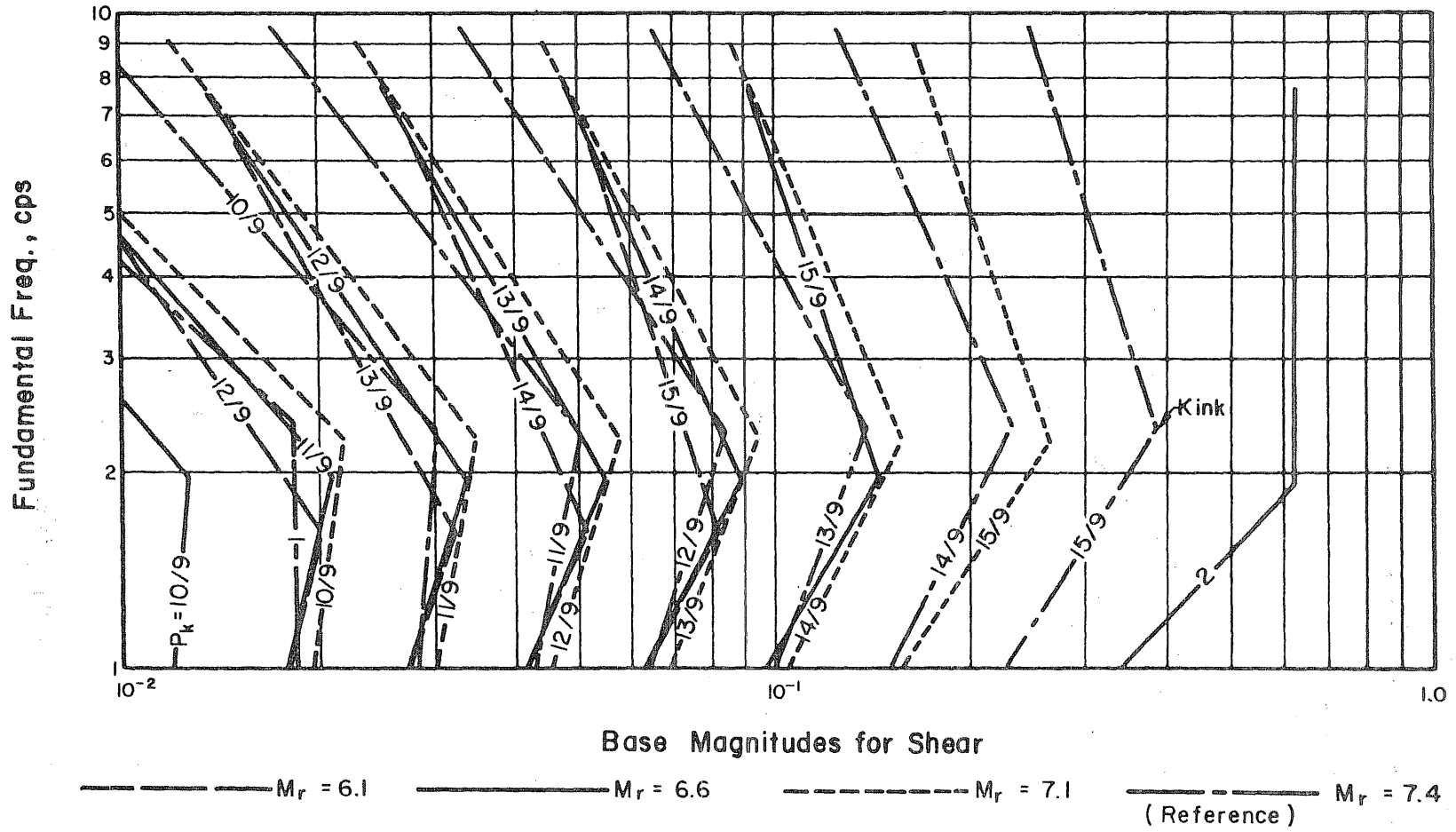

FIG. 15 BASE MAGNITUDES FOR SHEAR-EFFECT OF EARTHQUAKE MAGNITUDE (MODEL IOSA)

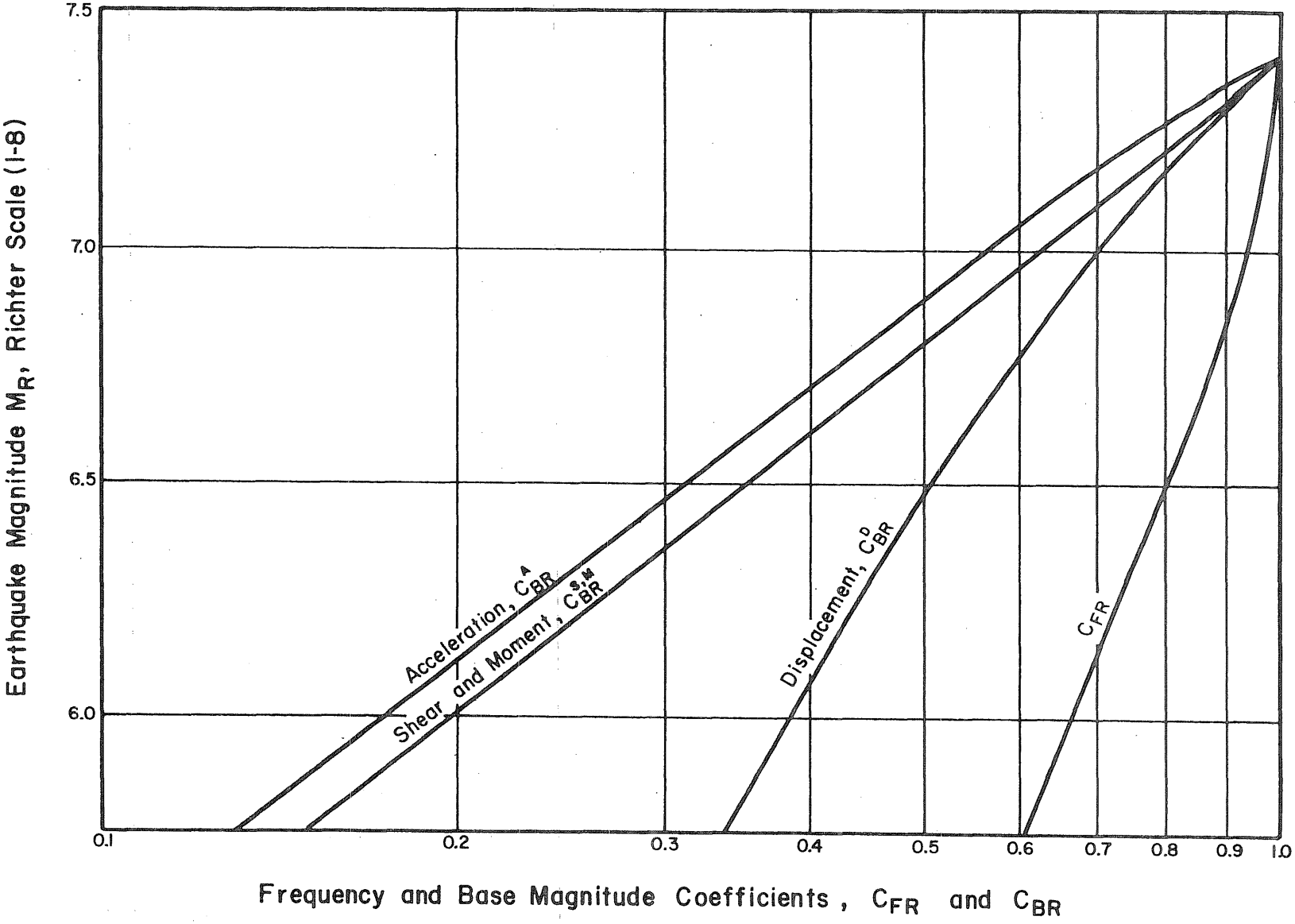

FIG. 16 SCALING BASE MAGNITUDE AND FREQUENCY COEFFICIENTS, FOR EARTHQUAKE MAGNITUDE

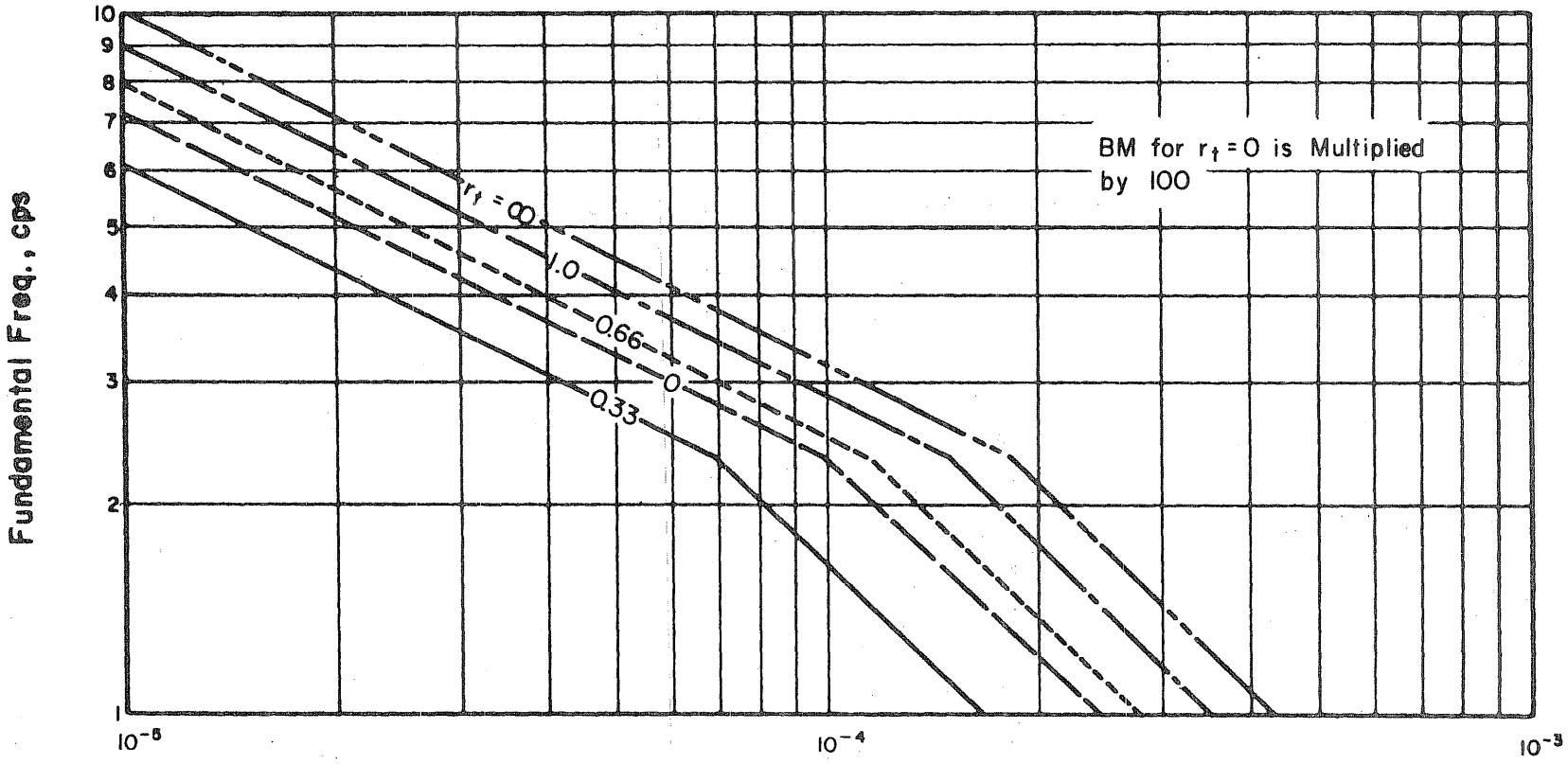

FIG. 17 BASE MAGNITUDES FOR DISPLACEMENT-EFFECT OF TYPE OF BUILDING

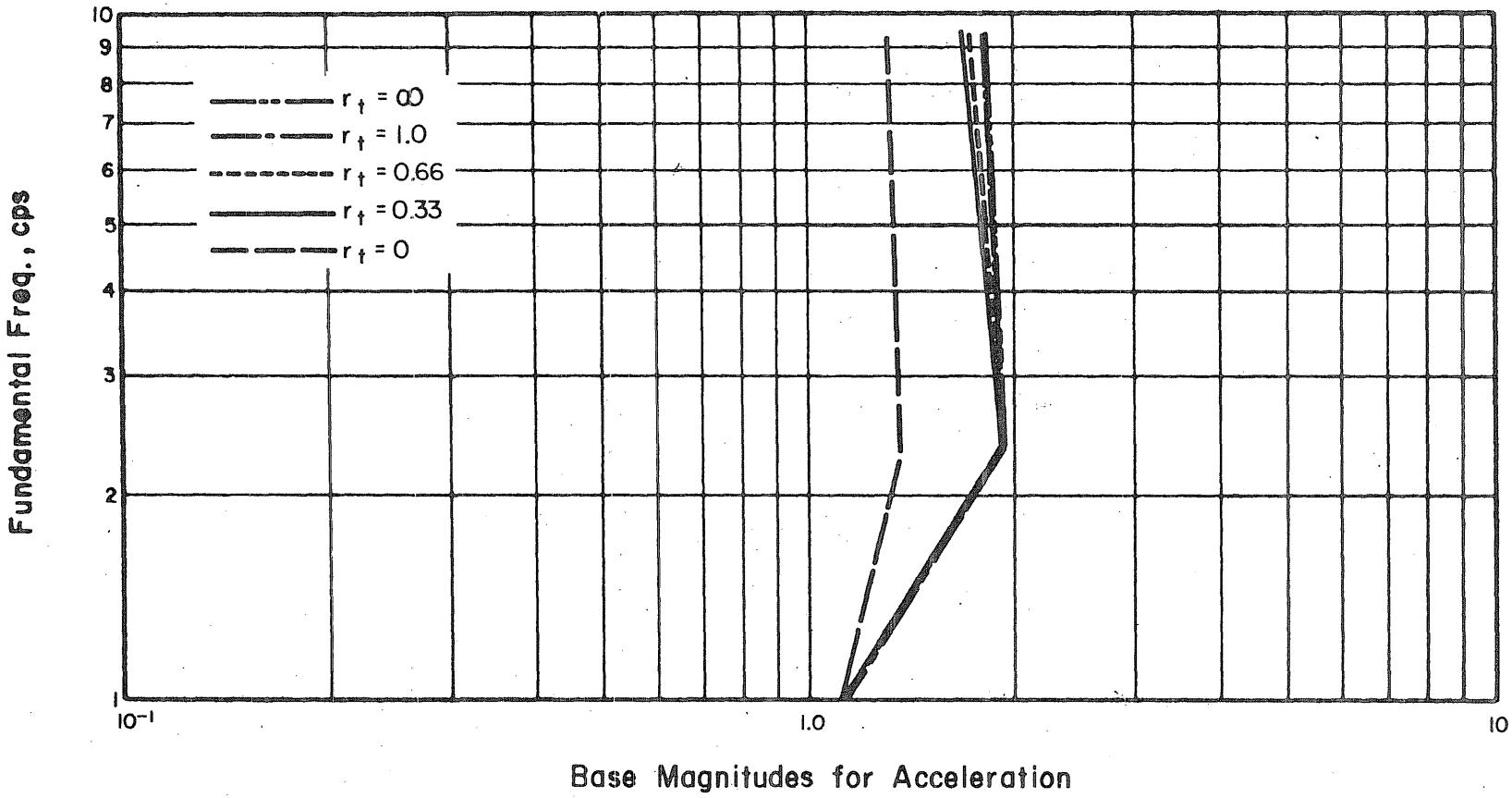

FIG. 18 BASE MAGNITUDES FOR ACCELERATION—EFFECT OF TYPE OF BUILDING

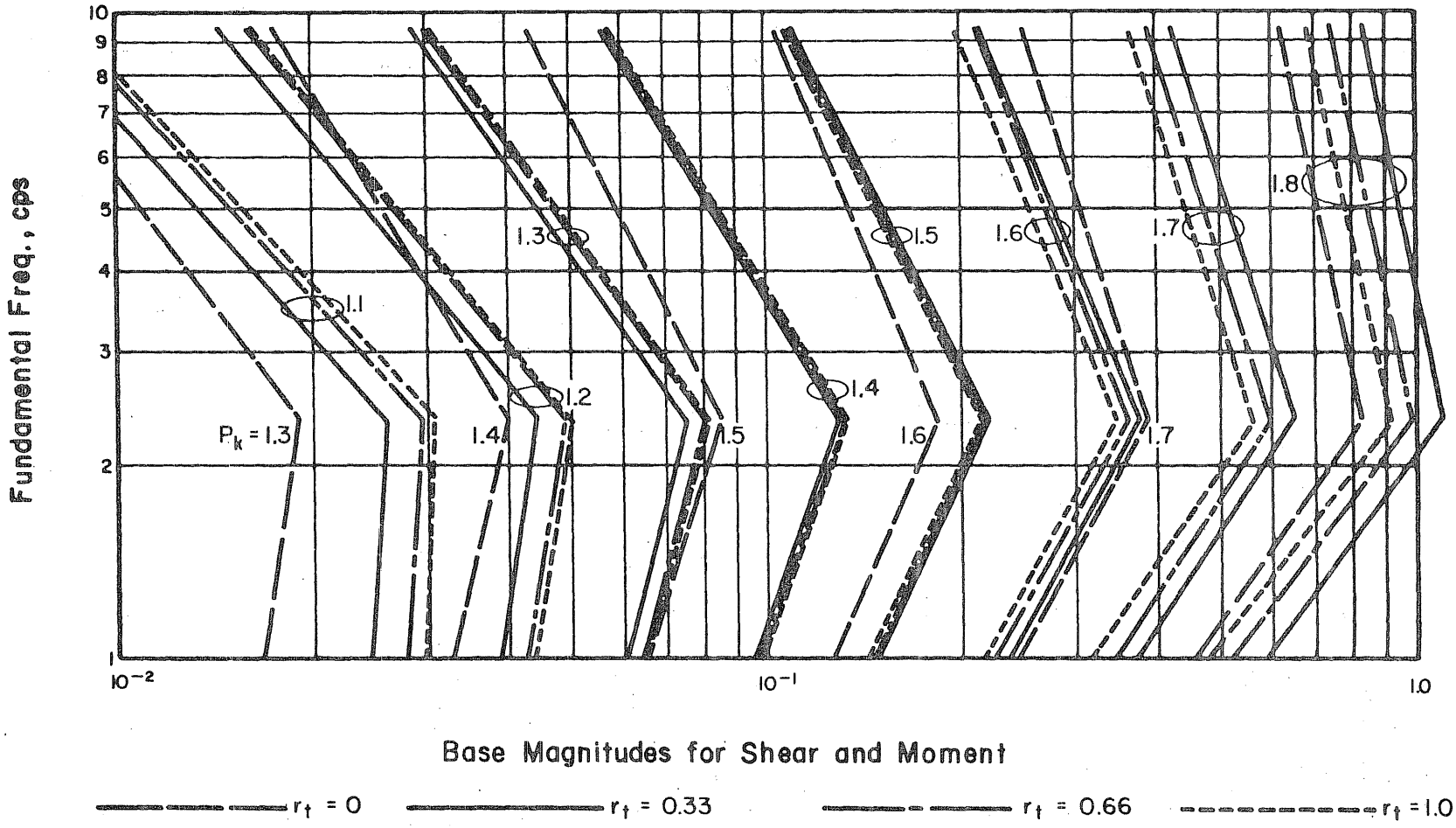

FIG. 19 BASE MAGNITUDES FOR SHEAR AND MOMENT—EFFECT OF TYPE OF BUILDING

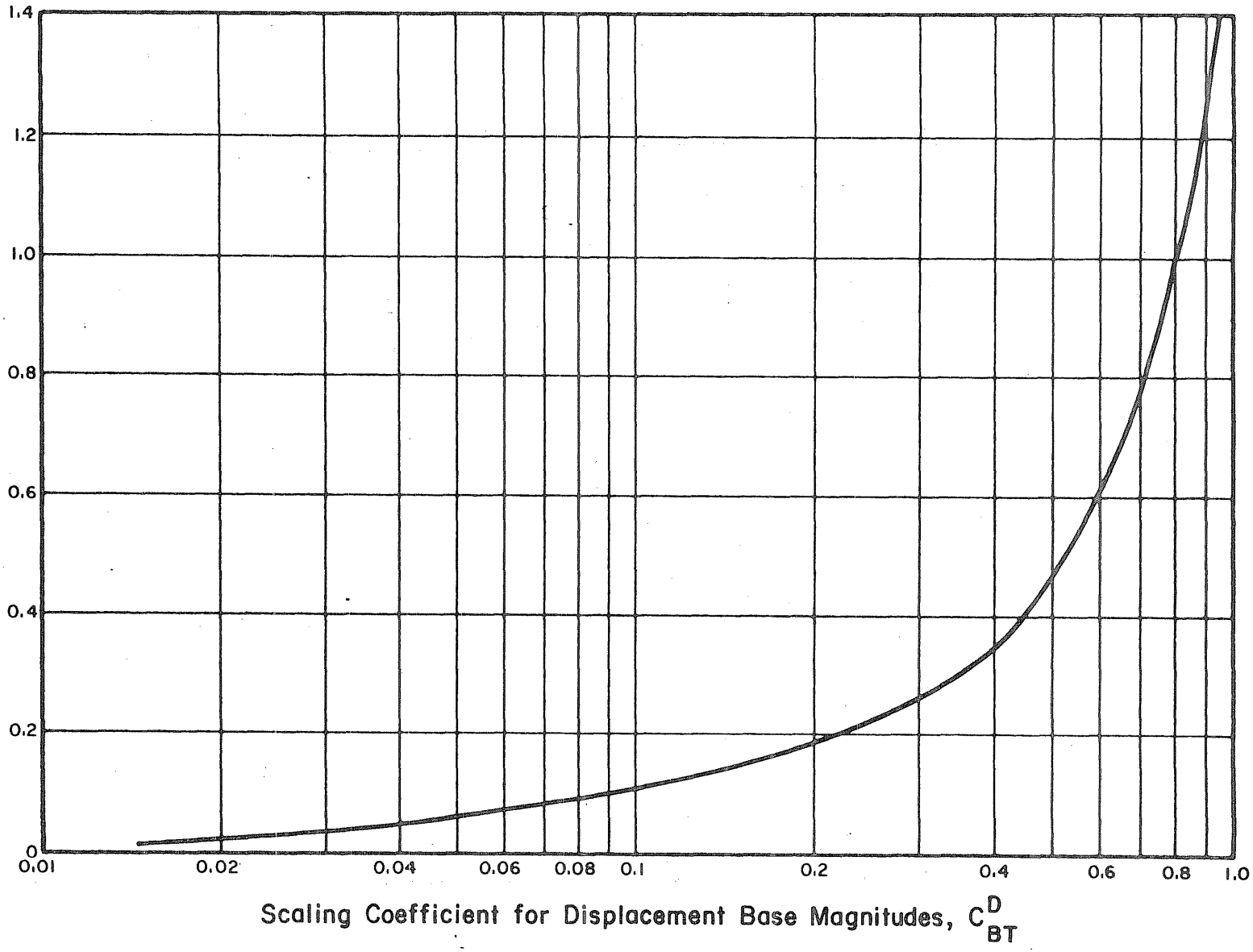

FIG. 20 SCALING COEFFICIENTS FOR DISPLACEMENT BASE MAGNITUDES, DUE TO TYPE OF BUILDING

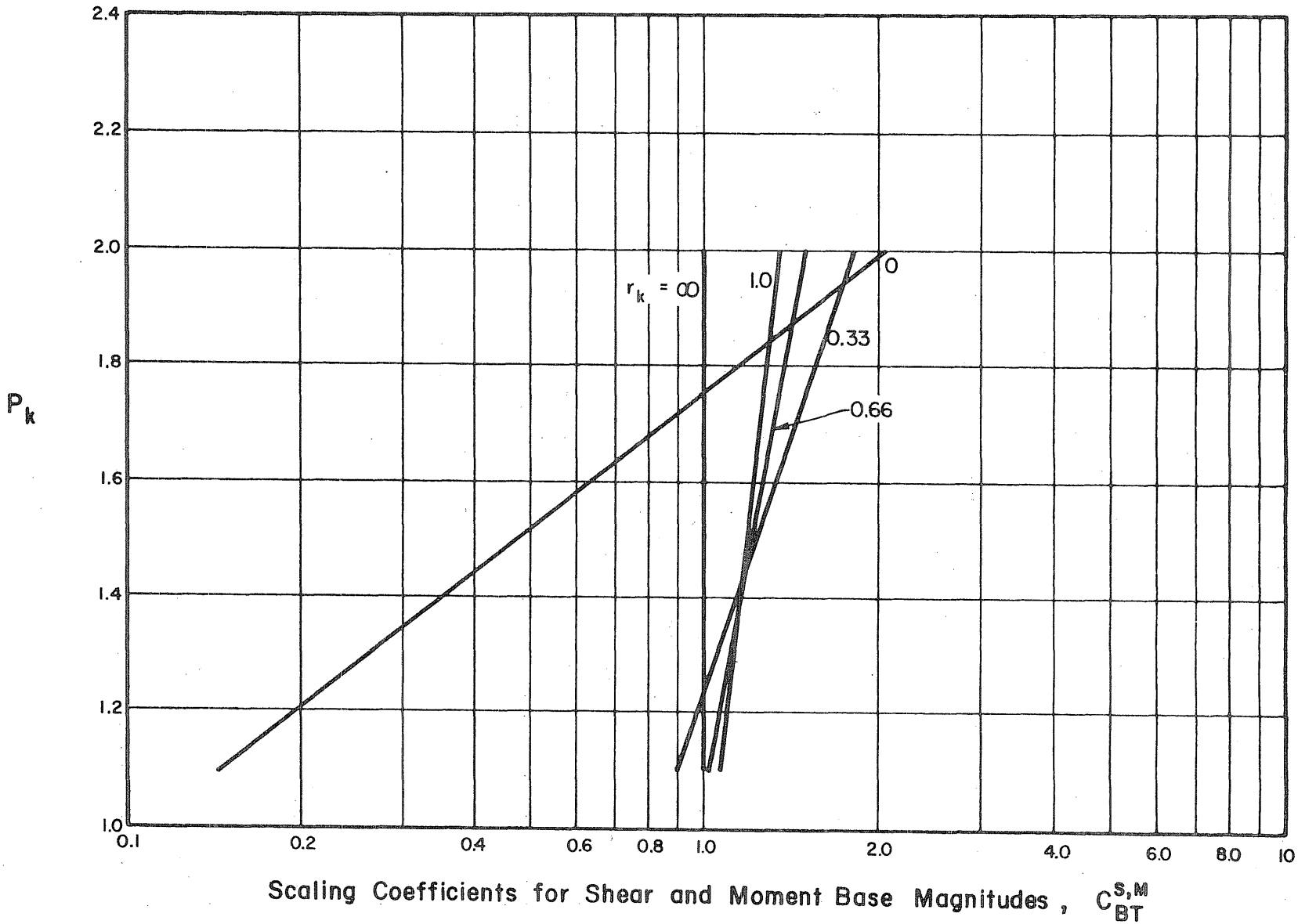

FIG. 21 SCALING COEFFICIENTS FOR SHEAR AND MOMENT BASE MAGNITUDES, DUE TO TYPE OF BUILDING

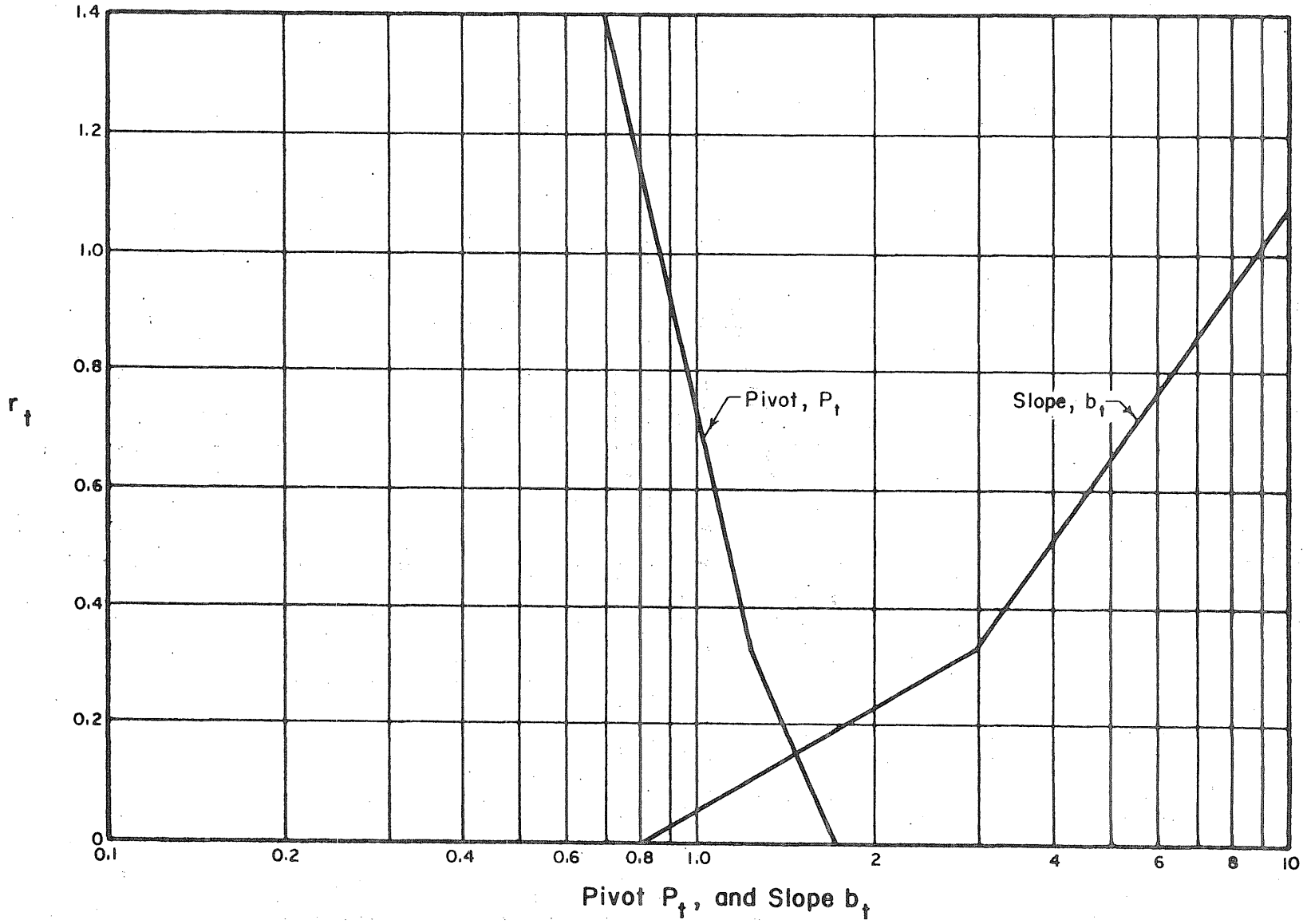

FIG. 22 PIVOT AND SLOPE FOR SCALING COEFFICIENTS FOR TYPE OF BUILDING, $C_{BT}^{S,M}$

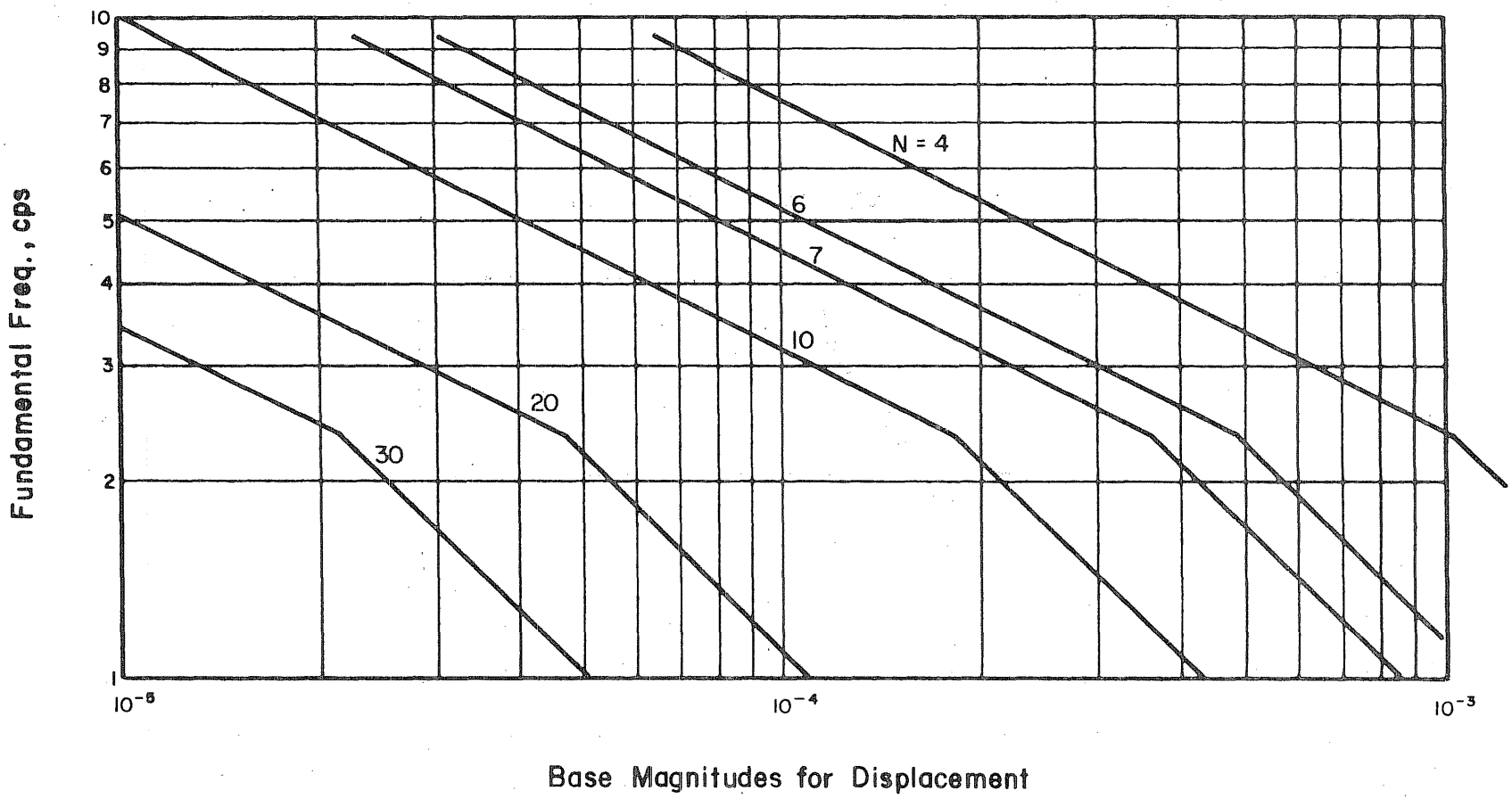

FIG. 23 BASE MAGNITUDES FOR DISPLACEMENT-EFFECT OF NUMBER OF STORIES N

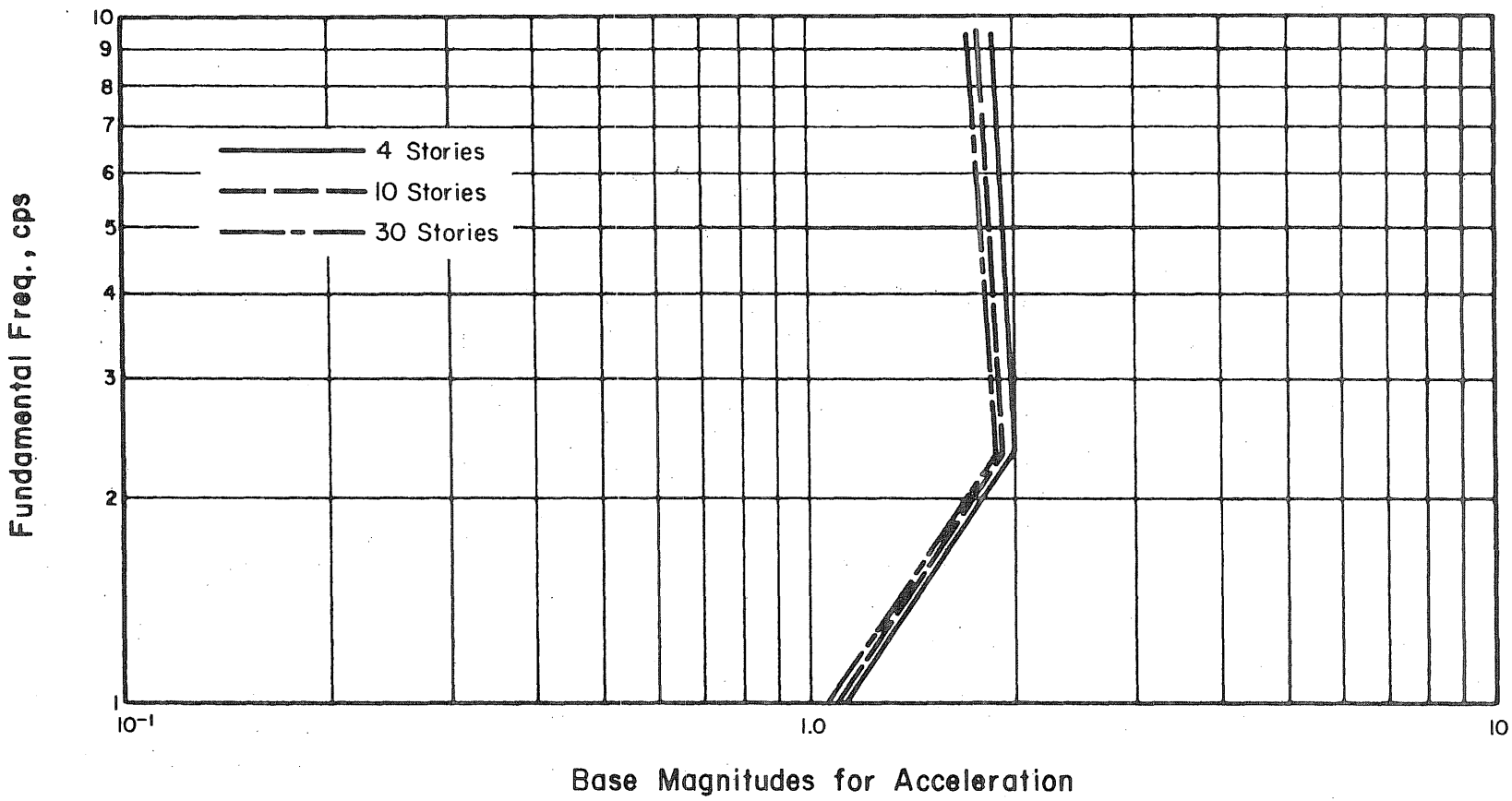

FIG. 24 BASE MAGNITUDES FOR ACCELERATION – EFFECT OF NUMBER OF STORIES N

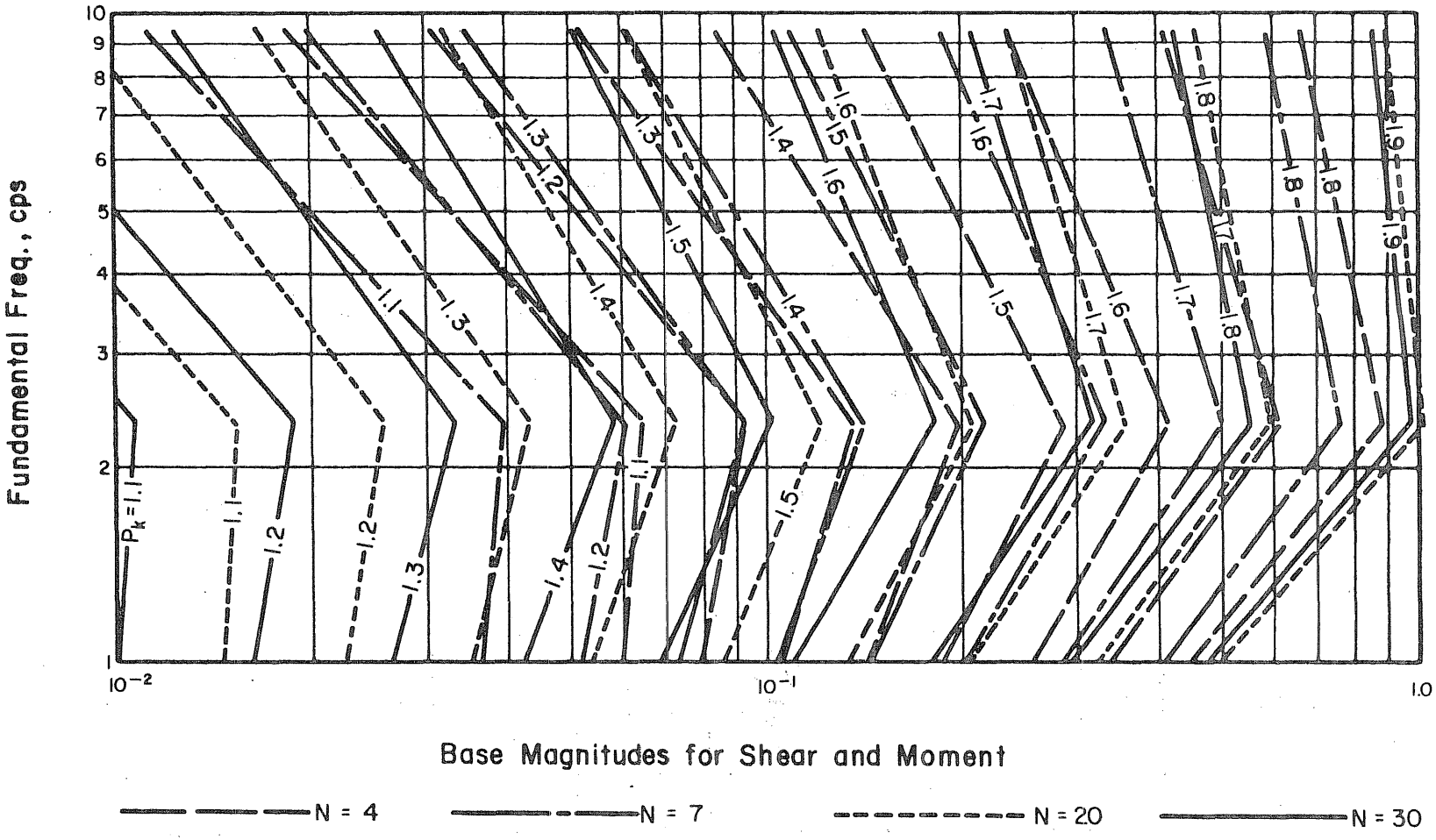

FIG. 25 BASE MAGNITUDES FOR SHEAR AND MOMENT – EFFECT OF NUMBER OF STORIES N

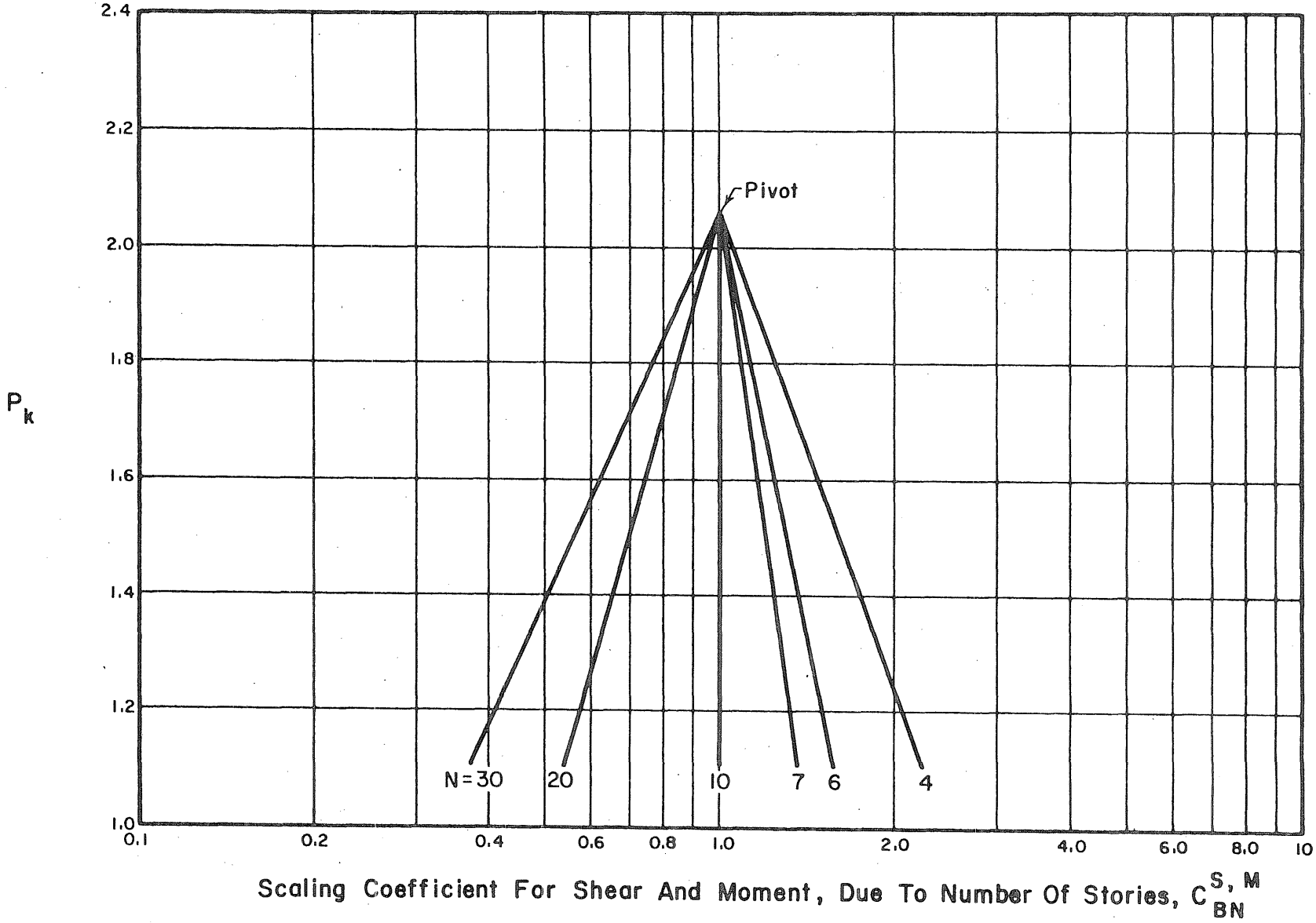

FIG. 26 SCALING COEFFICIENTS FOR SHEAR AND MOMENT, DUE TO NUMBER OF STORIES N

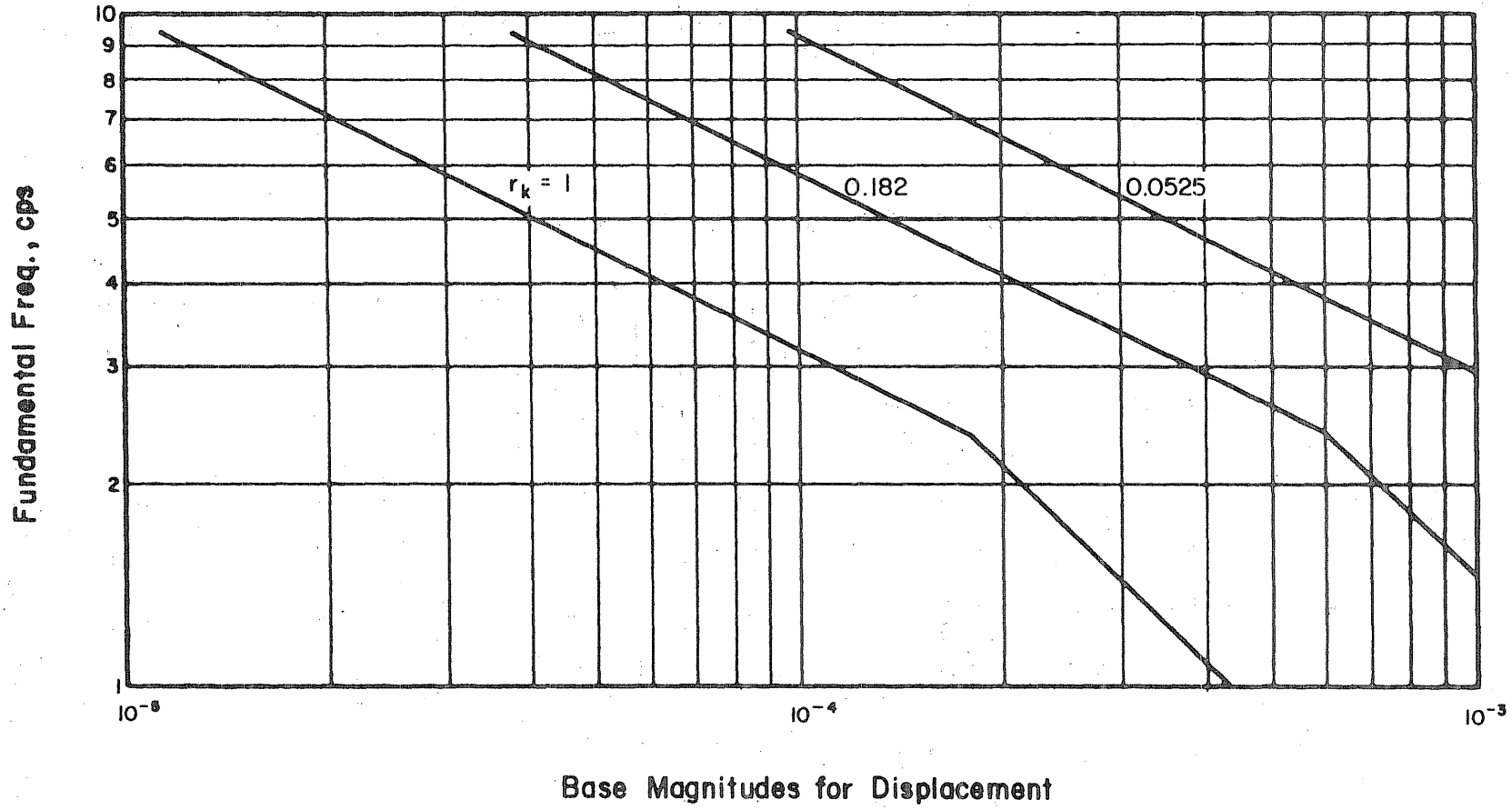

FIG. 27 BASE MAGNITUDES FOR DISPLACEMENT-EFFECT OF STIFFNESS DISTRIBUTION

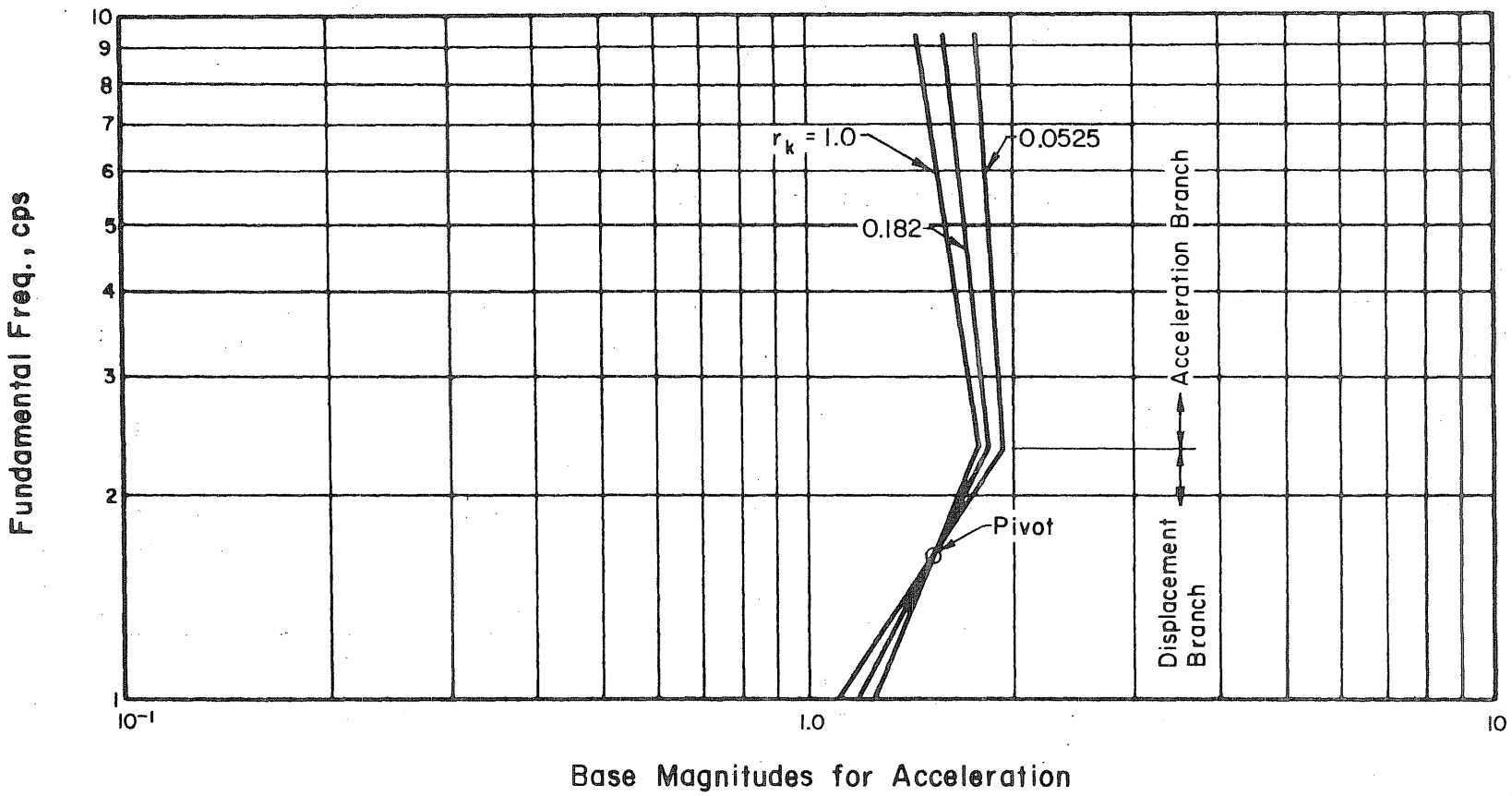

FIG. 28 BASE MAGNITUDES FOR ACCELERATION—EFFECT OF STIFFNESS DISTRIBUTION

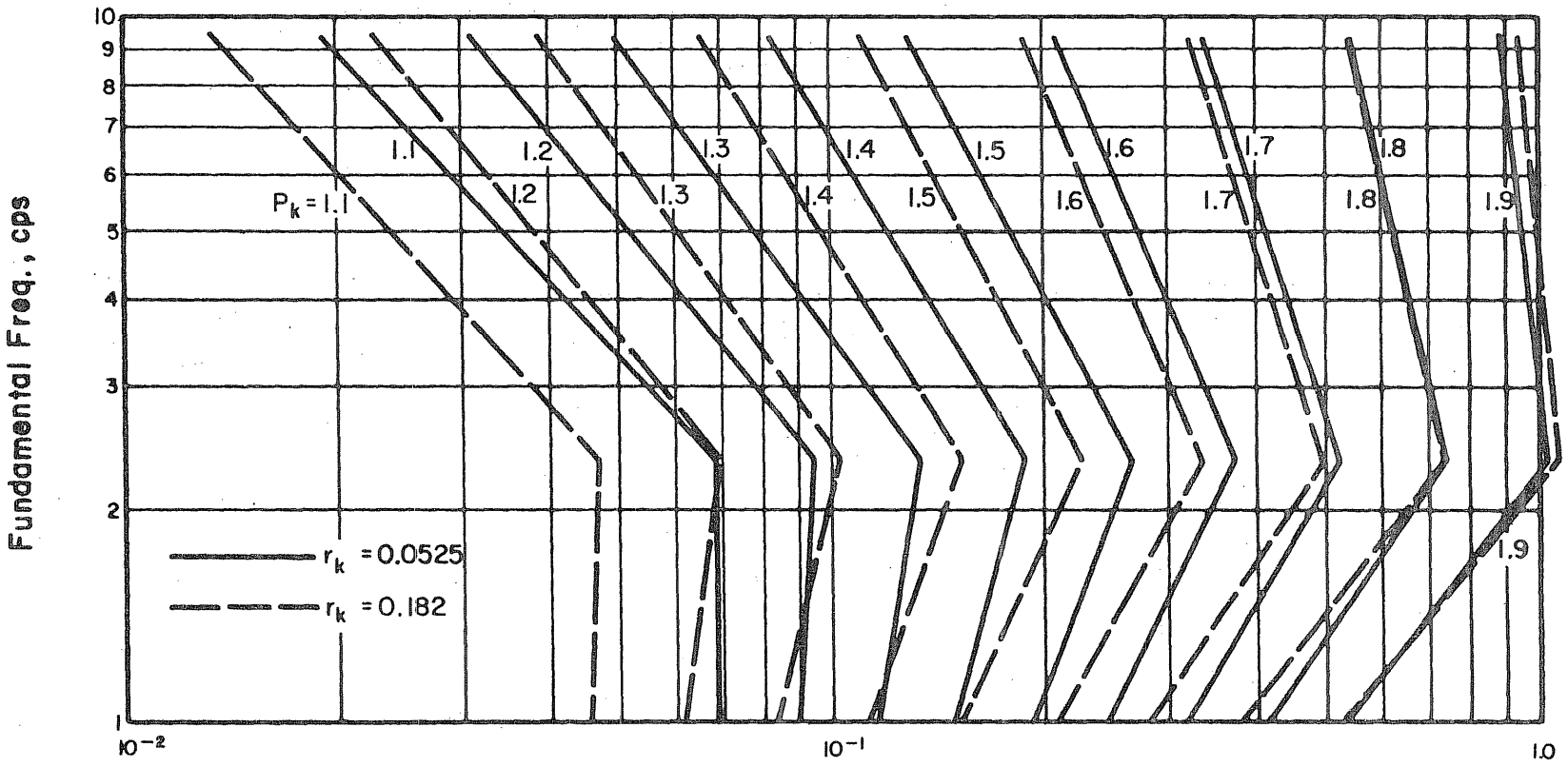

FIG. 29 BASE MAGNITUDES FOR SHEAR AND MOMENT – EFFECT OF STIFFNESS DISTRIBUTION

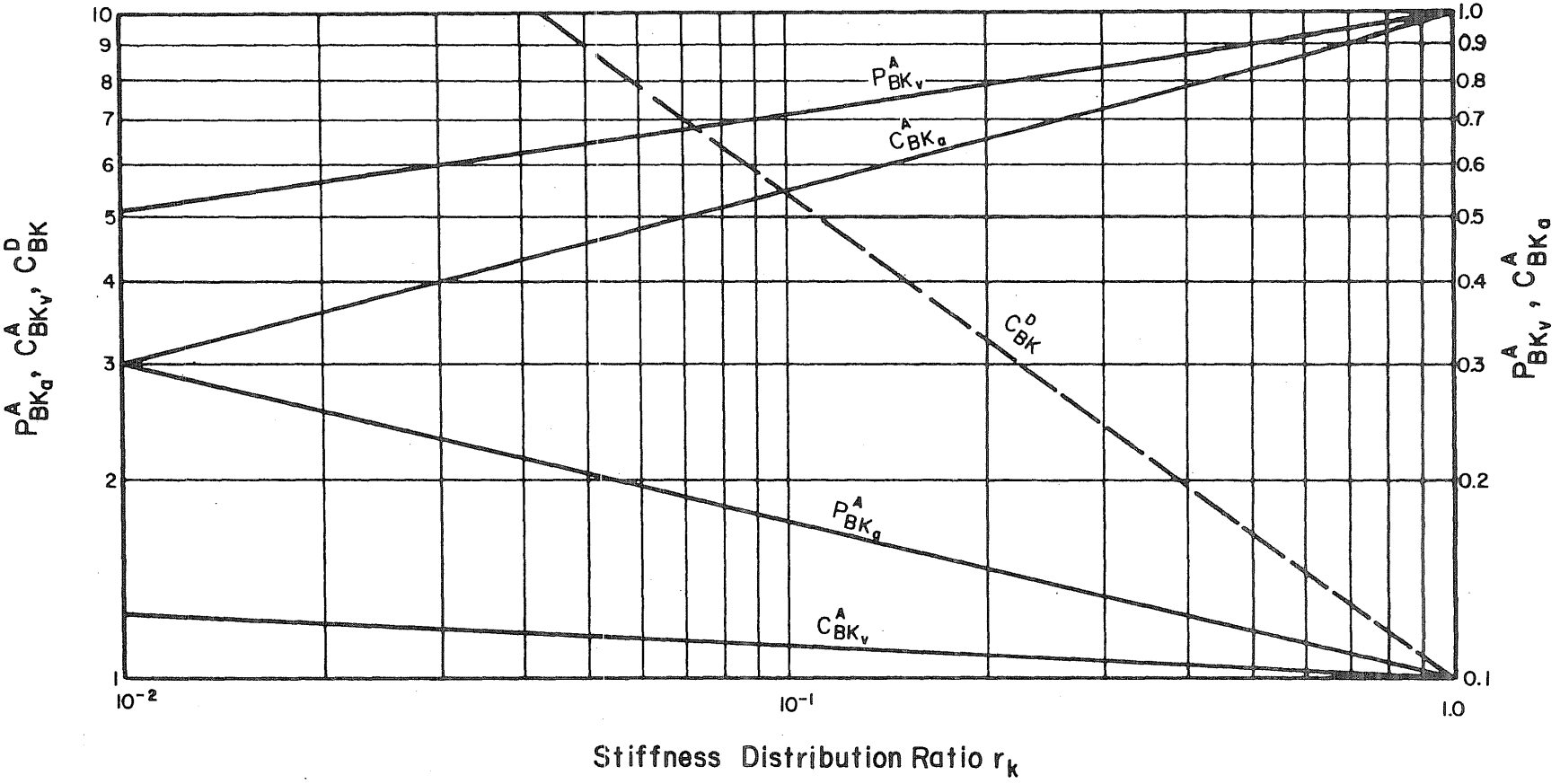

FIG. 30 SCALING POWERS AND COEFFICIENTS FOR DISPLACEMENT AND ACCELERATION BASE MAGNITUDES FOR EFFECT OF STIFFNESS DISTRIBUTION

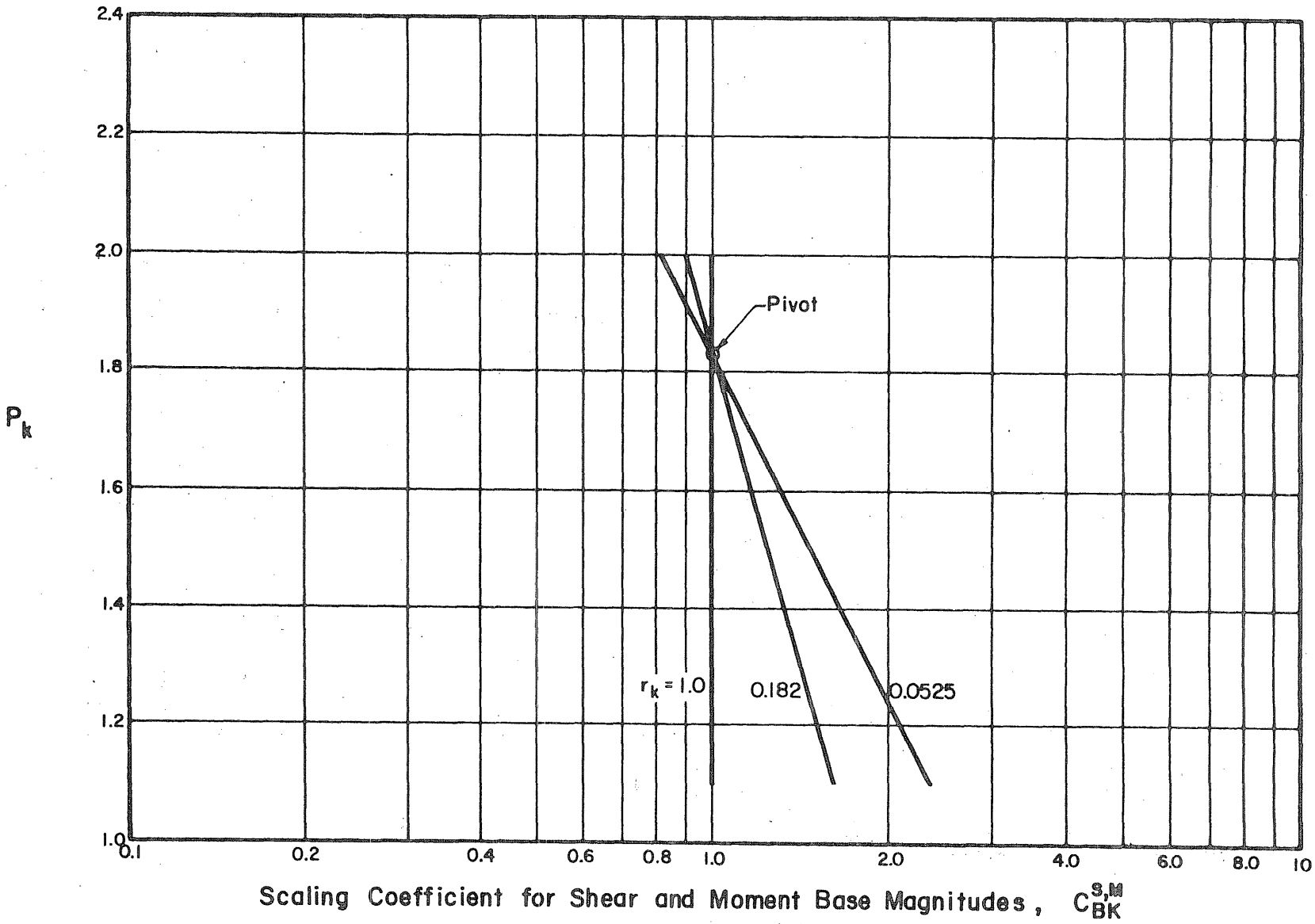

FIG. 31 SCALING COEFFICIENTS FOR SHEAR AND MOMENT BASE MAGNITUDES, DUE TO STIFFNESS DISTRIBUTION

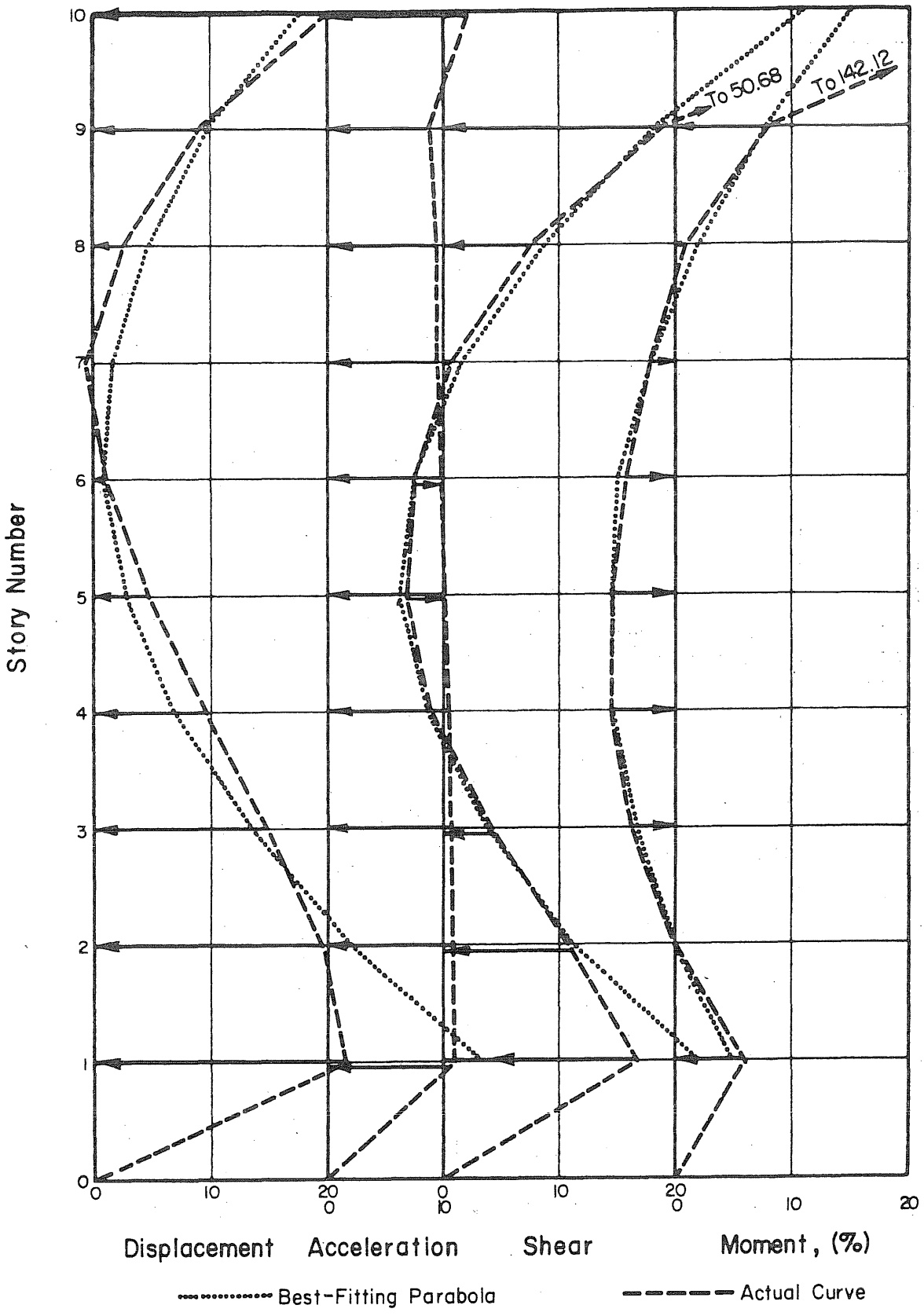

FIG. 32 SRSS VERTICAL VARIATION — MODEL IOSA, DISPLACEMENT BRANCH (f_1 = 0.142 cps)

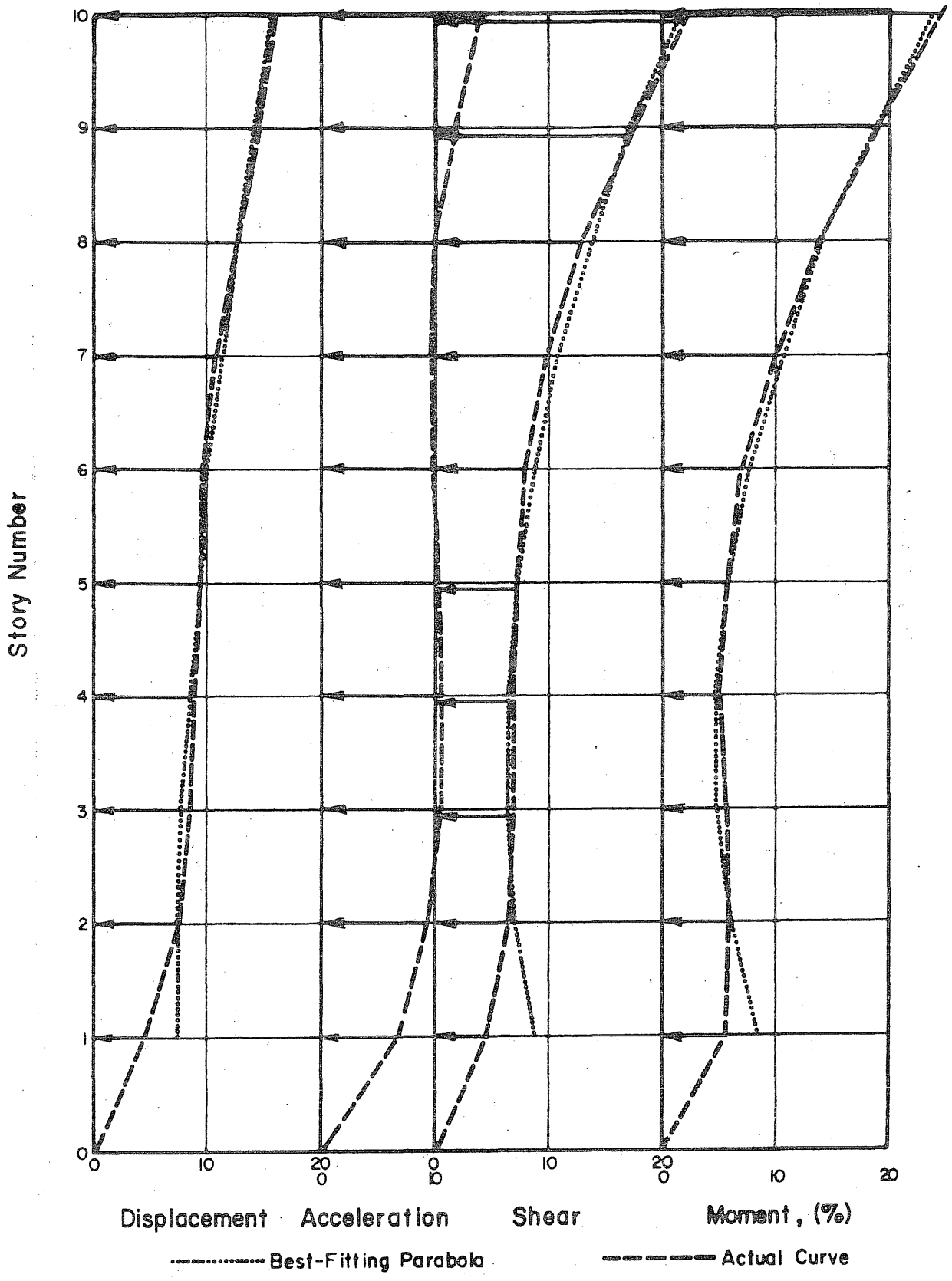

FIG. 33 SRSS VERTICAL VARIATION — MODEL IOSA, VELOCITY BRANCH (f_1 = 0.81 cps)

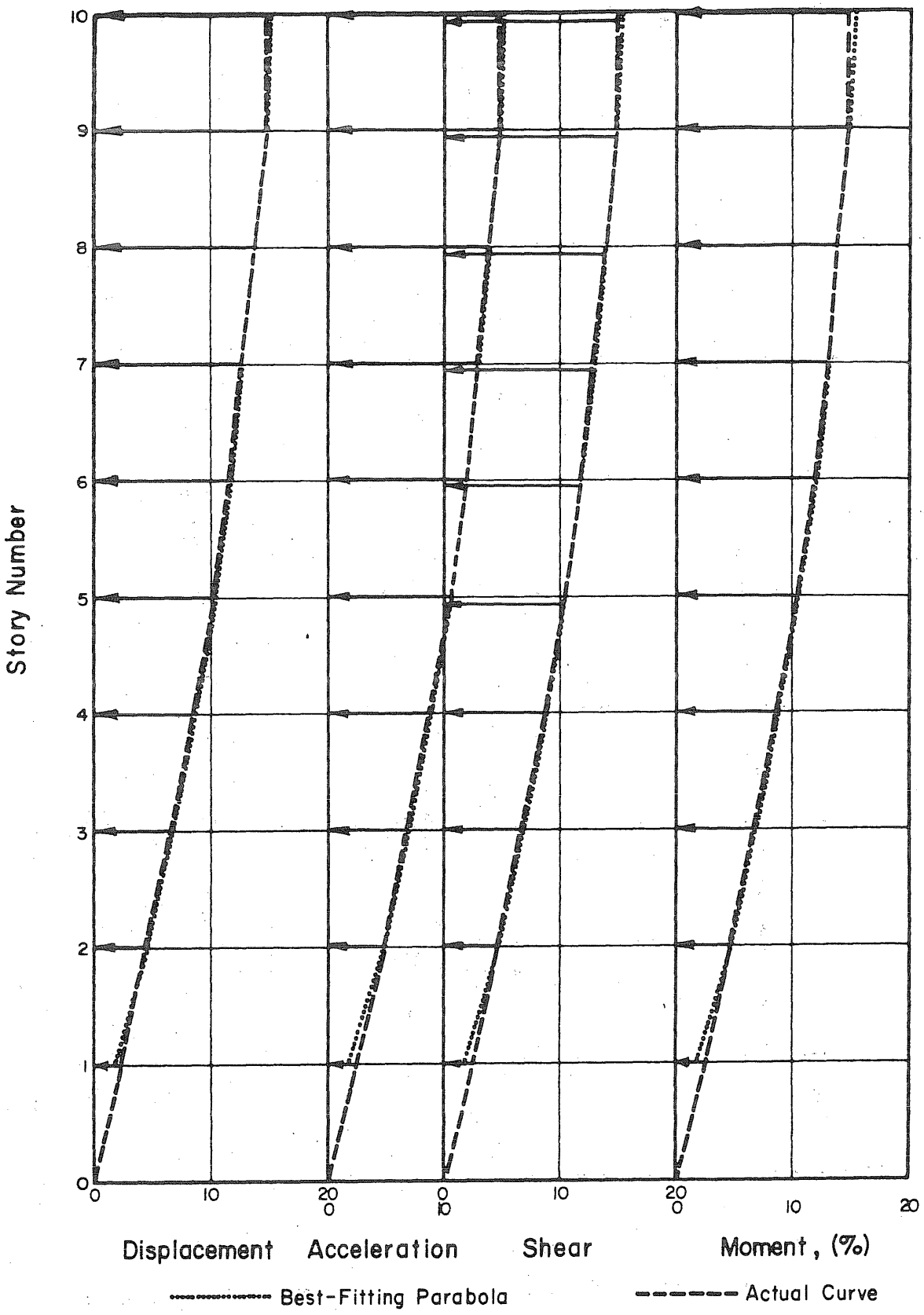

FIG. 34 SRSS VERTICAL VARIATION — MODEL IOSA, ACCELERATION BRANCH (f_1 = 9.40 cps)

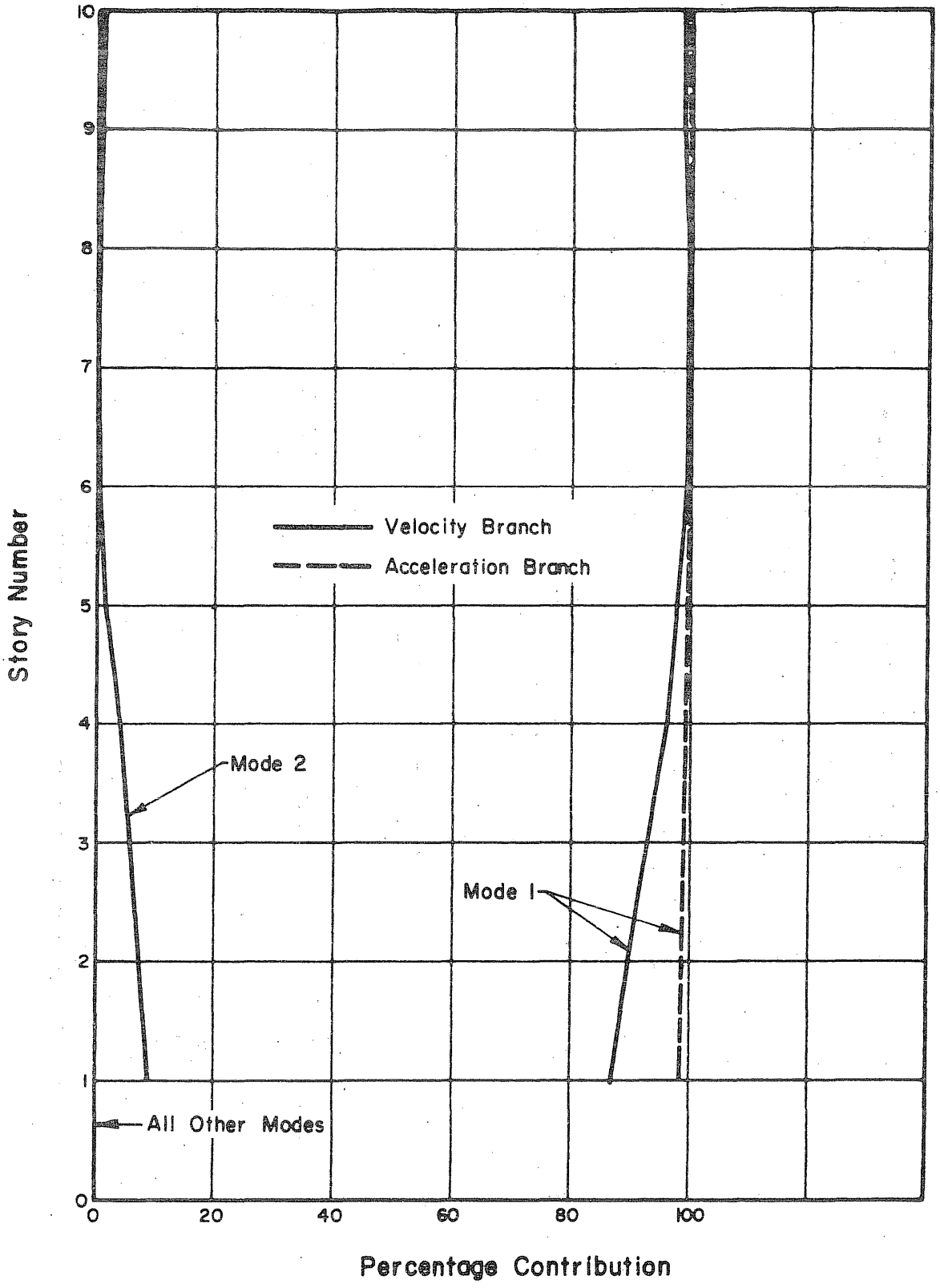

FIG. 35 SRSS CONTRIBUTIONS TO SPECTRAL DISPLACEMENTS (MODEL IOSA)

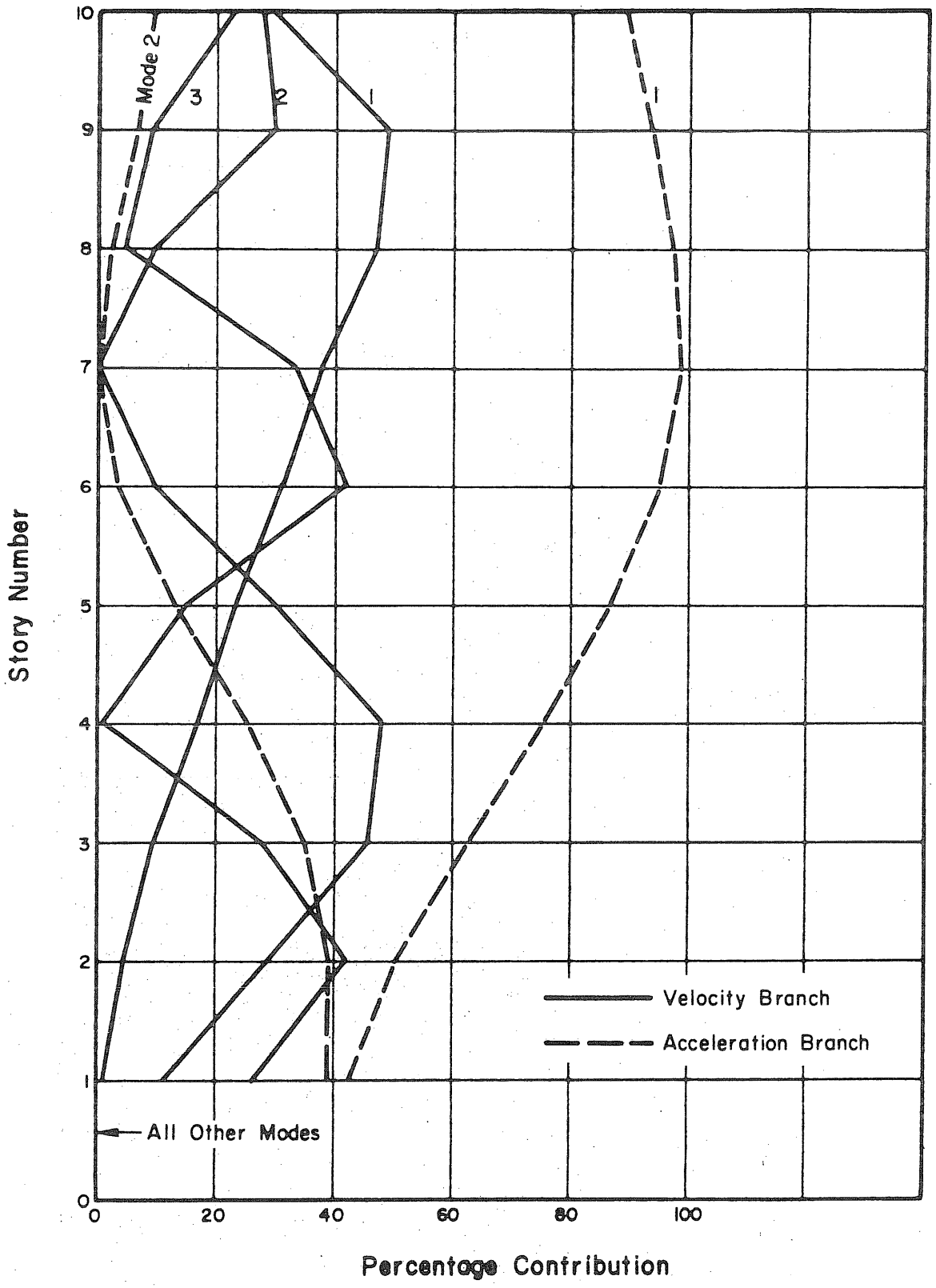

FIG. 36 SRSS CONTRIBUTIONS TO SPECTRAL ACCELERATIONS (MODEL 10SA)

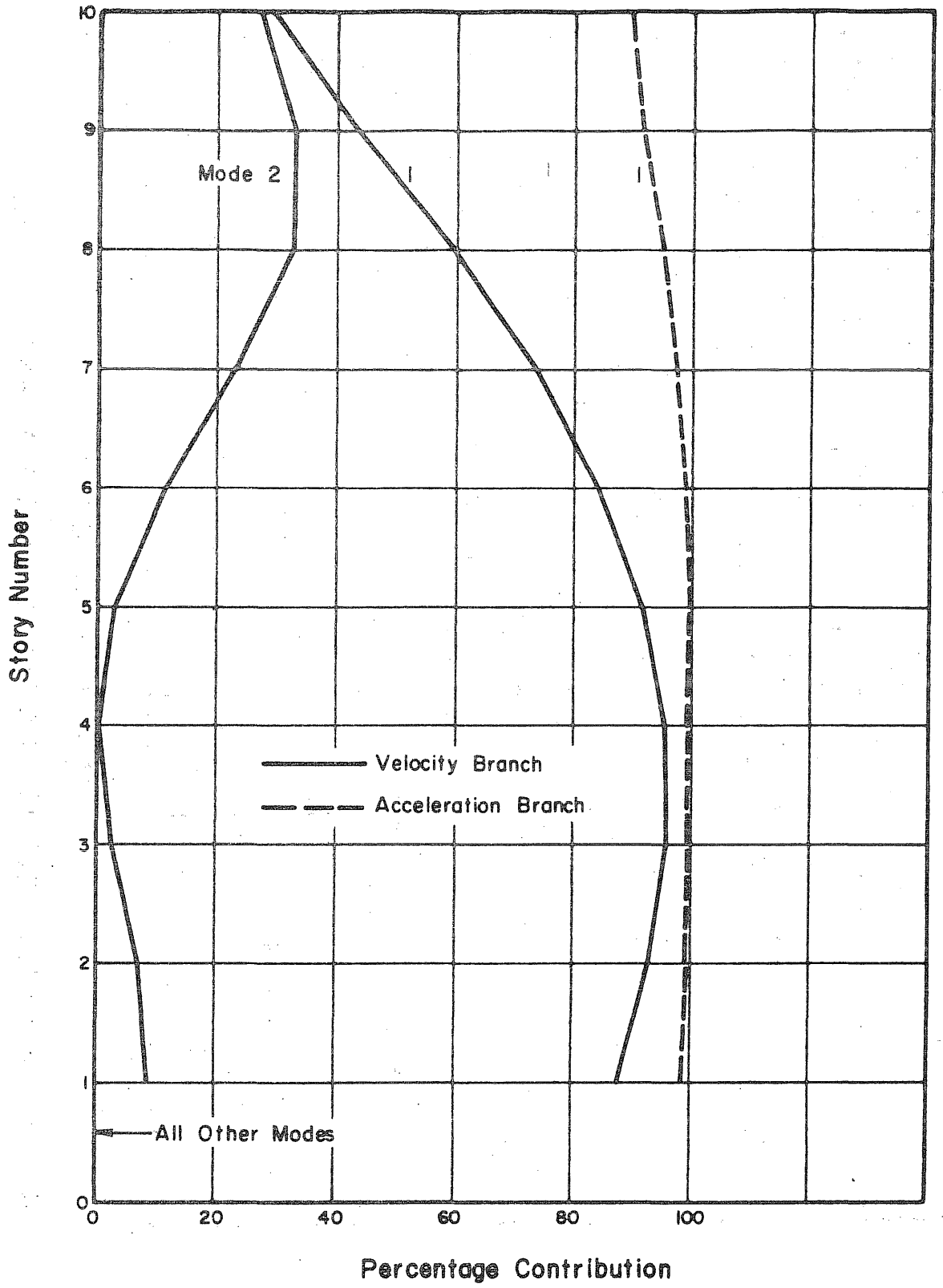

FIG. 37 SRSS CONTRIBUTIONS TO SPECTRAL SHEAR AND MOMENT (MODEL 10SA)

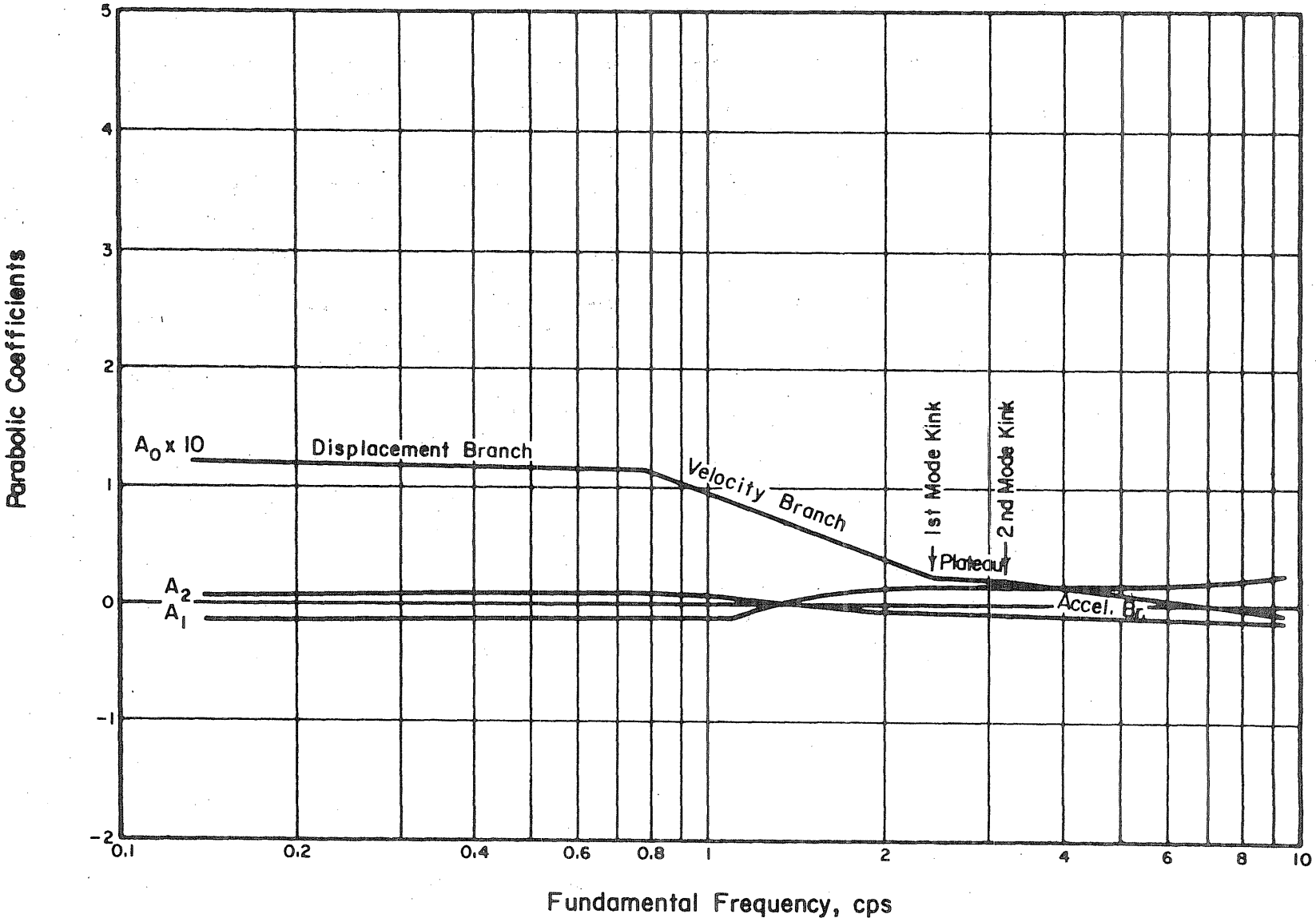

FIG. 38 PARABOLIC COEFFICIENTS FOR ACCELERATION— MODEL 10SA

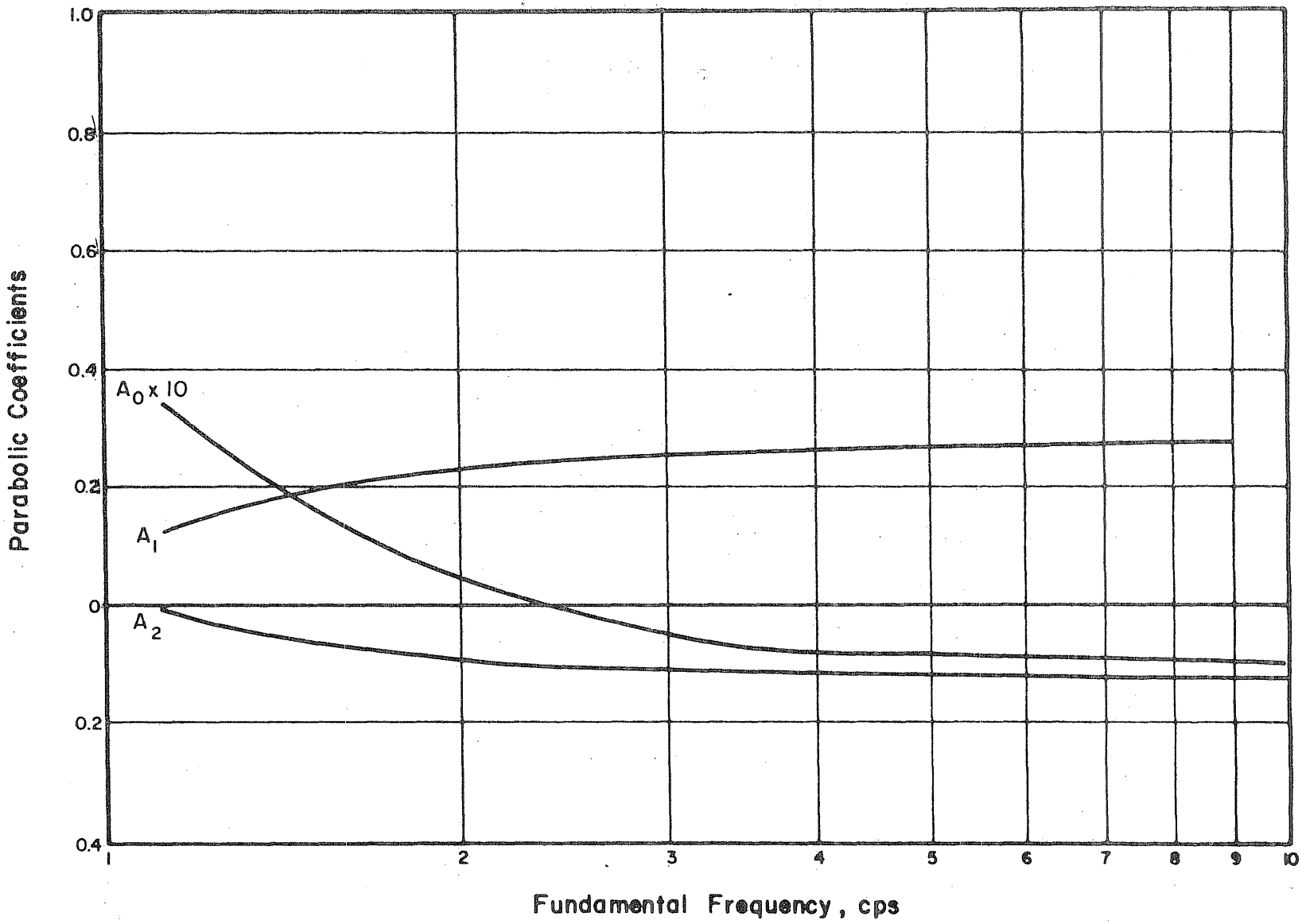

FIG. 39 PARABOLIC COEFFICIENTS FOR DISPLACEMENT—REFERENCE

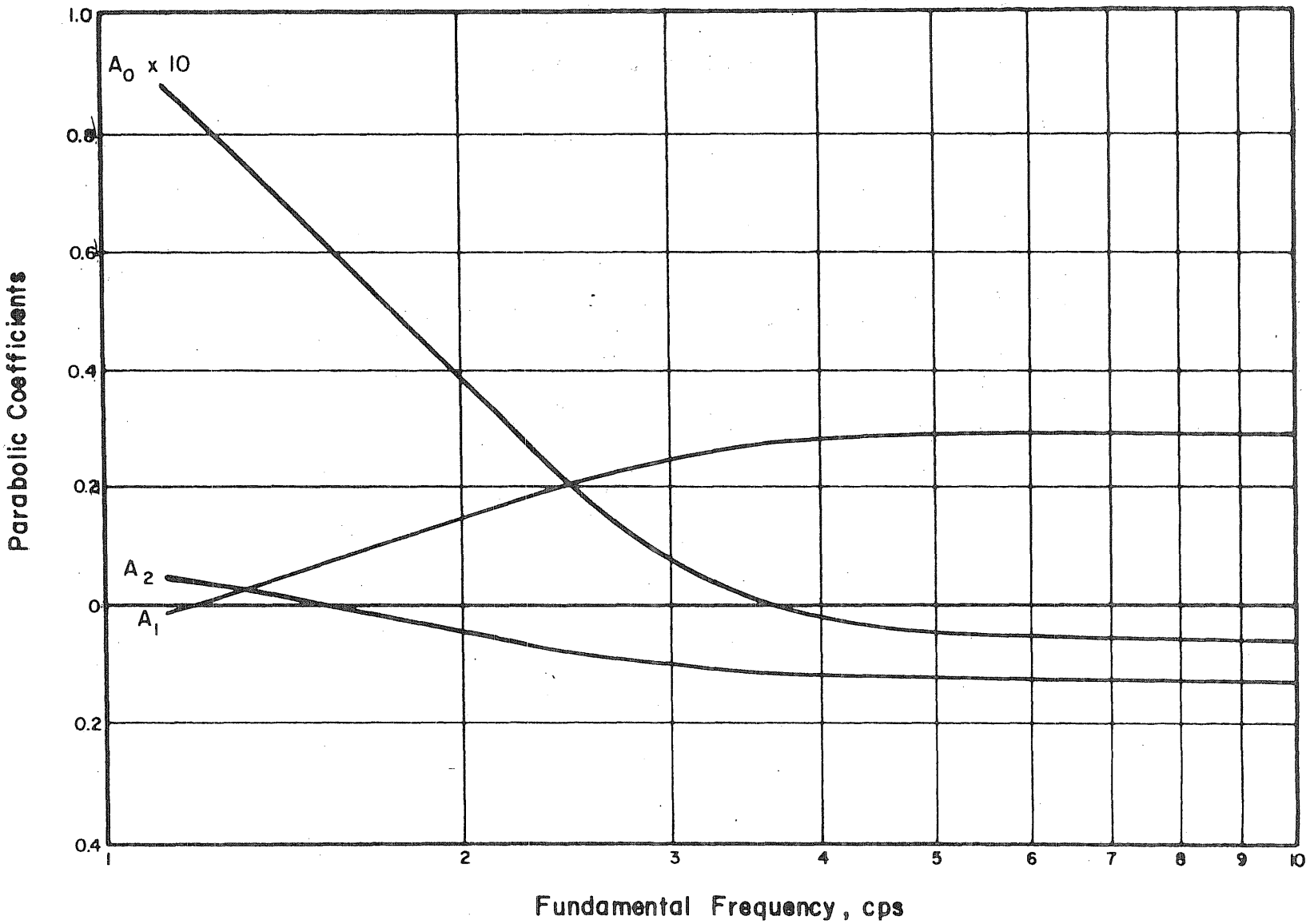

FIG. 40 PARABOLIC COEFFICIENTS FOR ACCELERATION—REFERENCE

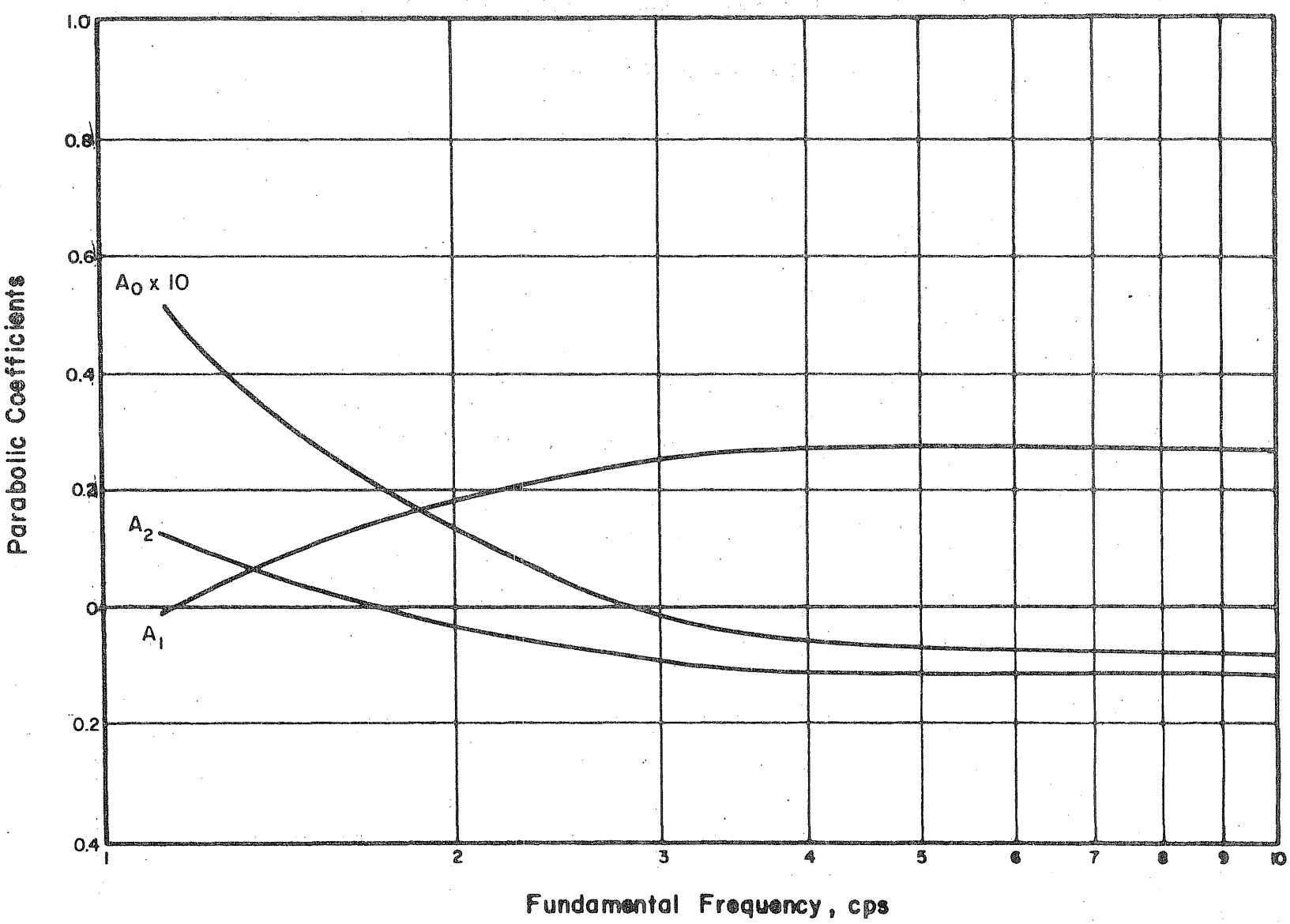

FIG. 41 PARABOLIC COEFFICIENTS FOR SHEAR AND MOMENT–REFERENCE

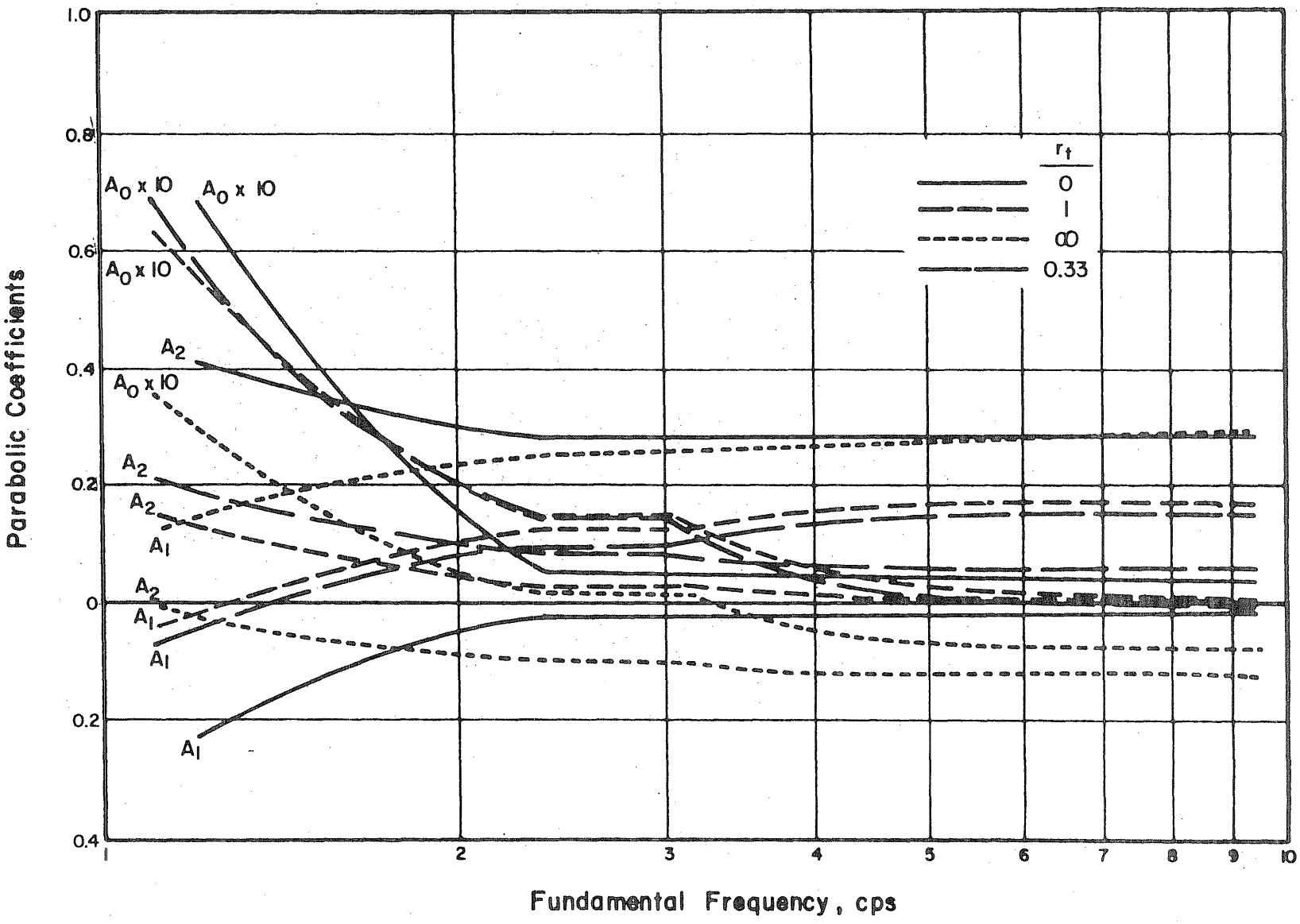

FIG. 42 PARABOLIC COEFFICIENTS FOR DISPLACEMENT — EFFECT OF TYPE OF BUILDING

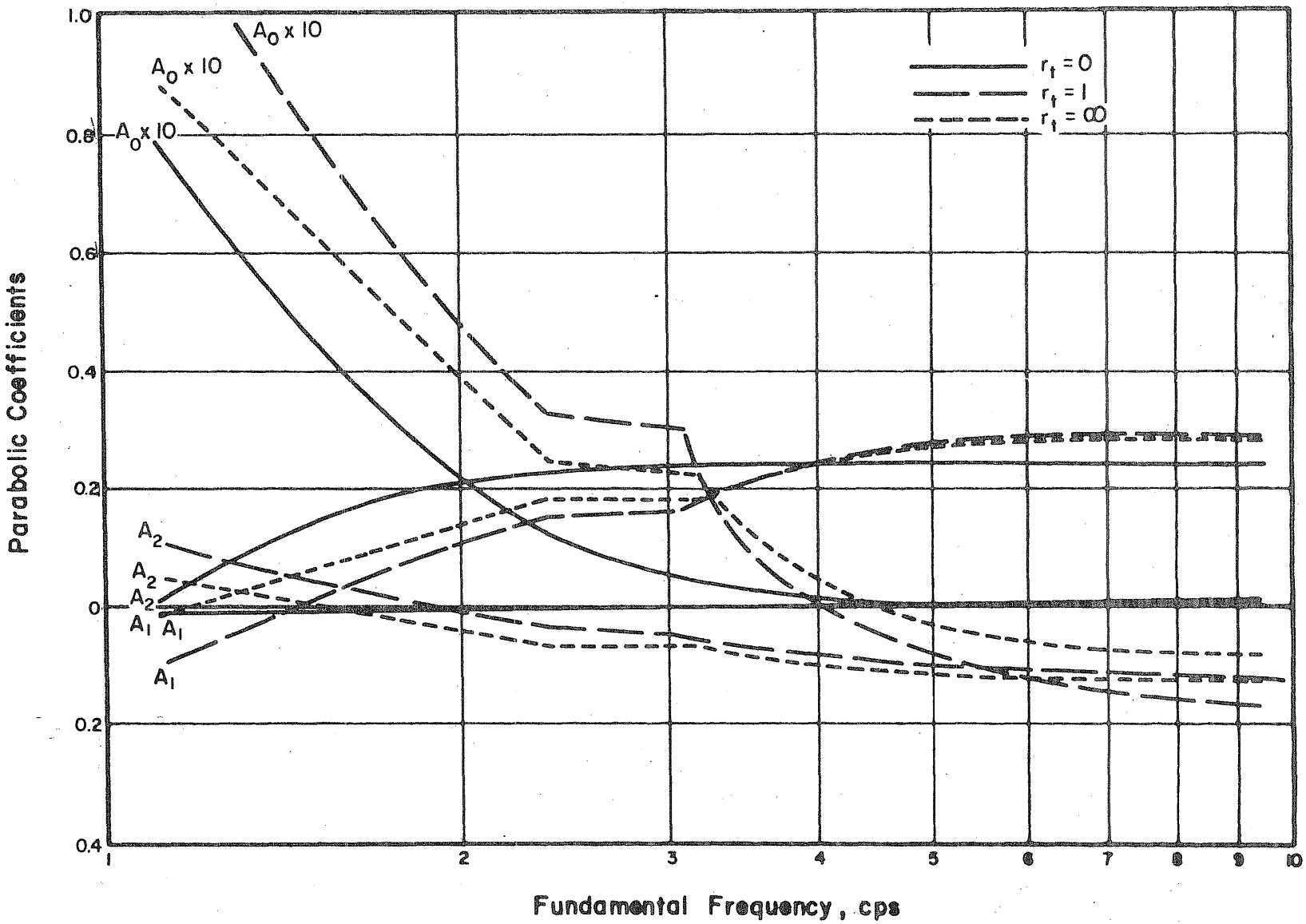

FIG. 43 PARABOLIC COEFFICIENTS FOR ACCELERATION—EFFECT OF TYPE OF BUILDING

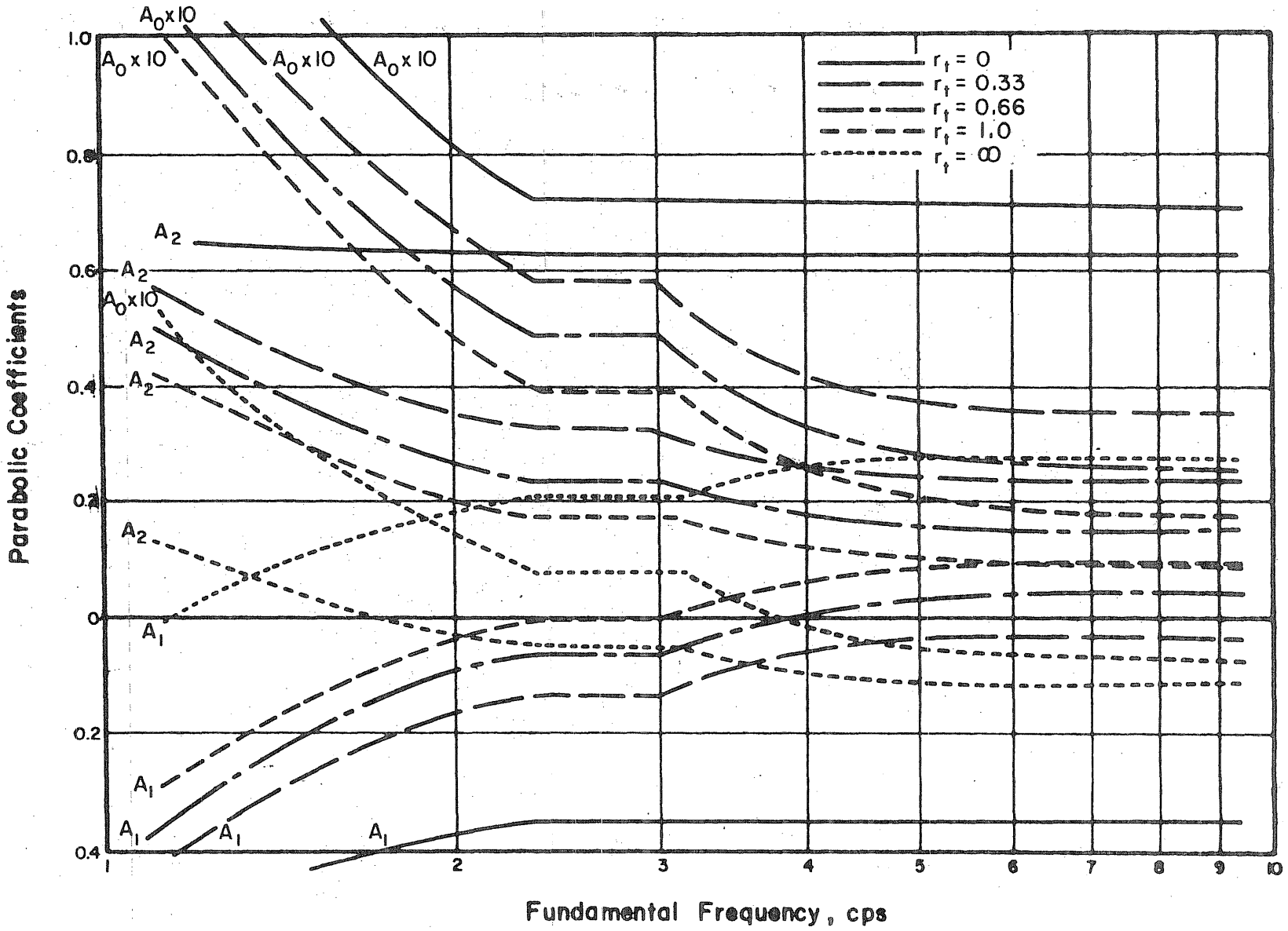

FIG. 44 PARABOLIC COEFFICIENTS FOR SHEAR AND MOMENT—EFFECT OF TYPE OF BUILDING

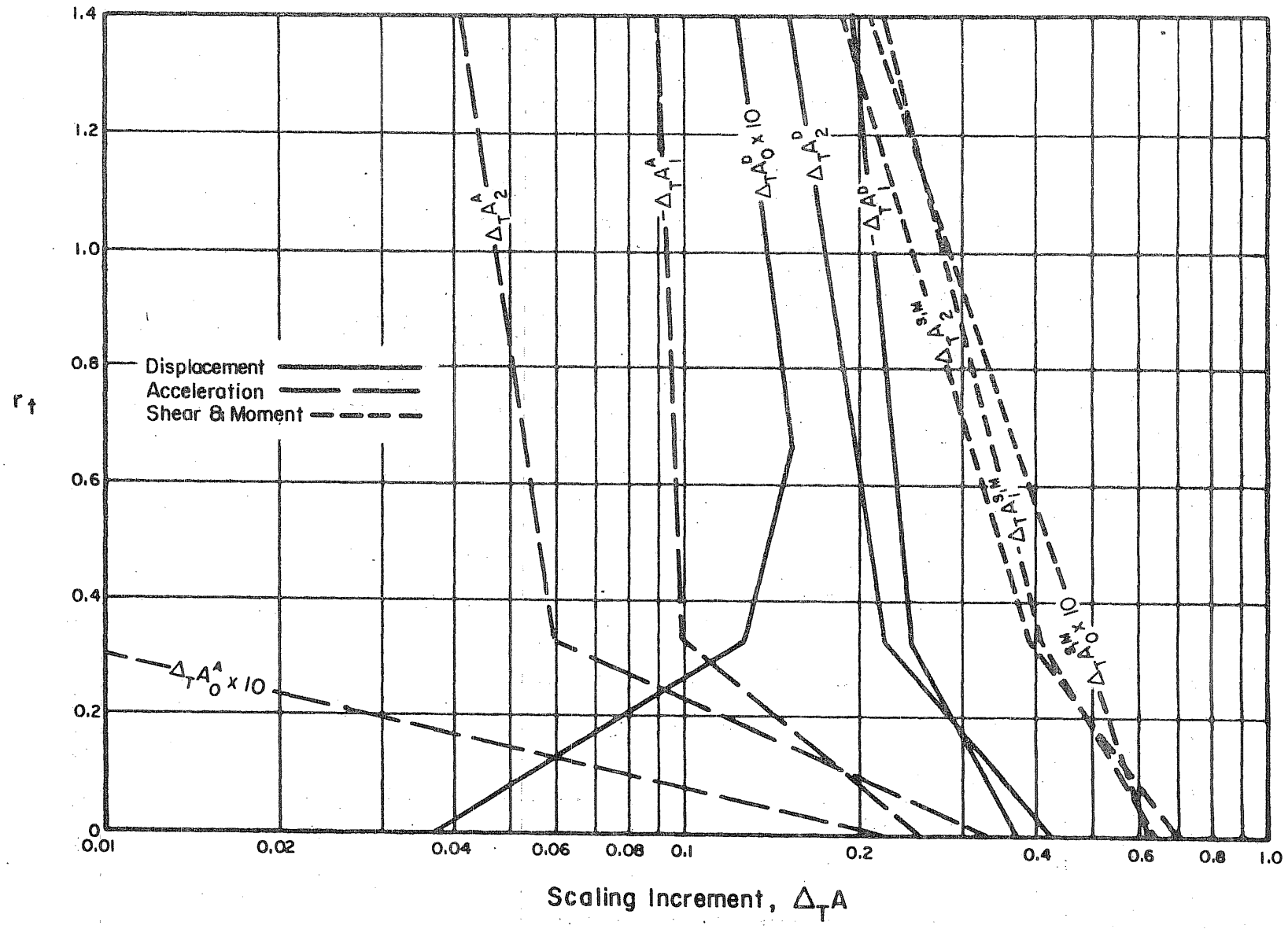

FIG. 45 SCALING INCREMENTS FOR TYPE OF BUILDING

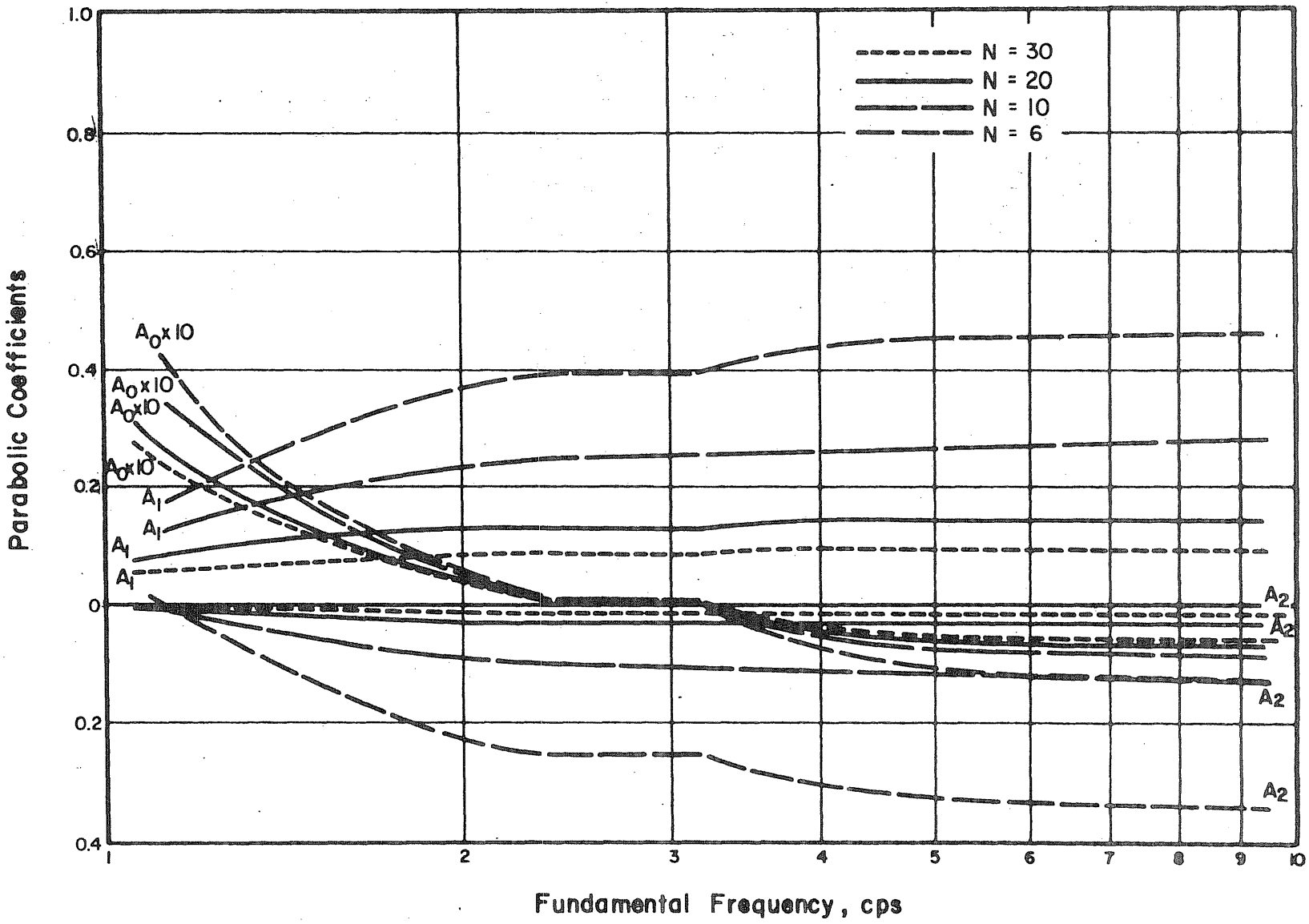

FIG. 46 PARABOLIC COEFFICIENTS FOR DISPLACEMENT—EFFECT OF NUMBER OF STORIES

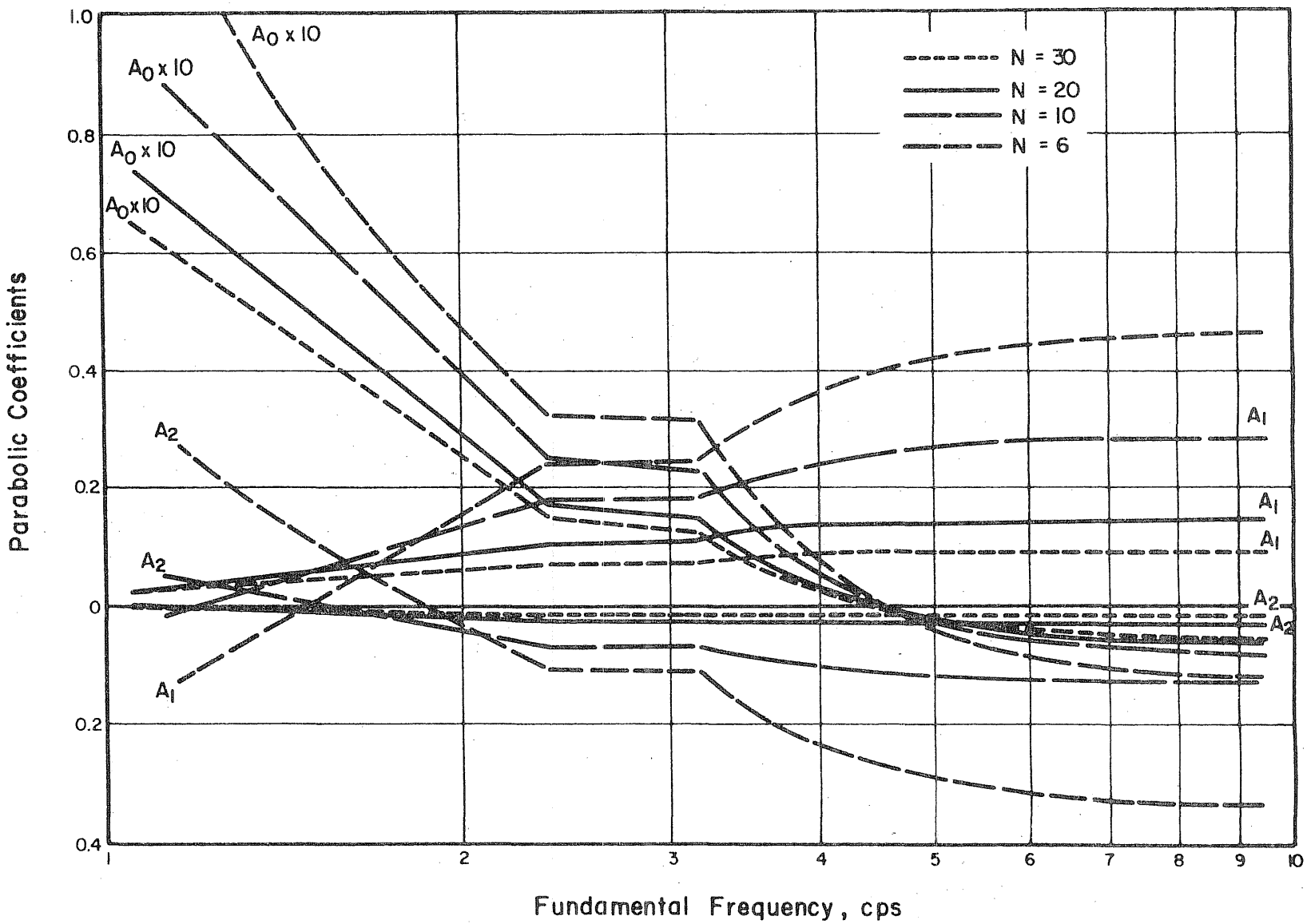

FIG. 47 PARABOLIC COEFFICIENTS FOR ACCELERATION—EFFECT OF NUMBER OF STORIES

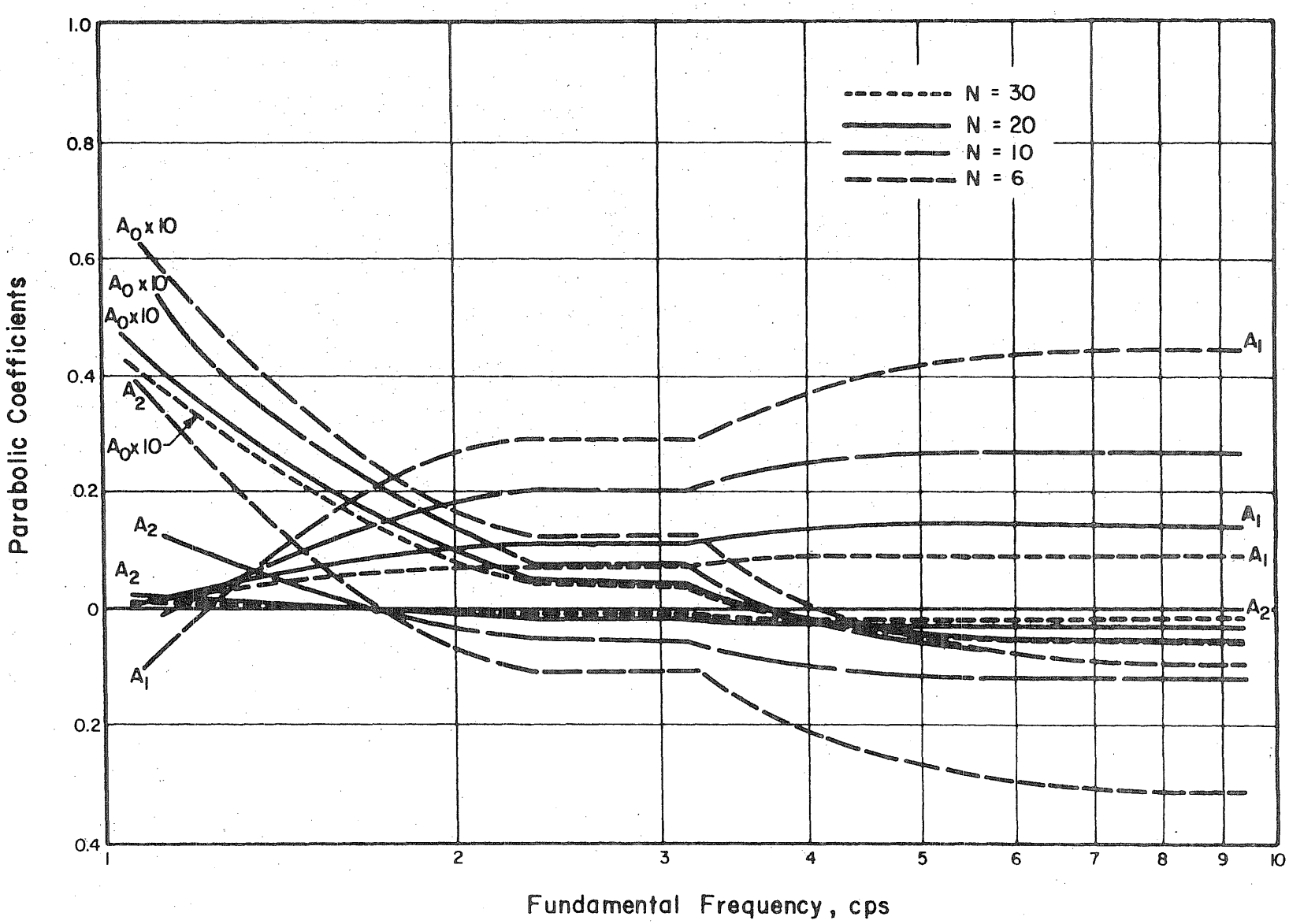

FIG. 48 PARABOLIC COEFFICIENTS FOR SHEAR AND MOMENT – EFFECT OF NUMBER OF STORIES

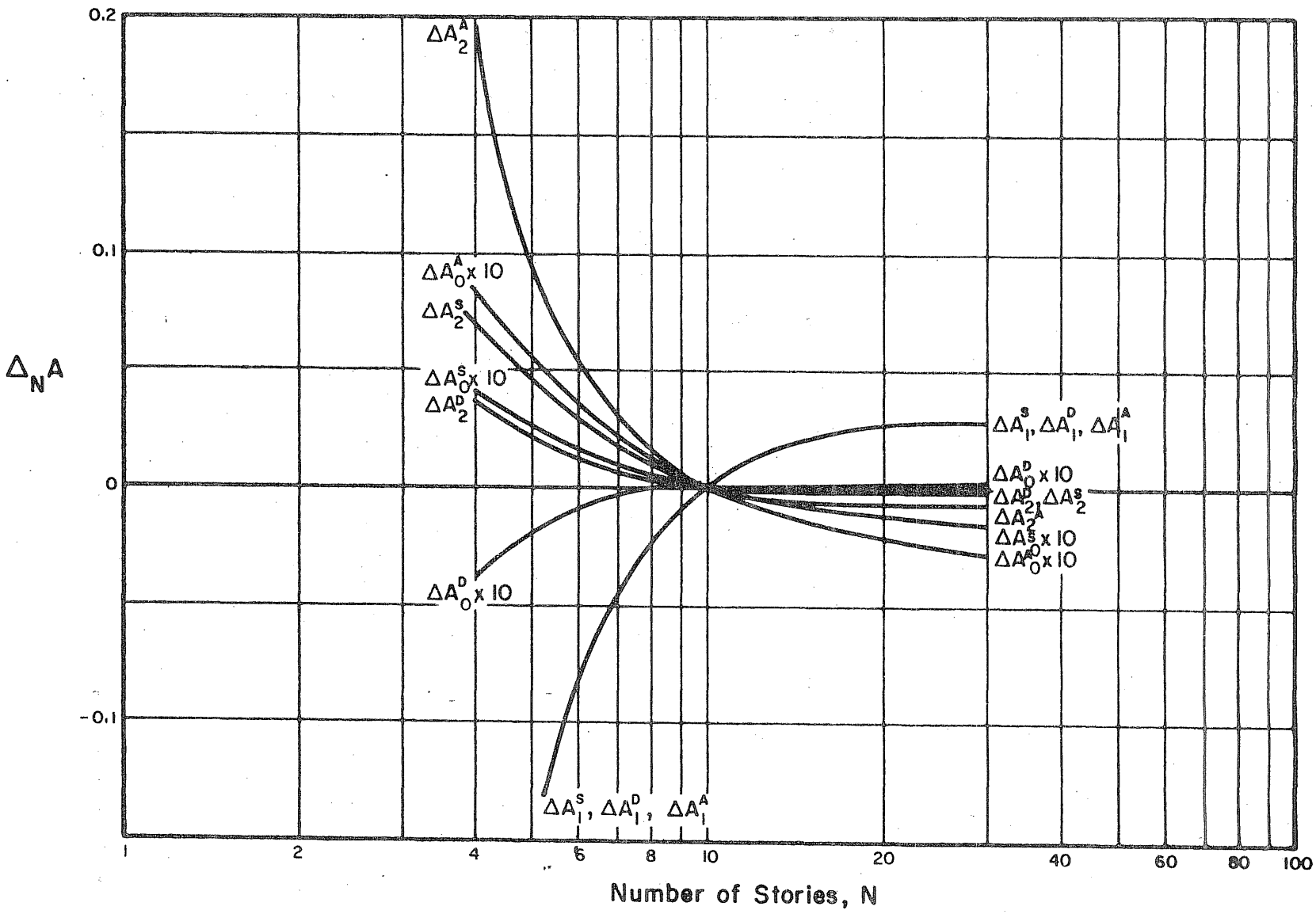

FIG. 49 SCALING INCREMENTS FOR NUMBER OF STORIES

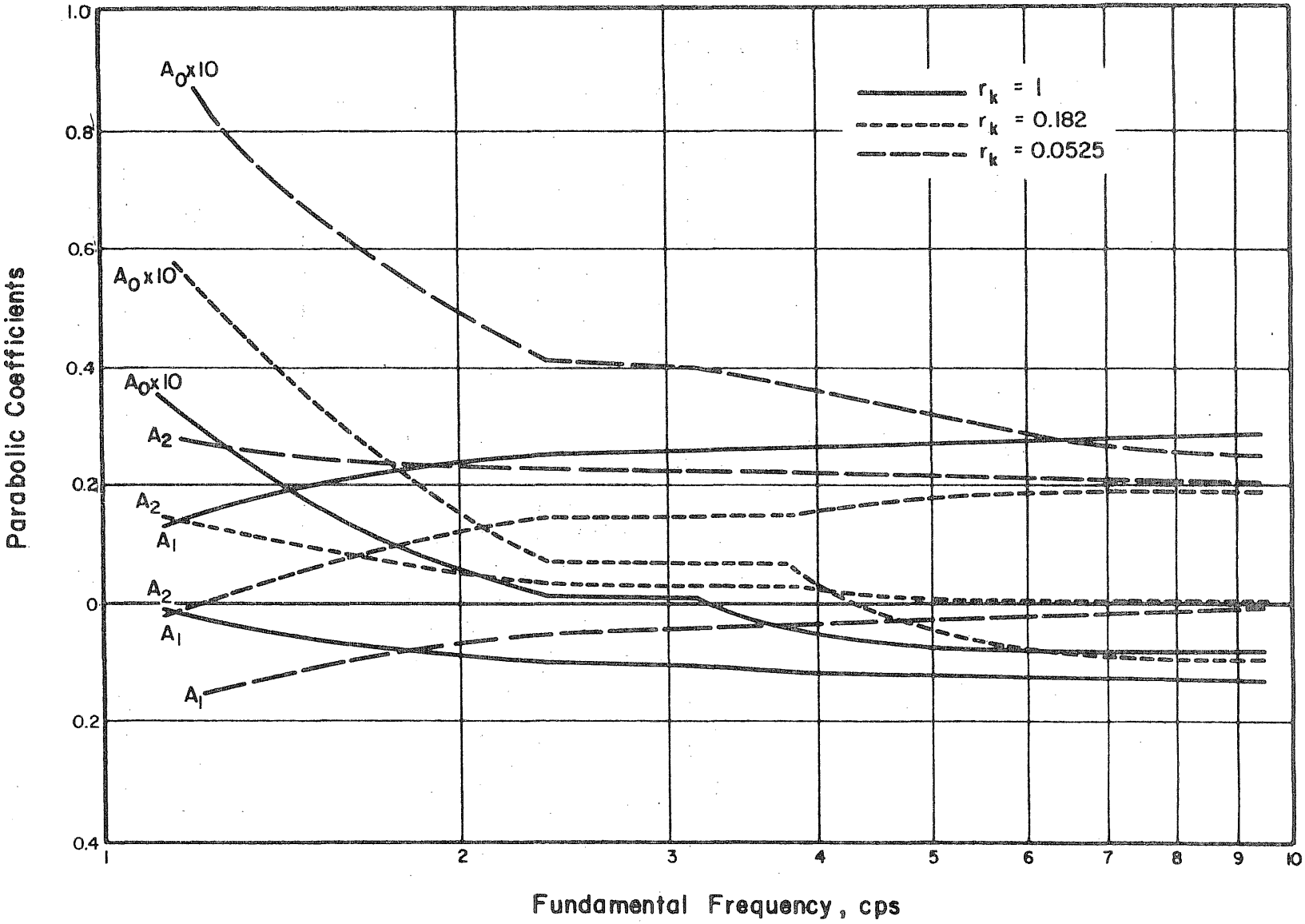

FIG. 50 PARABOLIC COEFFICIENTS FOR DISPLACEMENT—EFFECT OF STIFFNESS DISTRIBUTION

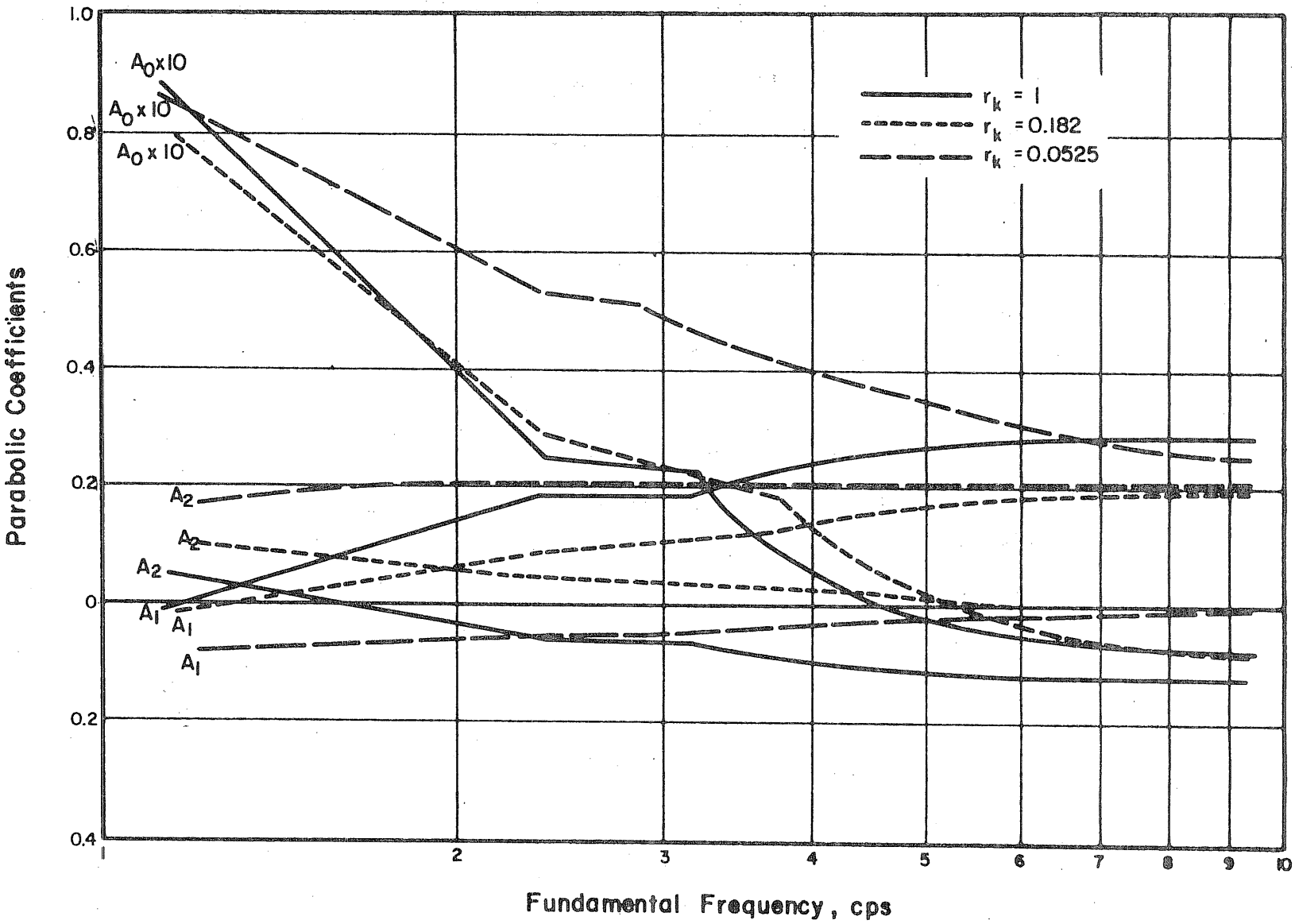

FIG. 51 PARABOLIC COEFFICIENTS FOR ACCELERATION-EFFECT OF STIFFNESS DISTRIBUTION

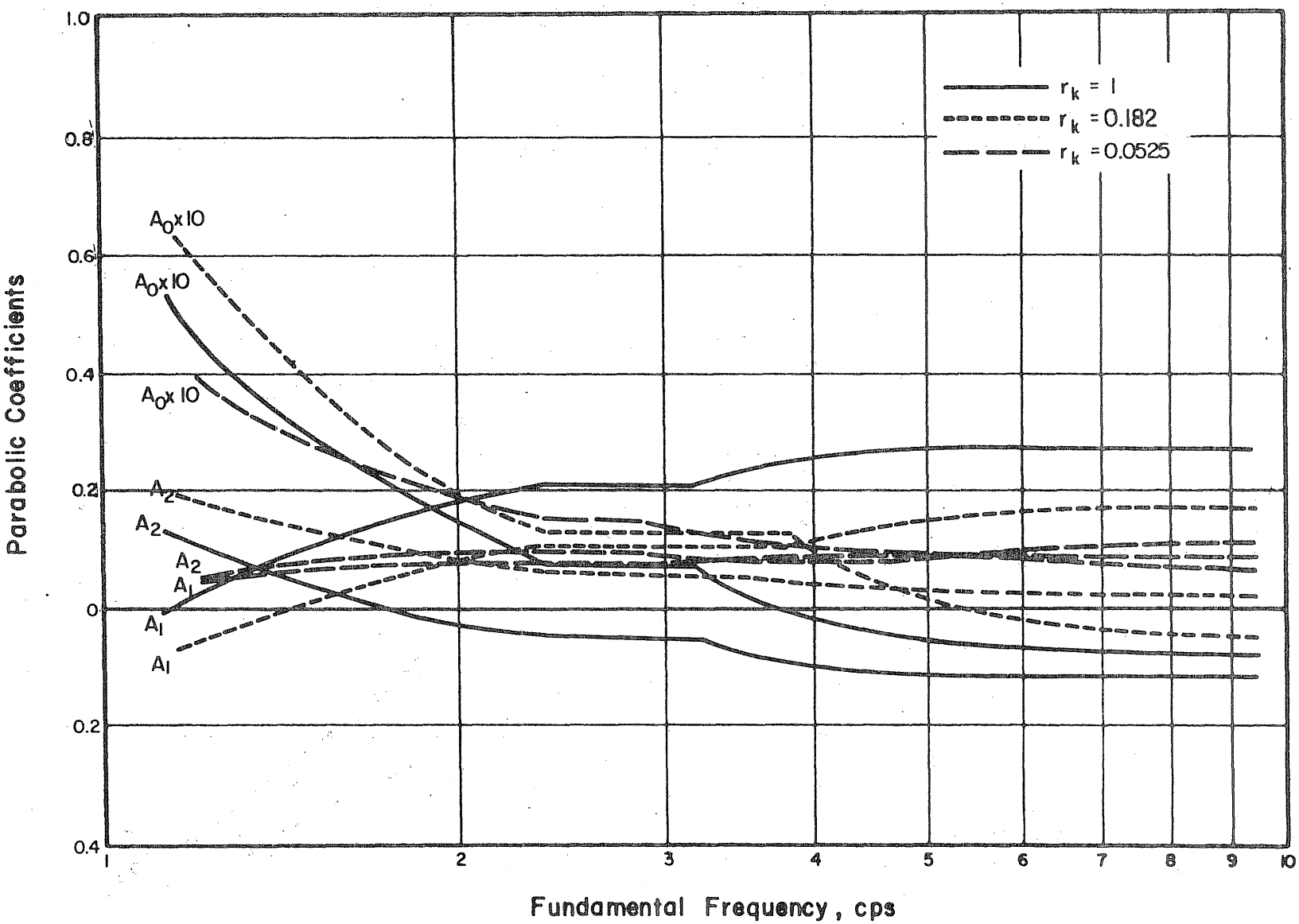

FIG. 52 PARABOLIC COEFFICIENTS FOR SHEAR AND MOMENT–EFFECT OF STIFFNESS DISTRIBUTION

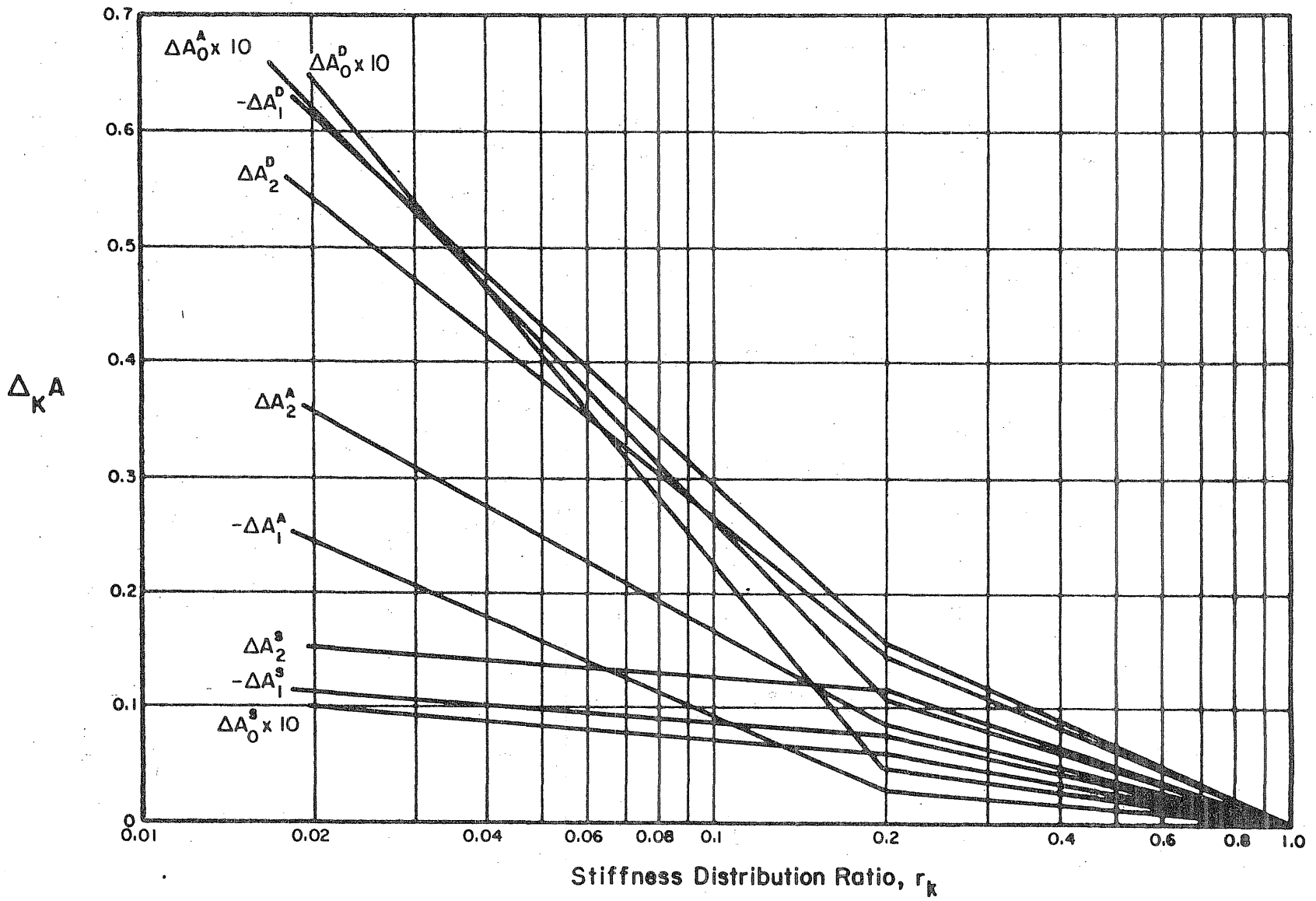

FIG. 53 SCALING INCREMENTS FOR STIFFNESS DISTRIBUTION

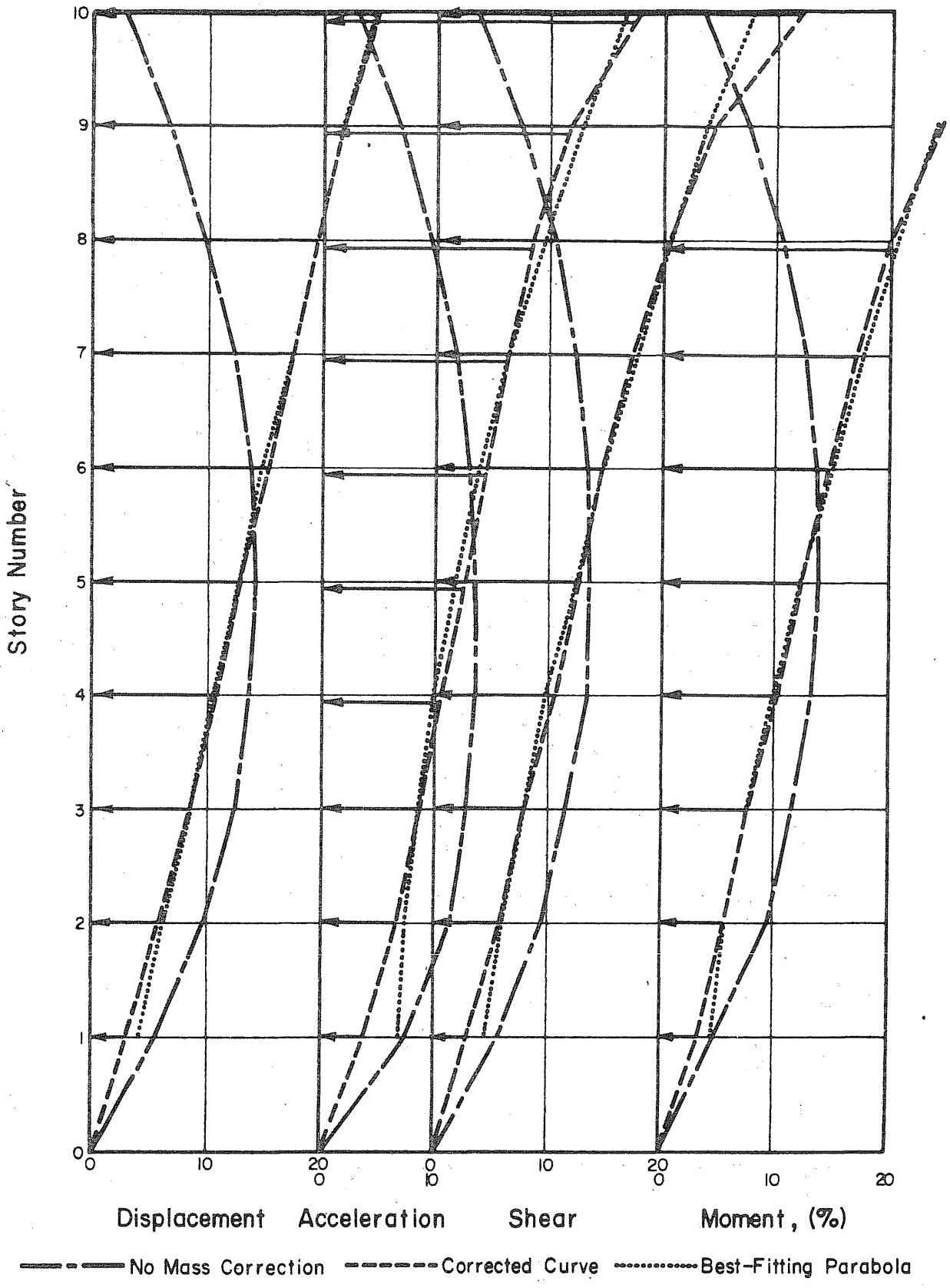

FIG. 54 SRSS VERTICAL VARIATION — MODEL IOSD, (f_1 = 2.4 cps)

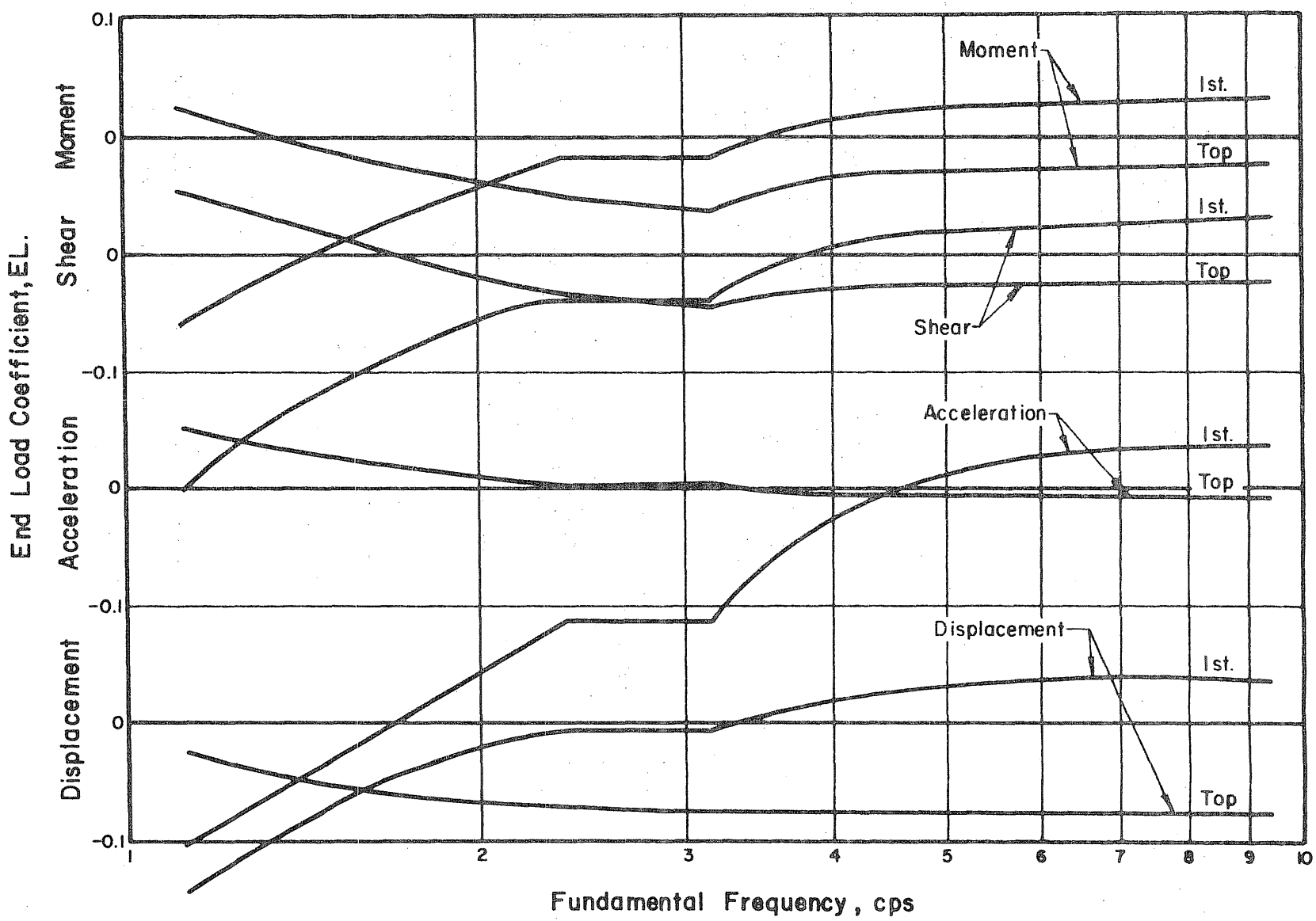

FIG. 55 END LOAD COEFFICIENTS AT FIRST AND TOP STORIES (MODEL IOSA)

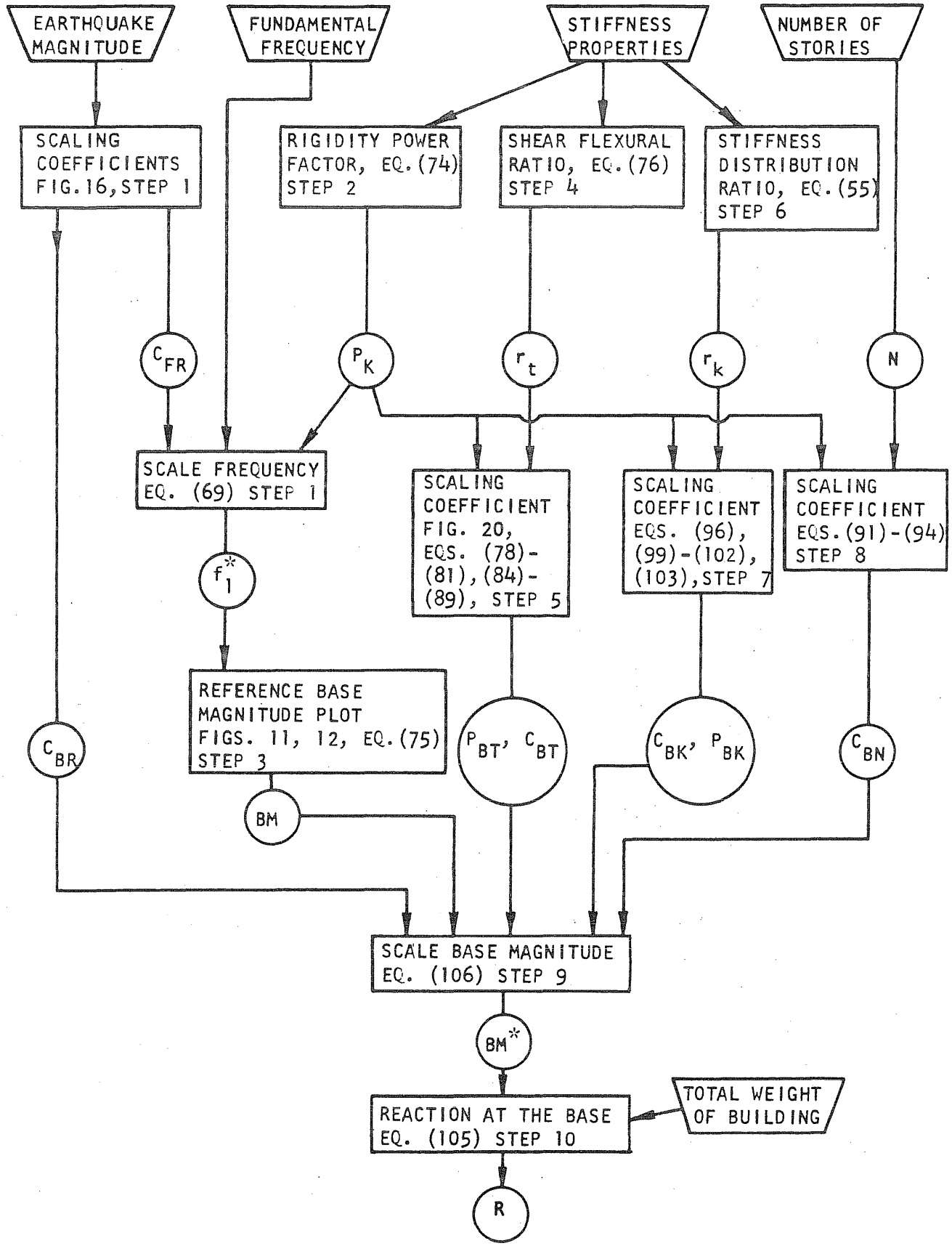

FIG. 56, COMPUTATIONAL PROCESS FOR BASE REACTION

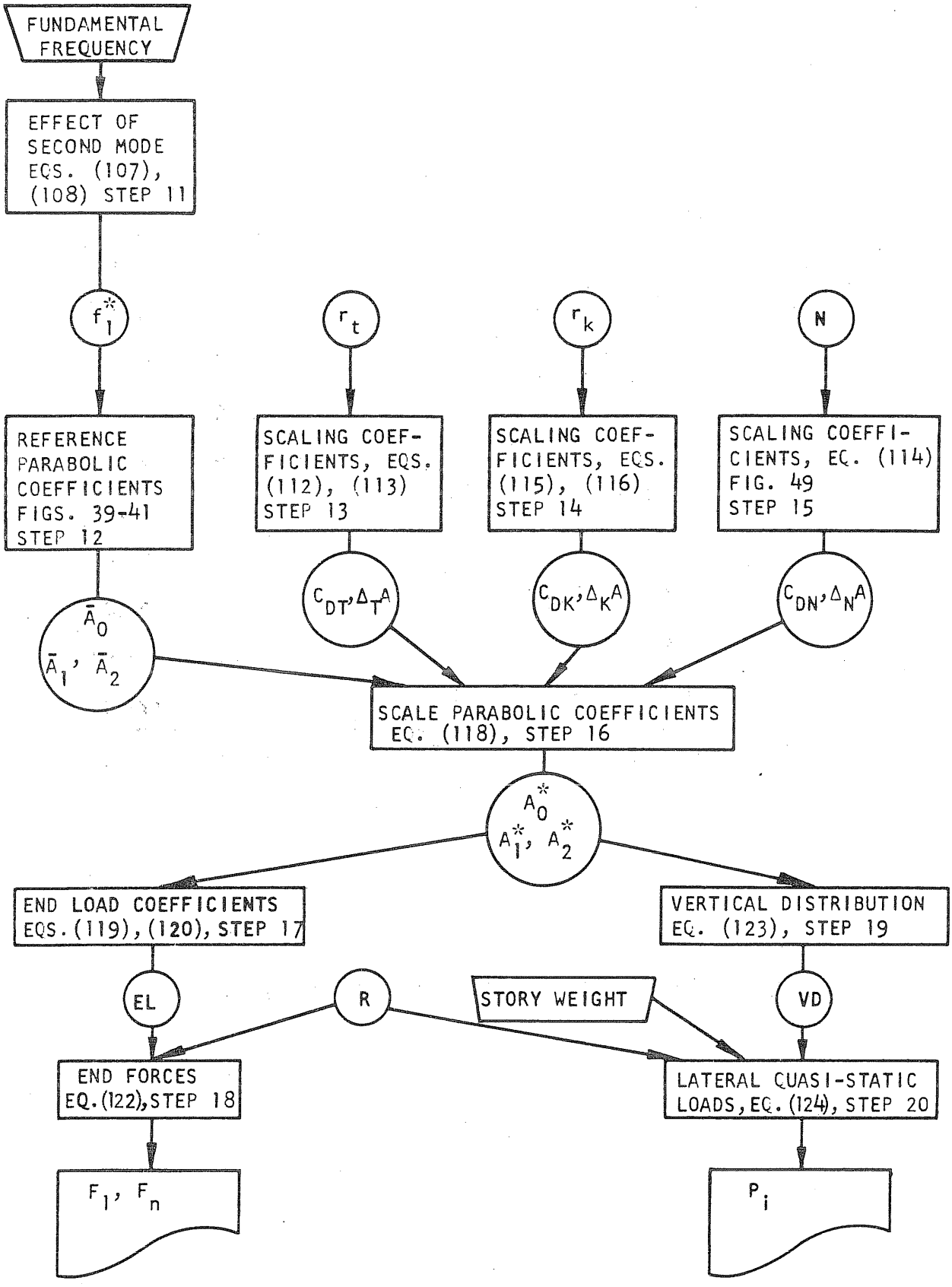

FIG. 57, COMPUTATIONAL PROCESS FOR QUASI-STATIC LATERAL DESIGN LOADS

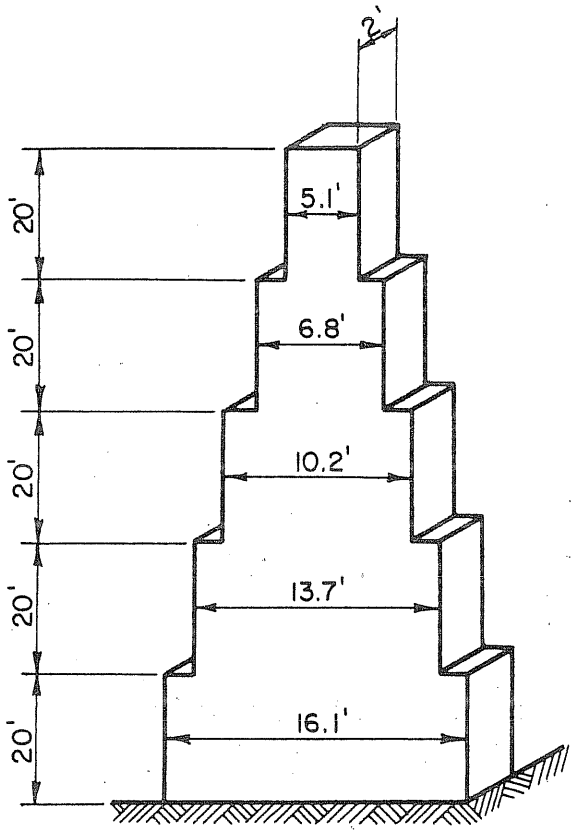

Story	ω_i (kips)	k_i (10^3k/in)
10	6.3	4.85
9	12.6	4.85
8	14.7	11.60
7	16.8	11.60
6	21.0	38.50
5	25.2	38.50
4	29.5	91.80
3	33.5	91.80
2	38.0	179.00
1	42.0	179.00
Total:	236.6	

FIG. 58 EXAMPLE 10-STORY SHEAR-WALL

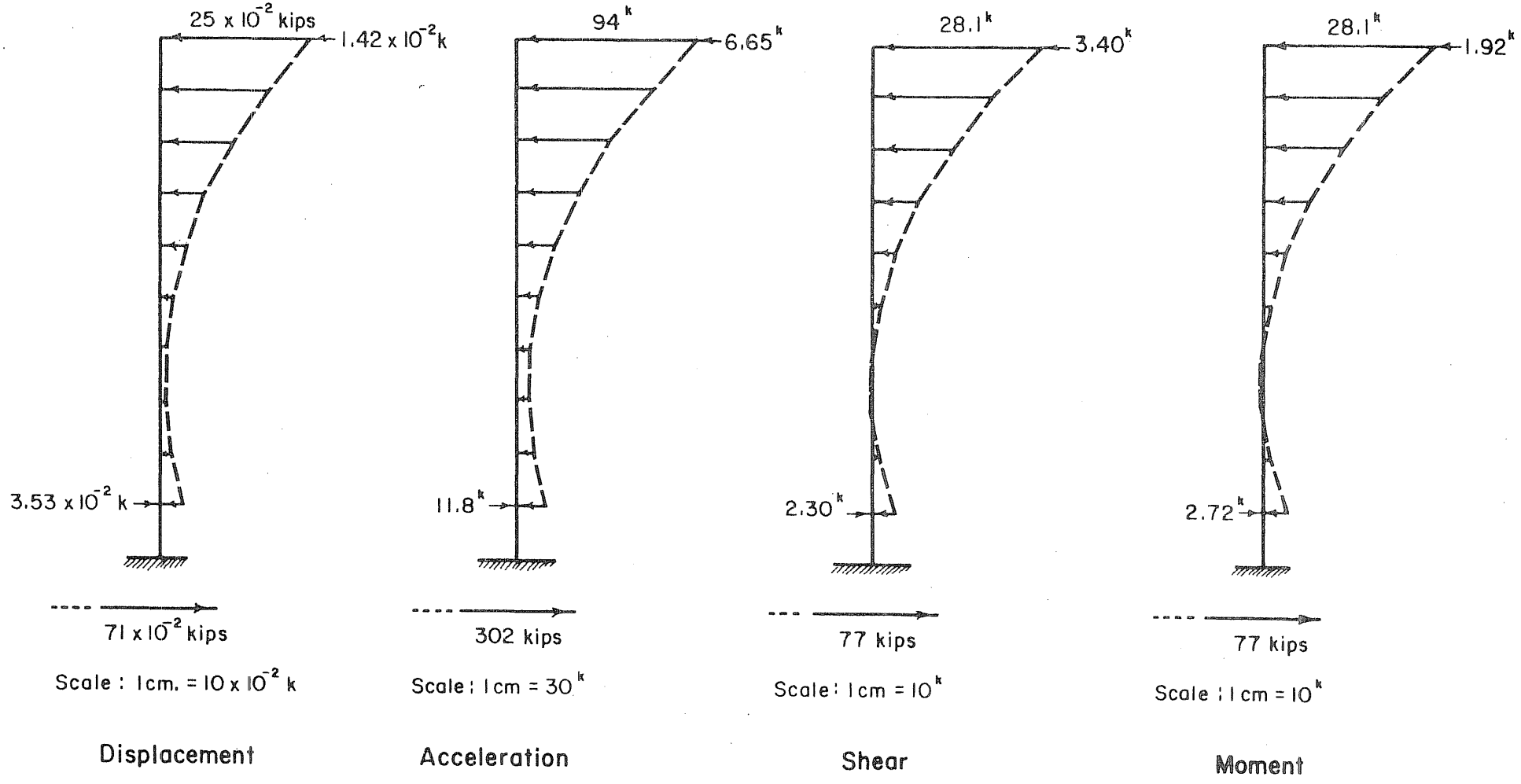

FIG. 59 EXAMPLE–QUASI–STATIC LATERAL DESIGN LOADS

PART 1 - GOVERNMENT

Administrative & Liaison Activities

Chief of Naval Research
Department of the Navy
Arlington, Virginia 22209
Attn: Code 423
439
468 (2)

Director
ONR Branch Office
495 Summer Street
Boston, Massachusetts 02210

Director
ONR Branch Office
219 S. Dearborn Street
Chicago, Illinois 60604

Director, Naval Research Laboratory
Attn: Library, Code 2029 (ONRL)
Washington, D. C. 20390 (5)

Commanding Officer
ONR Branch Office
207 West 24th Street
New York, New York 10011

Director
ONR Branch Office
1030 E. Green Street
Pasadena, California 91101

U. S. Naval Research Laboratory
Attn: Technical Information Div.
Washington, D. C. 20390 (6)

Defense Documentation Center
Cameron Station
Alexandria, Virginia 22314 (20)

Army

Commanding Officer
U. S. Army Research Office, Durham
Attn: Mr. J. J. Murray
CRD-AA-IP
Box CM, Duke Station
Durham, North Carolina 27706

Commanding Officer
AMXMR-ATL
Attn: Mr. J. Bluhm
U. S. Army Materials Res. Agcy.
Watertown, Massachusetts 02172

Watervliet Arsenal
MAGGS Research Center
Watervliet, New York
Attn: Director of Research

Radstone Scientific Info. Center
Chief, Document Section
U. S. Army Missile Command
Redstone Arsenal, Alabama 35809

Army R & D Center
Fort Belvoir, Virginia 22060

Technical Library
Aberdeen Proving Ground
Aberdeen, Maryland 21005

Navy

Commanding Officer and Director
Naval Ship Research & Development Center
Washington, D. C. 20390
Attn: Code 042 (Tech. Lib. Br.)
700 (Struc. Mech. Lab.)
720
725
800 (Appl. Math. Lab.)

901 (Dr. M. Strassberg)
941 (Dr. R. Liebowitz)
945 (Dr. W. S. Cramer)
960 (Mr. E. F. Noonan)
962 (Dr. E. Buchmann)

Aeronautical Structures Lab
Naval Air Engineering Center
Naval Base, Philadelphia, Pa. 19112

Naval Weapons Laboratory
Dahlgren, Virginia 22448

Naval Research Laboratory
Washington, D. C. 20390
Attn: Code 8400
8430
8440

Navy (cont'd)

Undersea Explosion Research Div.
Naval Ship R & D Center
Norfolk Naval Shipyard
Portsmouth, Virginia 23709
Attn: Mr. D. S. Cohen
Code 780

Nav. Ship R & D Center
Annapolis Division
Code 257, Library
Annapolis, Maryland 21402

Technical Library
Naval Underwater Weapons Center
Pasadena Annex
3202 E. Foothill Blvd.
Pasadena, California 91107

U. S. Naval Weapons Center
China Lake, California 93557
Attn: Code 4062 Mr. W. Werback
4520 Mr. Ken Bischel

Naval Research Laboratory
Washington, D. C. 20390
Attn: Code 8400 Ocean Tech. Div.
8440 Ocean Structures
6300 Metallurgy Div.
6305 Dr. J. Krafft

Commanding Officer
U. S. Naval Civil Engr. Lab.
Code L31
Port Hueneme, California 93041

Shipyard Technical Library
Code 242 L
Portsmouth Naval Shipyard
Portsmouth, New Hampshire 03804

U. S. Naval Electronics Laboratory
Attn: Dr. R. J. Christensen
San Diego, California 92152

U. S. Naval Ordnance Laboratory
Mechanics Division
RFD 1, White Oak
Silver Spring, Maryland 20910

U. S. Naval Ordnance Laboratory
Attn: Mr. H. A. Perry, Jr.
Non-Metallic Materials Division
Silver Spring, Maryland 20910

Supervisor of Shipbuilding
U. S. Navy
Newport News, Virginia 23607

Shipyard Technical Library
Building 746, Code 303TL
Mare Island Naval Shipyard
Vallejo, California 94592

U. S. Navy Underwater Sound Ref. Lab.
Office of Naval Research
P. O. Box 8337
Orlando, Florida 32806

Technical Library
U. S. Naval Ordnance Station
Indian Head, Maryland 20640

U. S. Naval Ordnance Station
Attn: Mr. Garet Bornstein
Research & Development Division
Indian Head, Maryland 20640

Chief of Naval Operation
Department of the Navy
Washington, D. C. 20350
Attn: Code Op-03EG
Op-07T

Special Projects Office
(CNM-PM-1) (MUN)
Department of the Navy
Washington, D. C. 20360
Attn: NSP-001 Dr. J. P. Craven

Deep Submergence Sys. Project
(CNM-PM-11)
6900 Wisconsin Ave.
Chevy Chase, Md. 20015
Attn: PM-1120 S. Hersh

U. S. Naval Applied Science Lab.
Code 9832
Technical Library
Building 291, Naval Base
Brooklyn, New York 11251

Director, Aeronautical Materials Lab.
Naval Air Engineering Center
Naval Base
Philadelphia, Pennsylvania 19112

Navy (cont'd)

Naval Air Systems Command
Dept. of the Navy
Washington, D.C. 20360
Attn: NAIR 03 Res. & Technology
320 Aero. & Structures
5320 Structures
604 Tech. Library

Naval Facilities Engineering
Command
Dept. of the Navy
Washington, D.C. 20360
Attn: NFAC 03 Res. & Development
04 Engineering & Design
04128 Tech. Library

Naval Ship Systems Command
Dept. of the Navy
Washington, D.C. 20360
Attn: NSHIP 031 Ch. Scientists for R & D
0342 Ship Mats. & Structs.
037 Ship Silencing Div.
052 Shock & Blast Coord.
2052 Tech. Library

Naval Ship Engineering Center
Main Navy Building
Washington, D.C. 20360
Attn: NSEC 6100 Ship Sys. Engr. & Des. Dept.
61020 Computerated Ship Des.
6105 Ship Protection
6110 Ship Concept Design
6120 Hull Div. - J. Nachtsheim
6120D Hull Div. - J. Vasta
6132 Hull Structs. - (4)

Naval Ordnance Systems Command
Dept. of the Navy
Washington, D.C. 20360
Attn: NORD 03 Res. & Technology
035 Weapons Dynamics
9132 Tech. Library

Air Force

Commander WADD
Wright-Patterson Air Force Base
Dayton, Ohio 45433
Attn: Code WWRMDD
AFFDL (FDDS)

Wright-Patterson AFB (cont'd)
Attn: Structures Division
AFLC (MCEEA)
Code WWRC
AFML (MAAM)

Commander
Chief, Applied Mechanics Group
U. S. Air Force Inst. of Tech.
Wright-Patterson Air Force Base
Dayton, Ohio 45433

Chief, Civil Engineering Branch
WLRC, Research Division
Air Force Weapons Laboratory
Kirtland AFB, New Mexico 87117

Air Force Office of Scientific Res.
1400 Wilson Blvd.
Arlington, Virginia 22209
Attn: Mechs. Div.

NASA

Structures Research Division
National Aeronautics & Space Admin.
Langley Research Center
Langley Station
Hampton, Virginia 23365
Attn: Mr. R. R. Heldenfels, Chief

National Aeronautic & Space Admin.
Associate Administrator for Advanced
Research & Technology
Washington, D.C. 20546

Scientific & Tech. Info. Facility
NASA Representative (S-AK/DL)
P. O. Box 5700
Bethesda, Maryland 20014

National Aeronautic & Space Admin.
Code RV-2
Washington, D.C. 20546

Other Government Activities

Commandant
Chief, Testing & Development Div.
U. S. Coast Guard
1300 E Street, N. W.
Washington, D. C. 20226

Director
Marine Corps Landing Force Dev. Cen.
Marine Corps Schools
Quantico, Virginia 22134

Director
National Bureau of Standards
Washington, D. C. 20234
Attn: Mr. B. L. Wilson, EM 219

National Science Foundation
Engineering Division
Washington, D. C. 20550

Science & Tech. Division
Library of Congress
Washington, D. C. 20540

Director
STBS
Defense Atomic Support Agency
Washington, D. C. 20350

Commander Field Command
Defense Atomic Support Agency
Sandia Base
Albuquerque, New Mexico 87115

Chief, Defense Atomic Support Agency
Blast & Shock Division
The Pentagon
Washington, D. C. 20301

Director, Defense Research & Engr.
Technical Library
Room 3C-128
The Pentagon
Washington, D. C. 20301

Chief, Airframe & Equipment Branch
FS-120
Office of Flight Standards
Federal Aviation Agency
Washington, D. C. 20553

Chief, Division of Ship Design
Maritime Administration
Washington, D. C. 20235

Deputy Chief, Office of Ship Constr.
Maritime Administration
Washington, D. C. 20235
Attn: Mr. U. L. Russo

Mr. Milton Shaw, Director
Div. of Reactor Devel. & Technology
Atomic Energy Commission
Germantown, Md. 20767

Ship Hull Research Committee
National Research Council
National Academy of Sciences
2101 Constitution Avenue
Washington, D. C. 20418
Attn: Mr. A. R. Lytle

PART 2 - CONTRACTORS AND OTHER
TECHNICAL COLLABORATORS

Universities

Professor J. R. Rice
Division of Engineering
Brown University
Providence, Rhode Island 02912

Dr. J. Tinsley Oden
Dept. of Engr. Mechs.
University of Alabama
Hunstville, Alabama

Professor M. E. Gurtin
Dept. of Mathematics
Carnegie Institute of Technology
Pittsburgh, Pennsylvania 15213

Professor R. S. Rivlin
Center for the Application of Mathematics
Lehigh University
Bethlehem, Pennsylvania 18015

Professor Julius Miklowitz
Division of Engr. & Applied Sciences
California Institute of Technology
Pasadena, California 91109

Professor George Sih
Department of Mechanics
Lehigh University
Bethlehem, Pennsylvania 18015

Dr. Harold Liebowitz, Dean
School of Engr. & Applied Sciences
George Washington University
725 23rd Street
Washington, D. C. 20006

Universities (cont'd)

Professor Eli Sternberg
Div. of Engr. & Applied Sciences
California Institute of Technology
Pasadena, California 91109

Professor Paul M. Naghdi
Div. of Applied Mechanics
Etcheverry Hall
University of California
Berkeley, California 94720

Professor Wm. Prager
Revelle College
University of California
P. O. Box 109
La Jolla, California 92037

Professor J. Baltrukonis
Mechanics Division
The Catholic Univ. of America
Washington, D. C. 20017

Professor A. J. Durelli
Mechanics Division
The Catholic Univ. of America
Washington, D. C. 20017

Professor H. H. Bleich
Department of Civil Engineering
Columbia University
Amsterdan & 120th Street
New York, New York 10027

Professor R. D. Mindlin
Department of Civil Engineering
Columbia University
S. W. Mudd Building
New York, New York 10027

Professor F. L. DiMaggio
Department of Civil Engineering
Columbia University
616 Mudd Building
New York, New York 10027

Professor A. M. Freudenthal
Department of Civil Engr. &
Engr. Mechs.
Columbia University
New York, New York 10027

Professor B. A. Boley
Dept. of Theor, & Appl. Mechs.
Cornell University
Ithaca, New York 14850

Professor P. G. Hodge
Department of Mechanics
Illinois Institute of Technology
Chicago, Illinois 60616

Dr. D. C. Drucker
Dean of Engineering
University of Illinois
Urbana, Illinois 61803

Professor N. M. Newmark
Dept. of Civil Engineering
University of Illinois
Urbana, Illinois 61803

Professor A. R. Robinson
Dept. of Civil Engineering
University of Illinois
Urbana, Illinois 61803

Professor S. Taira
Department of Engineering
Kyoto University
Kyoto, Japan

Professor James Mar
Massachusetts Inst. of Tech.
Rm. 33-318
Dept. of Aerospace & Astro.
77 Massachusetts Avenue
Cambridge, Massachusetts 02139

Professor E. Reissner
Dept. of Mathematics
Massachusetts Inst. of Tech.
Cambridge, Massachusetts 02139

Professor William A. Nash
Dept. of Mechs. & Aerospace Engr.
University of Massachusetts
Amherst, Massachusetts 01002

Library (Code 0384)
U. S. Naval Postgraduate School
Monterey, California 93940

Professor Arnold Allentuch
Department of Mechanical Engineering
Newark College of Engineering
323 High Street
Newark, New Jersey 07102

Universities (cont'd)

Professor E. L. Reiss
Courant Inst. of Math. Sciences
New York University
4 Washington Place
New York, New York 10003

Professor Bernard W. Shaffer
School of Engrg. & Science
New York University
University Heights
New York, New York 10453

Dr. Francis Cozzarelli
Div. of Interdisciplinary
Studies and Research
School of Engineering
State University of New York
Buffalo, New York 14214

Professor R. A. Douglas
Dept. of Engr. Mechs.
North Carolina St. Univ.
Raleigh, North Carolina 27606

Dr. George Herrmann
The Technological Institute
Northwestern University
Evanston, Illinois 60201

Professor J. D. Achenbach
Technological Institute
Northwestern University
Evanston, Illinois 60201

Director, Ordnance Research Lab.
Pennsylvania State University
P. O. Box 30
State College, Pennsylvania 16801

Professor Eugene J. Skudrzyk
Department of Physics
Ordnance Research Lab.
Pennsylvania State University
P. O. Box 30
State College, Pennsylvania 16801

Dean Oscar Baguio
Assoc. of Struc. Engr. of
the Philippines
University of Philippines
Manila, Philippines

Professor J. Kempner
Dept. of Aero. Engr. & Applied Mech.
Polytechnic Institute of Brooklyn
333 Jay Street
Brooklyn, New York 11201

Professor J. Klosner
Polytechnic Institute of Brooklyn
333 Jay Street
Brooklyn, New York 11201

Professor A. C. Eringen
Dept. of Aerospace & Mech. Sciences
Princeton University
Princeton, New Jersey 08540

Dr. S. L. Koh
School of Aero., Astro. & Engr. Science
Purdue University
Lafayette, Indiana 47907

Professor R. A. Schapery
Purdue University
Lafayette, Indiana 47907

Professor E. H. Lee
Div. of Engr. Mechanics
Stanford University
Stanford, California 94305

Dr. Nicholas J. Hoff
Dept. of Aero. & Astro.
Stanford University
Stanford, California 94305

Professor Max Anliker
Dept. of Aero. & Astro.
Stanford University
Stanford, California 94305

Professor J. N. Goodier
Div. of Engr. Mechanics
Stanford University
Stanford, California 94305

Professor H. W. Liu
Dept. of Chemical Engr. & Metal.
Syracuse University
Syracuse, New York 13210

Professor Markus Reiner
Technion R & D Foundation
Haifa, Israel

Universities (cont'd)

Professor Tsuyoshi Hayashi
Department of Aeronautics
Faculty of Engineering
University of Tokyo
BUNKYO-KU
Tokyo, Japan

Professor J. E. Fitzgerald, Ch.
Dept. of Civil Engineering
University of Utah
Salt Lake City, Utah 84112

Professor R. J. H. Bollard
Chairman, Aeronautical Engr. Dept.
207 Guggenheim Hall
University of Washington
Seattle, Washington 98105

Professor Albert S. Kobayashi
Dept. of Mechanical Engr.
University of Washington
Seattle, Washington 98105

Officer-in-Charge
Post Graduate School for Naval Off.
Webb Institute of Naval Arch.
Crescent Beach Road, Glen Cove
Long Island, New York 11542

Librarian
Webb Institute of Naval Arch.
Crescent Beach Road, Glen Cove
Long Island, New York 11542

Solid Rocket Struc. Integrity Cen.
Dept. of Mechanical Engr.
Professor F. Wagner
University of Utah
Salt Lake City, Utah 84112

Dr. Daniel Frederick
Dept. of Engr. Mechs.
Virginia Polytechnic Inst.
Blacksburgh, Virginia

Industry and Research Institutes

Dr. James H. Wiegand
Senior Dept. 4720, Bldg. 0525
Ballistics & Mech. Properties Lab.
Aerojet-General Corporation
P. O. Box 1947
Sacramento, California 95809

Mr. Carl E. Hartbower
Dept. 4620, Bldg. 2019 A2
Aeroject-General Corporation
P. O. Box 1947
Sacramento, California 95809

Mr. J. S. Wise
Aerospace Corporation
P. O. Box 1300
San Bernardino, California 92402

Dr. Vito Salerno
Applied Technology Assoc., Inc.
29 Church Street
Ramsey, New Jersey 07446

Library Services Department
Report Section, Bldg. 14-14
Argonne National Laboratory
9700 S. Cass Avenue
Argonne, Illinois 60440

Dr. M. C. Junger
Cambridge Acoustical Associates
129 Mount Auburn Street
Cambridge, Massachusetts 02138

Dr. F. R. Schwarzl
Central Laboratory T.N.O.
Schoenmakerstraat 97
Delft, The Netherlands

Research and Development
Electric Boat Division
General Dynamics Corporation
Groton, Connecticut 06340

Supervisor of Shipbuilding, USN, and
Naval Insp. of Ordnance
Electric Boat Division
General Dynamics Corporation
Groton, Connecticut 06340

Dr. L. H. Chen
Basic Engineering
Electric Boat Division
General Dynamics Corporation
Groton, Connecticut 06340

Dr. Wendt
Valley Forge Space Technology Cen.
General Electric Co.
Valley Forge, Pennsylvania 10481

Dr. Joshua E. Greenspon
J. G. Engr. Research Associates
3831 Menlo Drive
Baltimore, Maryland 21215

Industry & Research Inst. (cont'd)

Dr. Walt. D. Pilkey
IIT Research Institute
10 West 35 Street
Chicago, Illinois 60616

Library Newport News Shipbuilding
& Dry Dock Company
Newport News, Virginia 23607

Mr. J. I. Gonzalez
Engr. Mechs. Lab.
Martin Marietta
MP - 233
P. O. Box 5837
Orlando, Florida 32805

Dr. E. A. Alexander
Research Dept.
Rocketdyne D.W., NAA
6633 Canoga Avenue
Canoga Park, California 91304

Mr. Cezar P. Nuguid
Deputy Commissioner
Philippine Atomic Energy Commission
Manila, Philippines

Dr. M. L. Merritt
Division 5412
Sandia Corporation
Sandia Base
Albuquerque, New Mexico 87115

Director
Ship Research Institute
Ministry of Transportation
700, SHINKAWA
Mitaka
Tokyo, Japan

Dr. H. N. Abramson
Southwest Research Institute
8500 Culebra Road
San Antonio, Texas 78206

Dr. R. C. DeHart
Southwest Research Institute
8500 Culebra Road
San Antonio, Texas 78206

Dr. M. L. Baron
Paul Weidlinger, Consulting Engr.
777 Third Ave - 22nd Floor
New York, New York 10017

Mr. Roger Weiss
High Temp. Structs. & Materials
Applied Physics Lab.
8621 Georgia Ave.
Silver Spring, Md.

Mr. William Caywood
Code BBE
Applied Physics Lab.
8621 Georgia Ave.
Silver Spring, Md.

Mr. M. J. Berg
Engineering Mechs. Lab.
Bldg. R-1, Rm. 1104A
TRW Systems
1 Space Park
Redondo Beach, California 90278

Unclassified

Security Classification

DOCUMENT CONTROL DATA - R & D

Security classification of title, body of abstract and indexing annotation must be entered when the overall report is classified)

1. ORIGINATING ACTIVITY (Corporate author)	2a. REPORT SECURITY CLASSIFICATION
University of Illinois at Urbana-Champaign Department of Civil Engineering	Unclassified
	2b. GROUP

3. REPORT TITLE

QUASI-STATIC LATERAL DESIGN LOADS FOR EARTHQUAKE RESISTANT STRUCTURES

4. DESCRIPTIVE NOTES (Type of report and, inclusive dates)

5. AUTHOR(S) (First name, middle initial, last name)

Gabriel Estrada-Uribe

6. REPORT DATE	7a. TOTAL NO. OF PAGES	7b. NO. OF REFS
June, 1971	171	28

8a. CONTRACT OR GRANT NO.	9a. ORIGINATOR'S REPORT NUMBER(S)
N000-14-67-A-0305-0010	Structural Research Series No. SRS 378
b. PROJECT NO. Navy A-0305-0010	
c.	9b. OTHER REPORT NO(S) (Any other numbers that may be assigned this report)
d.	

10. DISTRIBUTION STATEMENT

Qualified requesters may obtain copies of this report from DDC.

11. SUPPLEMENTARY NOTES	12. SPONSORING MILITARY ACTIVITY
	Office of Naval Research Structural Mechanics Branch Department of the Navy

13. ABSTRACT

Different types of structures including frames, shear walls, box systems, chimneys, towers, masts, etc., were simulated by means of a mathematical model. The structural properties of the model such as mass and stiffness matrices were defined using matrix compression techniques. Equations of motion were then formulated and solved using a digital computer to obtain eigenvalues and eigenvectors. Finally, after performing a modal analysis, quasi-static loads were evaluated for the various responses of interest, namely displacements, accelerations, shears, and overturning moments. These forces were such that when applied to the model they would produce an equivalent dynamic response of the structure.

The effect of parameters such as earthquake magnitude, rigidity of the structures, shear-flexural ratio, stiffness and mass distribution, and number of stories, upon the responses of the structure, were analyzed independently. From the data obtained, a method of predicting a set of design quasi-static lateral loads that would yield responses greater than or equal to those given by a complete modal analysis was developed. The recommended systematic method of predicting quasi-static loads for earthquake resistant structures is presented and illustrated by means of an example.

DD FORM 1 NOV 65 1473 (PAGE 1)

S/N 0101-807-6811

Unclassified

Security Classification

A-31408

14. KEY WORDS	LINK A		LINK B		LINK C	
	ROLE	WT	ROLE	WT	ROLE	WT
Earthquake						
Design loads						
Global analysis						
Structural Response						
Spectral						